Energy Transfer Mechanism in Lanthanide Complexes Studied by Time-Resolved Spectroscopy

宮崎, 栞

Doctoral thesis

Energy Transfer Mechanism in Lanthanide Complexes Studied by Time-Resolved Spectroscopy

Shiori Miyazaki

Department of Chemistry

Graduate School of Science

Kyushu University

August 2023

Contents

Chapter 1. Introduction

1-1 Background

1-1-1 Excited-state dynamics and time-resolved spectroscopy

When materials absorb light, they transition to an excited state, which exhibits different functions from the ground state (S_0). Currently, there is a growing emphasis on the research of light-emitting materials centered around luminescent molecules in various applications such as organic light-emitting diodes (OLEDs) *(1–4)*, organic semiconductor laser diodes (OSLDs) *(5–7)*, organic solar cells *(8,9)*, photon energy upconversion systems *(10–13)*, and bioimaging sensors *(14,15)*.

The value of luminescent materials rely on important optical properties such as luminescence efficiency and color quality based on International Commission on Illumination (CIE) *(16,17)*. Particularly, luminescence efficiency plays a crucial role in the practical utilization of luminescent materials. To enhance luminescence efficiency, precise design strategies for luminescent molecules are essential in materials development. In order to establish these design strategies for light-emitting materials, a detailed understanding of the luminescent mechanisms at the molecular level is essential.

However, efficient design strategies for achieving targeted photo-functions and improving luminescence efficiency are still being developed. Understanding the molecular-level mechanisms of these photo-functions is crucial for both molecular photochemistry and materials science. By gaining deeper insights into the luminescent processes and optimizing the molecular structures, researchers aim to develop novel light-emitting materials with enhanced performance and expanded applications.

Excited states, however, are transient species with short lifetimes. **Fig. 1-1** illustrates the dynamics of excited states in typical organic molecules, where relaxation processes occur on timescales ranging from femtoseconds to seconds. These processes compete with each other, resulting in complex dynamics, despite most functions being expressed at the lowest singlet (S_1) or triplet (T_1) excited states. To unravel the molecular-level mechanisms, real-time observation on the timescale corresponding to each process is necessary. For instance, since fluorescence typically occurs within nanoseconds, real-time observation using a system with a nanosecond or even shorter time resolution is essential to understand fluorescence processes effectively.

With the recent development of ultrashort pulsed laser sources, various time-resolved spectroscopy techniques have been developed to enable real-time observations of excited state dynamics. The time resolution of these spectroscopic methods is determined not only by the pulse width of the laser but also by the characteristics of the detection system. Moreover, each time-resolved spectroscopy method provides different types of information, and it is crucial to select an appropriate system that suits the specific dynamics of interest.

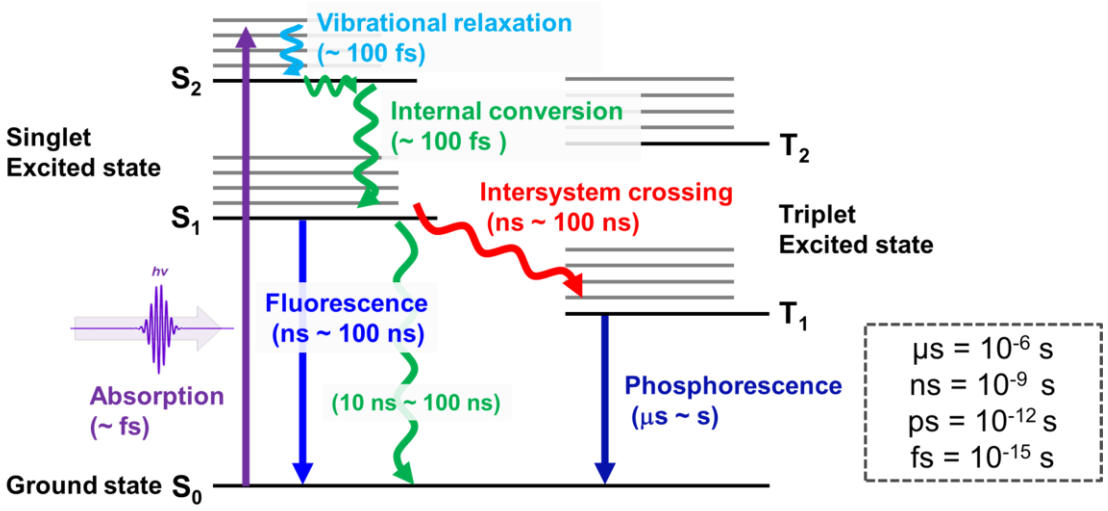

Figure 1-1 Schematic diagram of excited state dynamics in organic molecules (Jablonski diagram).

Two examples of widely used time-resolved spectroscopy methods are time-resolved photoluminescence spectroscopy (TR-PL) and transient absorption spectroscopy (TAS). TR-PL primarily provides information about emissive states, such as the fluorescence or phosphorescence decay time constants. On the other hand, TAS not only examines emissive states but also provides insights into dark states by monitoring the absorption of excited species. A comprehensive description of these spectroscopy methods is provided in **Chapter 2** of this thesis.

1-1-2 Rare earth and Lanthanoid

Rare earth ions, particularly trivalent rare earth ions, have garnered significant attention in the field of light-emitting materials. These ions possess distinct characteristics that differentiate them from luminescent molecules like organic compounds and transition metal complexes. Notable features include their narrow wavelength range for light absorption and emission, independence of emission and absorption transitions from the host materials, and remarkably long emission lifetimes, lasting on the order of milliseconds. These properties make trivalent rare earth ions highly promising for applications such as organic electroluminescence (EL) devices *(18–20)*, bioimaging sensors *(21–23)*, thermosensors *(24,25)* and security inks *(26, 27)*.

In this section, we will discuss rare earths and lanthanides. Rare earth elements refer to 17 elements, including scandium (Sc) with atomic number 21, yttrium (Y) with atomic number 39, and lanthanum (La) with number 57 to lutetium (Lu) with number 71, plus 14 elements. Among these, the 15 elements ranging from La to Lu (atomic numbers 57 to 71) are referred to as lanthanoids, while the 14 elements from cerium (Ce) to Lu (atomic numbers 58 to 71), which contain at least one 4f orbital electron, are specifically called lanthanides. **Fig. 1-2** shows the respective positions of rare earths, lanthanoids, and lanthanides on the periodic table.

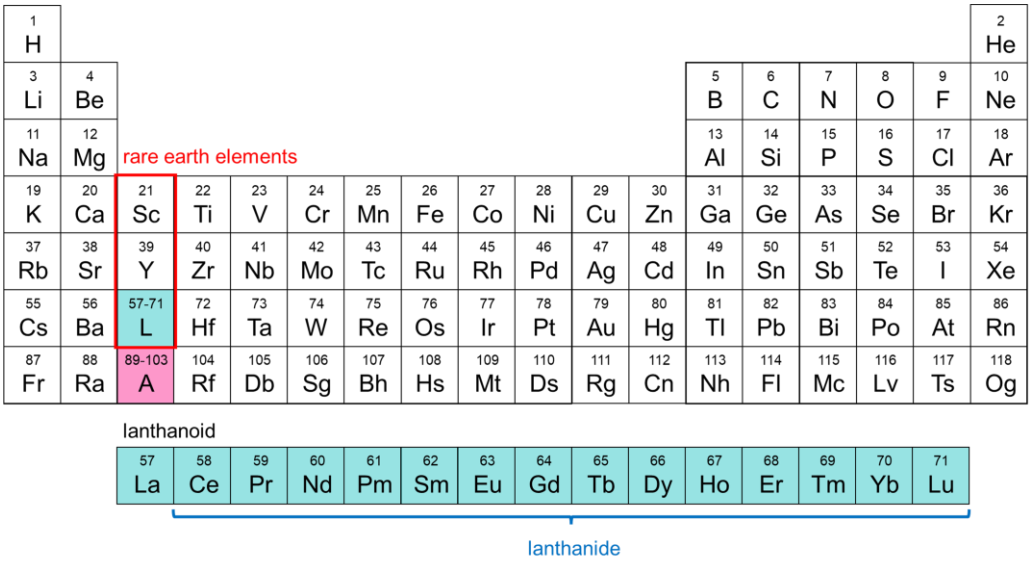

Figure 1-2 Rare earths and lanthanoids in the periodic table.

Table 1-1 shows the electron configuration of lanthanide atoms. Typically, electrons fill orbitals closer to the nucleus, but in the cases of La and Ce, electrons occupy the 5d orbitals instead of the 4f orbitals. From praseodymium (Pr) to europium (Eu), electrons sequentially occupy the 4f orbitals, with the 4f orbitals reaching a half-filled and stable state at Eu. Subsequently, in gadolinium (Gd), electrons fill the 5d orbital outside the 4f orbitals. However, starting from terbium (Tb), electrons once again occupy the 4f orbitals successively. In ytterbium (Yb), the 4f orbital achieves a stable closed-shell configuration, and in the subsequent Lu, electrons occupy the 5d orbitals outside the 4f orbitals. Normally, the lanthanide ions exhibit stability in the +3 valence state, with two electrons missing from the 6s orbital and one from the 4f orbital.

Table 1-1 Lanthanoide atoms and their electronic configuration.

atomic number	element number	name	4f	5s	5p	5d	6s
57	La	lanthanum	0	2	6	1	2
58	Ce	cerium	1	2	6	1	2
59	Pr	praseodymium	3	2	6		2
60	Nd	neodymium	4	2	6		2
61	Pm	promethium	5	2	6		2
62	Sm	samarium	6	2	6		2
63	Eu	europium	7	2	6		2
64	Gd	gadolinium	7	2	6	1	2
65	Tb	terbium	9	2	6		2
66	Dy	dysprosium	10	2	6		2
67	Ho	holmium	11	2	6		2
68	Er	erbium	12	2	6		2
69	Tm	thulium	13	2	6		2
70	Yb	ytterbium	14	2	6		2
71	Lu	lutetium	14	2	6	1	2

1-1-3 Photochemistry of Lanthanide

Trivalent lanthanide ions (Ln(III)) have attracted attention as luminescent materials due to their long-lived luminescence with high color purity, which remains unaffected by the ambient environment. In Ln(III), the majority of electronic transitions involved in light absorption and emission are 4f-4f transitions, shielded by 5s and 5p orbitals. The luminescence originating from these shielded 4f-4f transitions is minimally influenced by steric structures or coordination environments, resulting in relatively stable absorption positions, smaller Stokes shifts, narrower emission half-widths, and higher color purity. Moreover, the non-degeneracy of the 4f orbitals, due to their shielding, allows Ln(III) complexes to maintain their intricate split states, accurately represented by the original term symbols.

Fig. 1-3 shows the emission spectra of typical Ln(III) complexes, demonstrating their sharp and long-lived emission in the visible and near-infrared regions, attributed to 4f-4f transitions *(28)*. For instance, Tm(III) exhibits blue emission, Tb(III) emits green light, Dy(III) emits yellow, Eu(III) displays red luminescence, and Sm(III) emits deep red light in the visible region. Yb(III), Nd(III), and Er(III) exhibit emission in the near-infrared region.

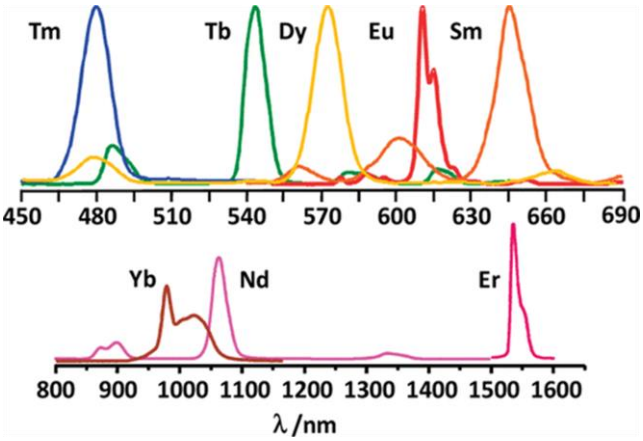

Figure 1-3 luminescence spectra of Ln(III).*(28)*

Due to the low absorption coefficient of Ln(III) (ε = 0.1-10 M^{-1} cm^{-1}), direct photoexcitation becomes challenging. Therefore, organic ligands with high absorption coefficients (ε = 10^3-10^5 M^{-1} cm^{-1}) have been employed as antennas to achieve strongly luminescent Ln(III) complexes through energy transfer from the antenna ligands to the central metal ion *(28–32)*. Ligand design has primarily focused on three aspects: enabling Laporte-forbidden 4f-4f transitions, suppressing non-radiative relaxation, and achieving highly efficient intramolecular energy transfer. Many Ln(III) complexes have been developed considering these terms.

Efforts have been made to enhance the emission of Laporte-forbidden 4f-4f transitions by introducing asymmetric complex structures fields that facilitate 4f-4f transitions as electric dipole transitions *(33,34)*. In terms of suppressing non-radiative relaxation and achieving efficient energy transfer, β-diketonate ligands have gained attention. Particularly, β-diketone ligands with CF bonds instead of CH bonds such as thenoyltrifluoroacetonate and hexafluoroacetylacetonate have been shown to reduce the non-radiative relaxation rate constant of Ln(III) complexes *(35–37)*. This is important because high-energy vibrations, such as the OH stretch in water, can quench the luminescence of Ln(III) ions *(38–40)*.

Phosphine oxide linkers have emerged as suitable candidates for suppressing the nonradiative relaxation of Eu(III) ions due to their low vibrational energy. Many Eu(III) complexes containing a phosphine oxide linker and β-diketonate ligands, exhibiting a high total photoluminescence quantum yield (PLQY) and long luminescence lifetime have been reported *(33,41–46)*. Moreover, ligands have been designed to tune their energy levels, which has proven to be an important factor in improving energy transfer efficiency.

Many Ln(III) complexes with high energy transfer efficiency have been reported

by appropriately designing the energy levels of the ligands. It is well-known that the energy level of the ligand T_1 state plays a crucial role in improving energy transfer efficiency *(47)*. **Fig. 1-4** provides an overview of intramolecular energy transfer of a Ln(III) complex. When the energy transfer from the ligand to Ln(III) occurs through the T_1 state of the ligand, it is important for the energy level of the ligand T_1 state to be higher than the energy acceptance state of Ln(III) *(48–50)*. Conversely, if the T_1 state of the ligand is close to the lowest excited level of Ln(III), a reverse energy transfer from Ln(III) to the ligand can occur *(25, 51–53)*. **Fig. 1-5** presents a Dieke's diagram *(54)* that systematically summarizes the energy levels of Ln(III).

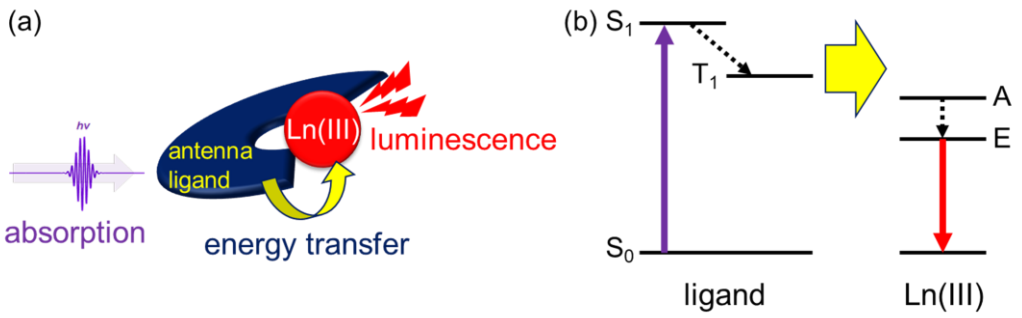

Figure 1-4 (a) Overview of intramolecular energy transfer. (b) Schematic diagram of energy transfer process (A: energy acceptance state of Ln(III), E: emission state of Ln(III)).

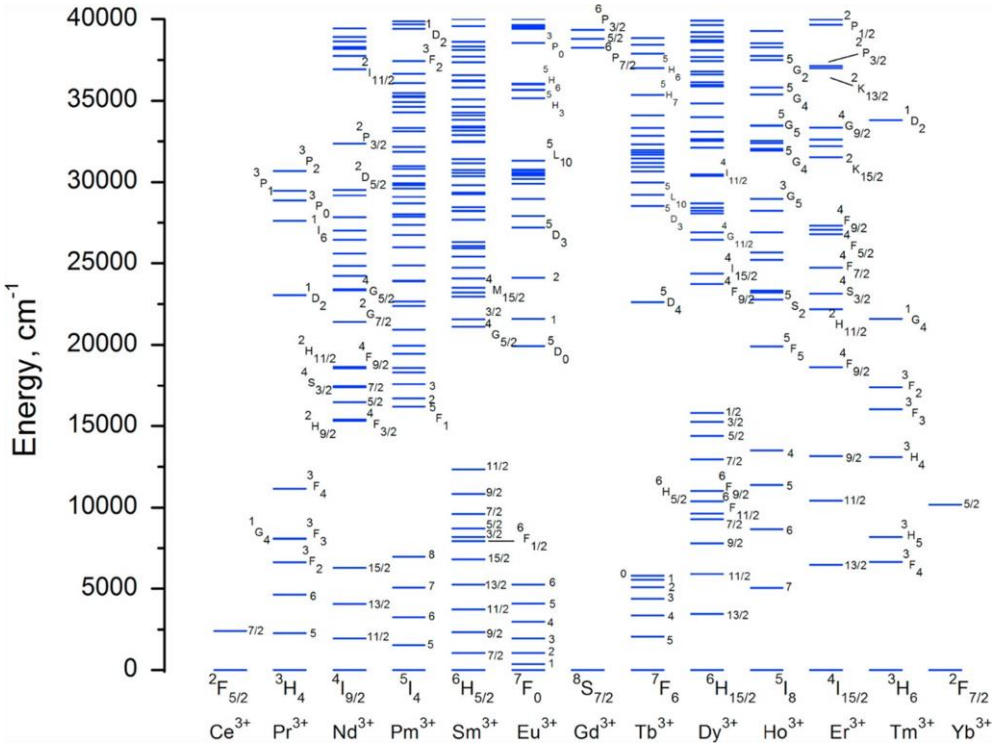

Figure 1-5 Dieke's diagram *(54)*.

1-1-4 Studies on energy transfer mechanism in Ln(III) complex

Although many complexes have been designed using ligands based on the T_1 energy level of the ligand, it is not always the T_1 state of the ligand that serves as the pathway for energy transfer from the ligand to the central metal. **Fig. 1-6** shows that energy is transferred from the S_1 or T_1 state of the photoexcited ligand to the appropriate excited level of Ln(III). Two possible energy transfer mechanisms exist: Förster-type *(55)* and Dexter-type *(56)*. The Förster-type energy transfer mechanism arises from the interaction of transition dipole moments, whereas the Dexter-type energy transfer mechanism is caused by electron exchange interaction. Energy transfer from the S_1 state of the ligand to the central metal is considered a Förster-type or Dexter-type energy transfer mechanism. Conversely, energy transfer from the T_1 state of the ligand exclusively follows the Dexter-type energy transfer mechanism. This is due to the small transition dipole moment at the T_1 state, which precludes Förster-type energy transfer.

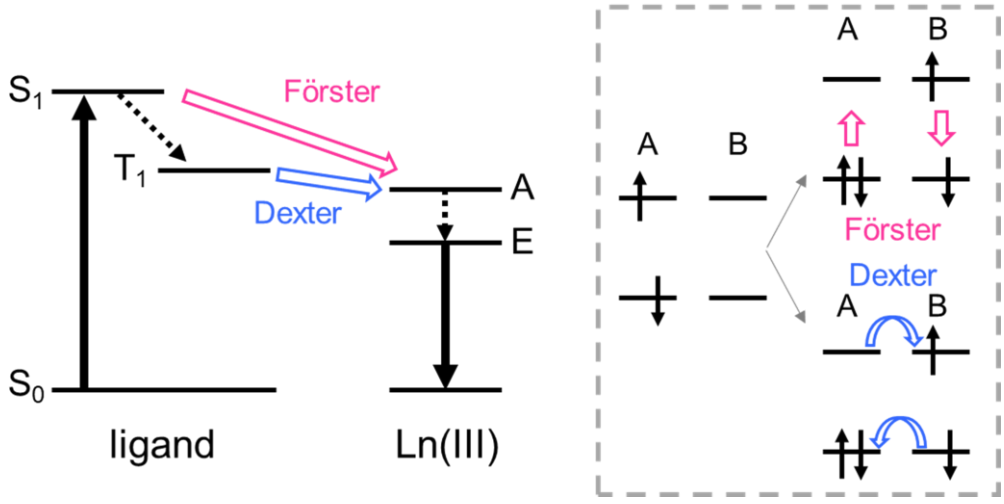

Figure 1-6 Jablonski diagram of the ligand and Ln(III) following photoexcitation, depicting the possible energy transfer pathways of Förster (shown in pink) and Dexter (shown in blue) mechanisms. (A: energy acceptance state of Ln(III), E: emission state of Ln(III)).

Elucidating the energy transfer process is crucial for establishing a ligand design strategy in Ln(III) complexes. Spectroscopic studies have been conducted to investigate the energy transfer mechanisms. It is important to note that the process can vary depending on the ligand and steric structure of the complex. TR-PL is effective to elucidate the emission dynamics in the Ln(III) complexes. In the case of Pr(III) complexes, Dexter-type energy transfer has been observed from the T_1 state of the ligand to the $^1I_6$ level of Pr(III) in $[Pr(phen)(DMF)_2(NO_3)_3]$ and from the T_1 state of the ligand to the $^1D_2$ state of Pr(III) in $[Pr(bathophen)_2(NO_3)_3]$ *(57–59)*. Similar investigations have been carried out for Eu(III) complexes using time-resolved spectroscopic measurements. It has revealed that energy transfer occurred from the S_1 state of the ligands in $[Eu(tta)_3]\cdot$dpbt *(60)*.

However, TR-PL measurement is unsuitable to direct observation of Dexter-type energy transfer mechanism. The TR-PL measurement can only indirectly observe the Dexter-type energy transfer mechanism in Ln(III) complexes. TAS is a powerful tool to observe the dynamics of non-emissive excited states such as triplet states of ligands. Fs-TAS and X-ray transient absorption spectroscopy have been employed to study the Eu(III) complexes with 1-hydroxypyridin-2-one ligands, leading to the observation of Dexter-type energy transfer from the ligand T_1 state to the Eu(III) ion *(61)*.

Despite these various studies on energy transfer mechanisms in Ln(III) complexes, the specific mechanism of intramolecular energy transfer from the ligand to the central metal in Ln(III) complexes with antenna ligands remains largely unknown. Designing ligands to control the energy transfer process represents a significant challenge. Further research in this area is necessary to advance our understanding and enable the design of highly efficient energy transfer systems.

1-2 Purpose and outline

The purpose of this research is to investigate the energy transfer mechanisms in Eu(III) complexes using TR-PL and TAS. By employing these advanced spectroscopic techniques, the author aims to gain a deeper understanding of the emission mechanism in Eu(III) complexes and facilitate the development of new materials.

Chapter 2 provides a detailed explanation of the time-resolved spectroscopy techniques used in this thesis, specifically TR-PL and fs-TAS, which are employed to investigate the energy transfer mechanisms.

Chapters 3 and 4 investigate the intramolecular energy transfer dynamics in Eu(III) complexes with β-diketonate ligands and phosphine oxide linkers, specifically $Eu(hfa)_3(DPPTO)_2$ (hfa: hexafluoroacetylacetonate, DPPTO: 2-diphenylphosphoryltriphenylene) and $Eu(hfa)_3(TPPO)_2$ (hfa: hexafluoroacetylacetonate, TPPO: triphenylphosphine oxide). Time-resolved spectroscopy is employed in solution to examine the overall energy transfer pathways and determine their corresponding time constants. These findings emphasize the importance of β-diketonate ligands in promoting efficient intramolecular energy transfer, establishing a foundation for the design and synthesis of highly luminescent Eu(III) complexes, and advancing the field of lanthanide-based light-emitting materials.

In **Chapter 3**, the energy transfer processes in the $Eu(hfa)_3(DPPTO)_2$ complex are examined using TR-PL. A dual energy transfer mechanism is discovered, involving both the conventional pathway through the T_1 state of the ligands and a fast pathway from the singlet excited states of the ligands to the $^5D_1$ state of Eu(III).

In **Chapter 4**, employing a combination of TR-PL and fs-TAS, the research demonstrates nearly perfect efficiency of energy transfer from the T_1 state of β-diketonate

ligands to the Eu(III) ions in $Eu(hfa)_3(TPPO)_2$. Furthermore, a novel pathway to the $^5D_2$ state of the Eu(III) ion is unveiled.

Chapter 5 shifts its focus to a Eu(III) complex doped host-guest film and investigates the enhancement of photoluminescence intensity through sensitization using intermolecular energy transfer. The study specifically examines a system composed of triazine-based host molecules and $Eu(hfa)_3(TPPO)_2$. By employing TR-PL and fs-TAS measurements, the author uncovers an energy transfer mechanism from the host molecules to the Eu(III) ions, which occurs through triplet states across multiple molecules with nearly perfect efficiency. This discovery paves the way for achieving highly efficient light harvesting in Eu(III) complexes and offers a straightforward solution-based fabrication process, holding significant promise for advancements in various light-emitting applications.

Chapter 6 concludes this thesis and discusses future perspectives for time-resolved spectroscopy and Ln(III) complexes.

Overall, this research employs advanced spectroscopic techniques to investigate the energy transfer mechanisms in Eu(III) complexes. By enhancing our understanding of the emission mechanism and facilitating materials development, this study contributes to the progress in the field of luminescent materials and holds great potential for applications in light-emitting technologies.

References

1. C. W. Tang, S. A. Vanslyke, Organic electroluminescent diodes. *Applied Physics Letters* **51**, 913–915 (1987).
2. M. A. Baldo, O. F. O'Brien, Y. You, A. Shoustikov, S. Sibley, M. E. Thompson, S. R. Forrest, Highly efficient phosphorescent emission from organic electroluminescent devices. *Nature* **395**, 151–154 (1998).
3. C. Adachi, M. A. Baldo, M. E. Thompson, S. R. Forrest, Nearly 100% internal phosphorescence efficiency in an organic light emitting device. *Journal of Applied Physics* **90**, 5048–5051 (2001).
4. H. Uoyama, K. Goushi, K. Shizu, H. Nomura, C. Adachi, Highly efficient organic light-emitting diodes from delayed fluorescence. *Nature* **492**, 234–238 (2012).
5. I. D. W. Samuel, G. A. Turnbull, Organic Semiconductor Lasers. *Chem. Rev.* **107**, *4*, 1272–1295 (2007).
6. A. J. C. Kuehne, M. C. Gather, Organic Lasers: Recent Developments on Materials, Device Geometries, and Fabrication Techniques. *Chem. Rev.* **116**, *21*, 12823–12864 (2016).
7. A. S. D. Sandanayaka, T. Matsushima, F. Bencheikh, S. Terakawa, W. J. Potscavage Jr., C. Qin, T. Fujihara, K. Goushi, J.-C. Ribierre, C. Adachi, Indication of current-injection lasing from an organic semiconductor. *Appl. Phys. Express* **12**, 061010 (2019).
8. B. O'Regan, M. A. Grätzel, A low-cost, high-efficiency solar cell based on dye-sensitized colloidal TiO_2 films. *Nature* **353**, 737 (1991).
9. A. Hagfeldt, M. Grätzel, Molecular photovoltaics. *Accounts of Chemical Research* **33**, 269–277 (2000).
10. T. N. Singh-Rachford, F. N. Castellano, Photon upconversion based on sensitized triplet-triplet annihilation. *Coordination Chemistry Reviews* **254**, 2560–2573 (2010).
11. P. Bharmoria, H. Bildirir, K. M.-Poulsen, Triplet–triplet annihilation based near infrared to visible molecular photon upconversion. *Chem. Soc. Rev.* **49**, 6529–6554 (2020).
12. J. Zhou, Q. Liu, W. Feng, Y. Sun, F. Li, Upconversion Luminescent Materials: Advances and Applications. *Chem. Rev.* **115**, *1*, 395–465 (2015).
13. N. Yanai, N. Kimizuka, New Triplet Sensitization Routes for Photon Upconversion: Thermally Activated Delayed Fluorescence Molecules, Inorganic Nanocrystals, and Singlet-to-Triplet Absorption. *Acc. Chem. Res.* **50**, *10*, 2487–2495 (2017).

14. M. Chalfie, Y. Tu, G. Euskirchen, W. W. Ward, D. C. Prasherf, Green Fluorescent Protein as a Marker for Gene Expression. *Science* **263**, 802–805 (1994).
15. H.-B. Cheng, Y. Li, B. Z. Tang, J. Yoon, Assembly strategies of organic-based imaging agents for fluorescence and photoacoustic bioimaging applications. *Chem. Soc. Rev.* **49**, 21–31 (2020).
16. W. D. Wright, A re-determination of the trichromatic coefficients of the spectral colours. *Trans. Opt. Soc.* **30**, 141 (1929).
17. J. Guild, The colorimetric properties of the spectrum. *Philosophical Transactions of the Royal Society of London. Series A* **230**, 149 (1931).
18. J. Kido, Y. Okamoto, Organo Lanthanide Metal Complexes for Electroluminescent Materials. *Chem. Rev.* **102**, 2357–2368 (2002).
19. L. Wang, Z. Zhao, C. Wei, H. Wei, Z. Liu, Z. Bian, C. Huang, Review on the Electroluminescence Study of Lanthanide Complexes. *Adv. Optical Mater.* **7**, 1801256 (2019).
20. K. Nehra, A. Dalal, A. Hooda, S. Bhagwan, R. K. Saini, B. Mari, S. Kumar, D. Singh, Lanthanides β-diketonate complexes as energy-efficient emissive materials: A review. *Journal of Molecular Structure* **1249**, 131531 (2022).
21. S. V. Eliseeva, J.-C. G. Bünzli, Lanthanide luminescence for functional materials and bio-sciences. *Chem. Soc. Rev.* **39**, 189–227 (2010).
22. X. Zhu , Q. Su , W. Feng, F. Li, Anti-Stokes shift luminescent materials for bio-applications. *Chem. Soc. Rev.* **46**, 1025–1039 (2017).
23. H. Dong, S.-R. Du, X.-Y. Zheng, G.-M. Lyu, L.-D. Sun, L.-D. Li, P.-Z. Zhang, C. Zhang, C.-H. Yan, Lanthanide Nanoparticles: From Design toward Bioimaging and Therapy. *Chem. Rev.* **115**, *19*, 10725–10815 (2015).
24. Y. Hasegawa, Y. Kitagawa, Thermo-sensitive luminescence of lanthanide complexes, clusters, coordination polymers and metal–organic frameworks with organic photosensitizers. *J. Mater. Chem. C* **7**, 7494–7511 (2019).
25. K. Miyata, Y. Konno, T. Nakanishi, A. Kobayashi, M. Kato, K. Fushimi, Y. Hasegawa, Chameleon Luminophore for Sensing Temperatures: Control of Metal-to-Metal and Energy Back Transfer in Lanthanide Coordination Polymers. *Angew. Chem. Int. Ed.* **52**, 6413–6416 (2013).
26. L. E. Mackenzie, R. Pal, Circularly polarized lanthanide luminescence for advanced security inks. *Nature Reviews Chemistry* **5**, 109–124 (2021).
27. J.-C. G. Bünzli, Rising Stars in Science and Technology: Luminescent Lanthanide Materials. *Eur. J. Inorg. Chem.* **2017**, *44*, 5058–5063 (2017).

28. J.-C. G. Bünzli, Lanthanide Luminescence for Biomedical Analyses and Imaging. *Chem. Rev.* **110**, 2729–2755 (2010).
29. S. I. Weissman, Intramolecular Energy Transfer The Fluorescence of Complexes of Europium. *J. Chem. Phys.* **10**, 214–217 (1942).
30. R.E. Whan, G.A. Crosby, Luminescence studies of rare earth complexes: Benzoylacetonate and dibenzoylmethide chelates. *J. Mol. Spectrosc.* **8**, 315 (1962).
31. Y. Hasegawa, Y. Wada, S. Yanagida, Strategies for the design of luminescent lanthanide(III) complexes and their photonic applications. *J. Photochem. Photobiol. C Rev.* **5**, 183–202 (2004).
32. J. -C. G. Bünzli, On the design of highly luminescent lanthanide complexes. *Cood. Chem. Rev.* **293–294**, 19–47 (2015).
33. K. Miyata, T. Nakagawa, R. Kawakami, Y. Kita, K. Sugimoto, T. Nakashima, T. Harada, T. Kawai, Y. Hasegawa, Remarkable Luminescence Properties of Lanthanide Complexes with Asymmetric Dodecahedron Structures. *Chem. Eur. J.* **17**, 521–528 (2011).
34. K. Yanagisawa, T. Nakanishi, Y. Kitagawa, T. Seki, T. Akama, M. Kobayashi, T. Taketsugu, H. Ito, K. Fushimi, Y. Hasegawa, Seven-Coordinate Luminophores: Brilliant Luminescence of Lanthanide Complexes withC_{3v} Geometrical Structures. *Eur. J. Inorg. Chem.* **28**, 4769–4774 (2015).
35. Y. Hasegawa, T. Ohkubo, K. Sogabe, Y. Kawamura, Y. Wada, N. Nakashima, S. Yanagida, Luminescence of Novel Neodymium Sulfonylaminate Complexes in Organic Media. *Angew. Chem. Int. Ed.* **39**, *2* (2000).
36. N. Filipescu, W. F. Sager, F. A. Serafin, Substituent Effects on Intramolecular Energy Transfer. II. Fluorescence Spectra of Europium and Terbium β-Diketone Chelates. *J. Phys. Chem.* **68**, *11*, 3324–3346 (1964).
37. Y. Hasegawa, K. Murakoshi, Y. Wada, S. Yanagida, J. Kim, N. Nakashima, T. Yamanaka, Enhancement of luminescence of Nd^{3+} complexes with deuterated hexafluoroacetylacetonato ligands in organic solvent. *Chem. Phys. Lett.*, **248**, 8–12 (1996).
38. Y. Haas, G. Stein, Pathways of Radiative and Radiationless Transitions in Europium (III) Solutions: the Role of High Energy Vibrations. *J. Phys. Chem.* **75**, *24*, (1971).
39. G. Stein, E. Würzberg, Energy gap law in the solvent isotope effect on radiationless transitions of rare earth ions. *J. Chem. Phys.* **62**, 208–213 (1975).

40. N. Filipescu, G. W. Mushrush, C. R. Hurt, N. Mcavoy, Fluorescence Quantum Efficiencies of Octa-coordinated Europium Homogeneous and Mixed Chelates in Organic Solvents. *Nature* **211**, 960–961 (1966).
41. D. B. A. Raj, B. Francis, M. L. P. Reddy, R. R. Butorac, V. M. Lynch, A. H. Cowley, Highly Luminescent Poly(Methyl Methacrylate)-Incorporated Europium Complex Supported by a Carbazole-Based Fluorinated β-Diketonate Ligand and a 4,5-Bis(diphenylphosphino)-9,9-dimethylxanthene Oxide Co-Ligand. *Inorg. Chem.* **49**, *19*, 9055–9063 (2010).
42. N. B. D. Lima, S. M. C. Gonçalves, S. A. Júnior, A. M. A. Simas, Comprehensive Strategy to Boost the Quantum Yield of Luminescence of Europium Complexes. *Sci. Rep.* **3**, 1–8 (2013).
43. Y. Kitagawa, R. Ohno, T. Nakanishi, K. Fushimi, Y. Hasegawa, Visible Luminescent Lanthanide Ions and a Large π-Conjugated Ligand System Shake Hands. *Phys. Chem. Chem. Phys.* **18**, 31012–31016 (2016)
44. K. Nakamura, Y. Hasegawa, H. Kawai, N. Yasuda, N. Kanehisa, Y. Kai, T. Nakamura, S. Yanagida, Y. Wada, Enhanced Lasing Properties of Dissymmetric Eu(III) Complex with Bidentate Phosphine Ligands. *J. Phys. Chem. A* **111**, 3029–3037 (2007).
45. Y. Kitagawa, F. Suzue, T. Nakanishi, K. Fushimi, Y. Hasegawa, A Highly Luminescent Eu(III) Complex Based on an Electronically Isolated Aromatic Ring System with Ultralong Lifetime. *Dalt. Trans.* **47**, 7327–7332 (2018).
46. Y. Hasegawa, M. Yamamuro, Y. Wada, N. Kanehisa, Y. Kai, A. Yanagida, Luminescent Polymer Containing the Eu(III) Complex Having Fast Radiation Rate and High Emission Quantum Efficiency. *J. Phys. Chem. A* **107**, 1697–1702 (2003).
47. M. Latva, H. Takalo, V-M. Mukkala, C. Matachescu, J. C. Rodriguez-Ubisd, J. Kankarea, Correlation between the Lowest Triplet State Energy Level of the Ligand and Lanthanide(III) Luminescence Quantum Yield. *J. Lumin*. **75**, 149–169 (1997).
48. G. A. Crosby, R. E. Whan, R. M. Alire, Intramolecular Energy Transfer in Rare Earth Chelates. Role of the Triplet State. *J. Chem. Phys.* **34**, 743–748 (1961).
49. G. A. Crosby, R. E. Whan, J. J. Freeman, SPECTROSCOPIC STUDIES OF RARE EARTH CHELATES. *J. Phys. Chem.* **66**, *12*, 2493–2499.
50. G. A. Crosby, Luminescent Organic Complexes of the Rare Earths. *Mol. Cryst.* **1**, 37–81 (1966).
51. S. Katagiri, Y. Hasegawa, Y. Wada, S. Yanagida, Thermo-sensitive Luminescence Based on the Back Energy Transfer in Terbium(III) Complexes. *Chem. Lett.* 33, 1438–1439 (2004).

52. S. Katagiri, Y. Tsukahara, Y. Hasegawa, Y. Wada, Energy-Transfer Mechanism in Photoluminescent Terbium(III) Complexes Causing Their Temperature-Dependence. *Bull. Chem. Soc. Jpn.* **80**, *8*, 1492–1503 (2007).
53. M. Yamamoto, Y. Kitagawa, T. Nakanishi, K. Fushimi, Y. Hasegawa, Ligand-Assisted Back Energy Transfer in Luminescent Tb^{III} Complexes for Thermosensing Properties. *Chem. Eur. J.* 24, 17719–17726 (2018).
54. C. -G. Ma, M. G. Brik, D.-X. Liu, B. Feng, Y. Tian, A. Suchocki, Energy level schemes of f^N electronic configurations for the di-, tri-, and tetravalent lanthanides and actinides in a free state. *J. Lumin.* **170**, 369–374 (2016).
55. T. Förster, Excitation transfer and internal conversion. *Chem. Phys. Lett.* **12**, 422–424 (1971).
56. D. L. Dexter, A Theory of Sensitized Luminescence in Solids. *J. Chem. Phys.* **21**, 836–850 (1953).
57. M. Hasegawa, A. Ishii, T. Yamazaki, S. Kishi, I. Yamazaki, Intramolecular Excited Energy Transfer from Phenanthroline Fluorophore to Pr(III) in a Metal Complex. *Chem. Lett.* **34**, 1418–1419 (2005).
58. M. Hasegawa, A. Ishii, S. Kishi, Picosecond Time-Resolved Luminescence of Pr(III) Complexes: Intramolecular Excitation Energy Transfer from Ligand to Pr(III). *J. Photochem. Photobiol*. *A* **178**, 220–224 (2006).
59. A. Ishii, S. Kishi, H. Ohtsu, T. Iimori, T. Nakabayashi, N. Ohta, N. Tamai, M. Melnik, M. Hasegawa, Y. Shigesato, Molecular Distortion Effect on ff-Emission in a Pr(III) Complex with 4,7-Diphenyl-1,10-Phenanthroline. *ChemPhysChem* **8**, 1345–1351 (2007).
60. C. Yang, L. M. Fu, Y. Wang, J. P. Zhang, W. T. Wong, X. C. Ai, Y. F. Qiao, B. S. Zou, L. L. Gui, A Highly Luminescent Europium Complex Showing Visible-Light-Sensitized Red Emission: Direct Observation of the Singlet Pathway. *Angew. Chem., Int. Ed.* 43, 5010– 5013 (2004).
61. M. W. Mara, D. S. Tatum, A. March, G. Doumy, E. G. Moore, K. N. Raymond, Energy Transfer from Antenna Ligand to Europium(III) Followed Using Ultrafast Optical and X-Ray Spectroscopy. *J. Am. Chem. Soc.* 141, 11071– 11081 (2019).

Chapter 2. Experimental methods

2-1 Time-resolved photoluminescence spectroscopy (TR-PL)

Multiple methods have been established to perform TR-PL, including optical Kerr gate spectroscopy, fluorescence upconversion spectroscopy, time-correlated single photon counting (TCSPC), and the method utilizing a streak camera. Each method possesses unique characteristics and should be selected based on specific requirements such as temporal resolution, sensitivity, simplicity, and the need for TR-PL spectra. Optical Kerr gate spectroscopy and fluorescence upconversion spectroscopy with femtosecond lasers enable sub-picosecond time resolution through the utilization of the optical Kerr effect and sum-frequency generation, respectively. While optical Kerr gate spectroscopy can also provide TR-PL spectra, its sensitivity may not be as high. TCSPC allows for the acquisition of PL decay curves with excellent sensitivity and a time resolution of a few picoseconds. By combining a streak camera with a spectrometer, a wavelength and time-resolved profile can be obtained through the wavelength dispersion of the spectrometer and the electrode sweep of the streak camera. As an example, **Fig. 2-1** shows a streak image of 2-diphenylphosphoryltriphenylene (DPPTO) in a THF solution. Streak cameras also offer a time resolution of a few nanoseconds.

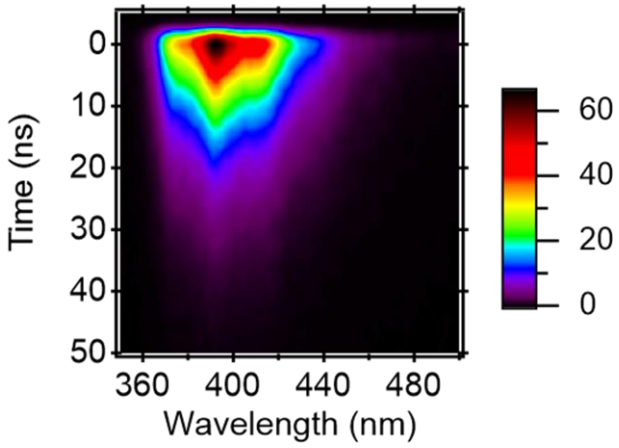

Figure 2-1 Streak image of DPPTO in THF solution.

Fig. 2-2 provides a brief overview of the operational principle of the streak camera *(1,2)*. Following dispersion by wavelength in a spectrometer, the emitted photons enter a streak tube. At the photocathode, the photons are converted into electrons, and the number of ejected electrons corresponds to the incident light intensity. These electrons traverse a sweep electrode, causing their trajectory to change along the vertical direction, ultimately reaching different positions on the microchannel plate (MCP). Within the MCP, the electrons undergo a process of amplification, multiplying their numbers by several thousand. Subsequently, the electrons collide with a phosphor screen, where they are reconverted into light. The light intensity is then detected by a charge-coupled device (CCD) sensor, enabling the acquisition of a streak image.

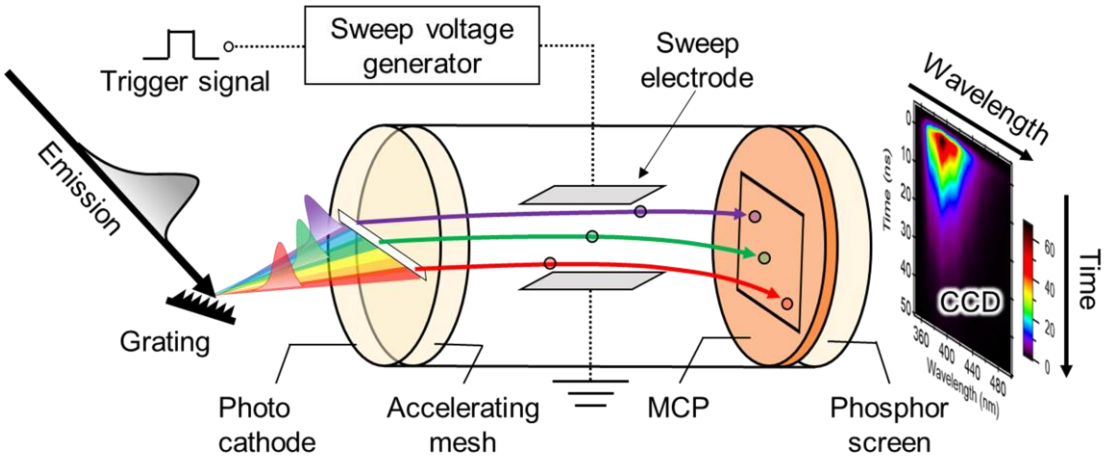

Figure 2-2 Operation principle of streak camera.

2-2 Transient absorption spectroscopy (TAS)

Well-known TAS methods include flash photolysis and pump-probe spectroscopy, which are widely used. Other TAS methods, such as the randomly interleaved pulse-train (RIPT) method *(3)* and the method using a streak camera *(4)*, have also been developed. In flash photolysis, a sample is excited by a pulsed laser and detected using continuous light, such as a xenon lamp. The change in absorbance is then observed using a high-speed response detector. Typically, the time resolution in flash photolysis is determined by the response time of the detector, resulting in time resolutions longer than a few nanoseconds. In the pump-probe method, measurements are conducted using two light pulses: a pump pulse and a probe pulse. Initially, the sample is excited by the pump pulse, similar to flash photolysis. Then, after a certain delay time, a probe pulse is irradiated, and the transmitted probe pulse is detected (**Fig. 2-3**). By acquiring the absorption spectra at different delay times, time-resolved information can be obtained. The time resolution in pump-probe spectroscopy relies on the pulse width and the accuracy of delay time control, rather than the response time of the detector. In an actual pump-probe spectroscopy system, the pump pulse is modulated by an optical chopper to detect the differential spectrum with and without pump pulse irradiation.

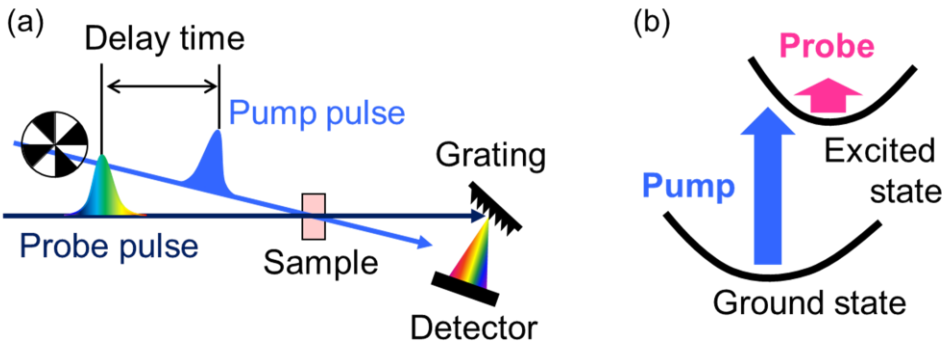

Figure 2-3 (a) Schematic diagram of pump-probe spectroscopy. (b) Energy diagram of pump-probe spectroscopy.

In pump-probe spectroscopy, the delay time is determined by the time difference between the pump and probe pulses, and there are two methods to control the delay time. One approach is to adjust the delay time by changing the optical path length of the pump and probe pulses (optical delay control, **Fig. 2-4a**). The delay time can be modified by using a translational stage with mirrors. For example, to achieve a delay time of 1 ps, the optical path length needs to be adjusted by 0.30 mm. An optical delay stage with a stepping motor can easily control the optical path lengths. However, for longer delay times, such as 10 ns, a significant optical path difference of 3 m is required, which becomes challenging to implement at the laboratory level. Generally, optical delay control is suitable for delay times up to 1 ns. On the other hand, electrical delay control becomes more useful for delay times of 1 ns or longer. In electrical delay control, the oscillation timing of two synchronized lasers is adjusted to control the delay time (electrically delay control, **Fig. 2-4b**). The time range of a few nanoseconds is typically challenging to measure, but pump-probe spectroscopy utilizing a combination of both delay control methods can overcome this difficulty. The RIPT method and the method using a streak camera are also effective for measurements in this timescale.

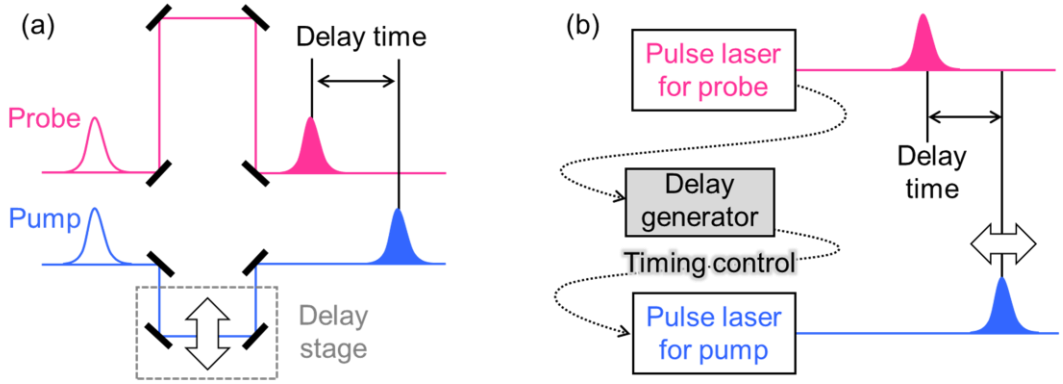

Figure 2-4 (a) Schematic diagram of delay time control by optical delay stage. (b) An example of electrical delay control system. In this system, the output signal of the laser for probe pulse is inserted into a delay generator to control the delay time and the output is used for control of oscillation timing of the laser for pump pulse.

References

1. Hamamatsu photonics. *Guide to Streak Cameras*. (2008).
2. Komura, M. & Itoh, S. Fluorescence measurement by a streak camera in a single-photon-counting mode. *Photosynthesis Research* **101**, 119–133 (2009).
3. Nakagawa, T., Okamoto, K., Hanada, H. & Katoh, R. Probing with randomly interleaved pulse train bridges the gap between ultrafast pump-probe and nanosecond flash photolysis. *Optics Letters* **41**, 1498 (2016).
4. Sumitani, M. & Yoshihara, K. Direct Observation of the Rate for Cis→Trans and Trans→Cis Photoisomerization of Stilbene with Picosecond Laser Photolysis. *Bulletin of the Chemical Society of Japan* **55**, 85–89 (1982).

Chapter 3.

Dual Energy Transfer Pathways from an Antenna Ligand to Lanthanide Ion in Trivalent Europium Complexes with Phosphine-Oxide Bridges

Shiori Miyazaki, Kiyoshi Miyata, Haruna Sakamoto, Fumiya Suzue, Yuichi Kitagawa, Yasuchika Hasegawa, and Ken Onda

The Journal of Physical Chemistry A **2020**, *124*, 33, 6601–6606.

Abstract

Trivalent europium (Eu(III)) complexes are attractive materials for luminescence applications if energy transfer from antenna ligands to the lanthanide ion is efficient. However, the microscopic mechanisms of the transfer remain elusive, and fundamental physical chemistry questions still require answers. We track the energy transfer processes in a luminescent complex $Eu(hfa)_3(DPPTO)_2$ (hfa: hexafluoroacetylacetonate, DPPTO: 2-diphenylphosphoryltriphenylene) using time-resolved photoluminescence spectroscopy (TR-PL). In addition to the conventional energy transfer pathway through the T_1 state of the ligands, we discovered fast energy transfer pathway directly from the singlet excited states of the ligands to the $^5D_1$ state of Eu(III). The short timescale of the energy transfer (3 ns, 200 ns) results in its high photoluminescence quantum yield. The discovery of the distinct energy transfer pathways from a single chromophore is important for establishing design strategies of luminescent complexes.

3-1 Introduction

Trivalent europium (Eu(III)) is attractive for luminescence applications because of its narrow line-width emission originating from a 4f-4f transition *(1-5)*. This narrow emission results from the screening by electronically occupied 5s/5p orbitals that isolate the 4f-4f transition from its environment. A primary challenge for the development of efficient phosphors based on Eu(III) materials is to overcome the small extinction coefficient ($\varepsilon < 10\ M^{-1}\ cm^{-1}$) of Eu(III). Approaches involving ligand engineering, to make luminescent Eu(III) complexes, are promising because of the controllability of the ligand fields of Eu(III) and enhancement of the photoluminescence quantum yield (PLQY), which result from antenna effects *(6-9)*.

Luminescent Eu(III) complexes have been mainly developed based on β-diketone ligands *(10)*. Recently, a phosphine oxide was found to be a suitable linker because of its small vibrational energy, which is beneficial for suppressing the non-radiative relaxation of Eu(III) *(11-15)*. Hasegawa and co-workers reported newly synthesized emissive Eu(III) complexes that were connected to antenna molecules using a phosphine-oxide linker *(6,7)*. However, the phosphine-oxide bridge can also be an isolator between the lanthanide ion and antenna molecules, which might prohibit efficient energy transfer from the antenna chromophores to Eu(III) *(16)*. Thus, gaining detailed information on the energy transfer and investigating the mechanistic reasons for an effective emission are extremely important.

Nevertheless, direct observation of the energy transfer dynamics is limited, and decent design strategies to make efficient Eu(III) complexes have not been established. The energy transfer is assumed to take place through the triplet excited state (T_1) of the antenna ligands *(17)*. This model actually works for several lanthanide complexes *(9,17-*

21). However, Yang *et al.* first observed the energy transfer dynamics in $[Eu(tta)_3]\cdot$dpbt complexes using time- and energy-resolved photoluminescence, and concluded that the energy transfer occurs from the singlet excited state (S_1) of the ligands *(22)*. Kasprzycka *et al.* recently proposed that energy transfer from the singlet excited states is also possible from the viewpoint of the energetics between the ligands and Eu(III) *(23)*. The detailed mechanisms of the energy transfer in Eu(III) complexes are still controversial.

Here, we focused on the $Eu(hfa)_3(DPPTO)_2$ (hfa: hexafluoroacetylacetonate, DPPTO: 2-diphenylphosphoryltriphenylene) complexes (**Fig. 3-1**), which show high PLQY (53%) *(7)* despite weak electronic couplings between the lanthanide ion and the antenna ligands through phosphine-oxide bridges, using time-resolved photoluminescence spectroscopy. We tracked the spectral change of the emission after optical excitation of antenna chromophores in the temporal range from sub-nanoseconds to hundreds of microseconds, which enabled us to thoroughly map out the dynamics of the energy flow in the complexes. We uncovered that the energy transfer from the antenna chromophore to Eu(III) takes place in less than a microsecond, despite the weak electronic coupling between the lanthanide ion and the antenna ligands. More importantly, the temporal changes of the emission spectra strongly suggested that the energy transfer pathway was not single: in addition to conventional energy transfer through the T_1 state of the ligands in ~200 ns, ultrafast energy transfer in ~3 ns was observed. The coexistence of the dual energy pathways is likely one of the origins of the high PLQY. The discovery has an important implication on the design strategies for the development of efficient energy transfer to maximize the antenna effect.

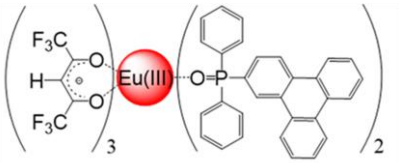

Figure 3-1 Chemical structure of $Eu(hfa)_3(DPPTO)_2$.

3-2 Experimental section

3-2-1 Sample preparation

$Eu(hfa)_3(DPPTO)_2$ was synthesized according to the reported procedure *(7)*. We prepared a solution of the complex in tetrahydrofuran (THF) purchased from Kanto Kagaku, Tokyo, Japan.

3-2-2 Time-resolved spectroscopy

TR-PL measurements were performed using a streak camera system (Hamamatsu C4780, time resolution: <30 ps) synchronized with a regenerative Ti:Sapphire amplifier (Spitfire Ace, ~120 fs, 1 kHz, 4 mJ/pulse, 800 nm). The samples were excited by the third harmonic of the fundamental pulse from the amplifier (267 nm). The polarization angles of the light for pumping/detection were set to the magic angle (54.7 deg) to avoid distortion of the temporal profiles from molecular orientation *(24)*. The excitation energy was kept to less than 0.8 mJ/cm^2. The concentration of the solutions was 1 mM.

3-3 Results and discussion

3-3-1 Assignment of absorption spectra

The absorption spectra of a solution of the complex $Eu(hfa)_3(DPPTO)_2$ and that of the ligand molecule DPPTO were almost identical in the region of 250–270 nm (**Fig. 3-2**), which indicated a weak electronic coupling between the lanthanide ion and the ligands. The strong absorption band spanning from 250 to 270 nm was mainly assigned to the S_0-S_n excitation of the triphenylene moiety in the ligands, whereas the shoulder observed at 300–340 nm mainly arose from hfa, as confirmed by the absorption spectrum of $Eu(hfa)_3(H_2O)_2$ *(7)*.

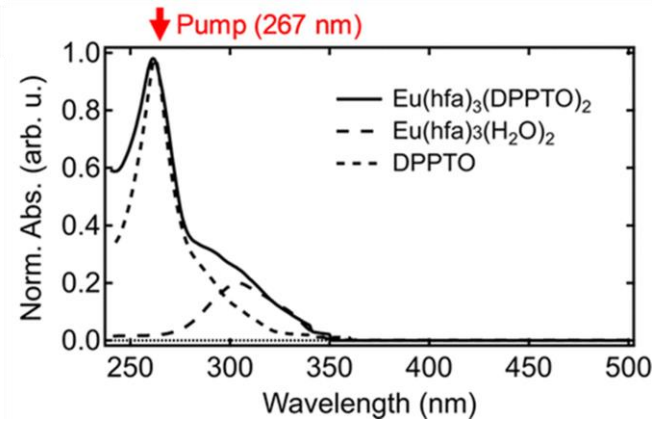

Figure 3-2 Absorption spectra of the solutions of the $Eu(hfa)_3(DPPTO)_2$ complex (solid line), the $Eu(hfa)_3(H_2O)_2$ complex (dotted line), and DPPTO (broken line). The arrow indicates the wavelength of the excitation pulse for our TR-PL measurements (267 nm).

3-3-2 Time-resolved photoluminescence spectroscopy

Fig. 3-3 shows the spectral evolution of the emission from $Eu(hfa)_3(DPPTO)_2$ in the solution after freeze-pump-thaw degassing. Immediately after the initial optical excitation of the triphenylene chromophore at 267 nm, a broad emission in the range from 360 to 500 nm was observed (**Fig. 3-3a, d**). This emission mainly originated in the fluorescence from the triphenylene (TPH) chromophores in the DPPTO ligands because the spectrum is much broader and higher in energy than that of the emission from Eu(III). As the emission of the ligands decays, the sharp emission from Eu(III) becomes dominant. All the observed bands correlate well to the diagram reported previously. The emission bands at 535, 555, and 585 nm, which manifested themselves in the time region of hundreds of nanoseconds (**Fig. 3-3b, e**), were assigned to the transitions of $^5D_1 \rightarrow {}^7F_1$, $^5D_1 \rightarrow {}^7F_2$, and $^5D_1 \rightarrow {}^7F_3$, respectively. The bands at 590 and 615 had the longest lifetime (**Fig. 3-3c, f**), and were assigned to $^5D_0 \rightarrow {}^7F_1$ and $^5D_0 \rightarrow {}^7F_2$, respectively. The most significant emission band at 615 nm was an electronic dipole allowed emission when

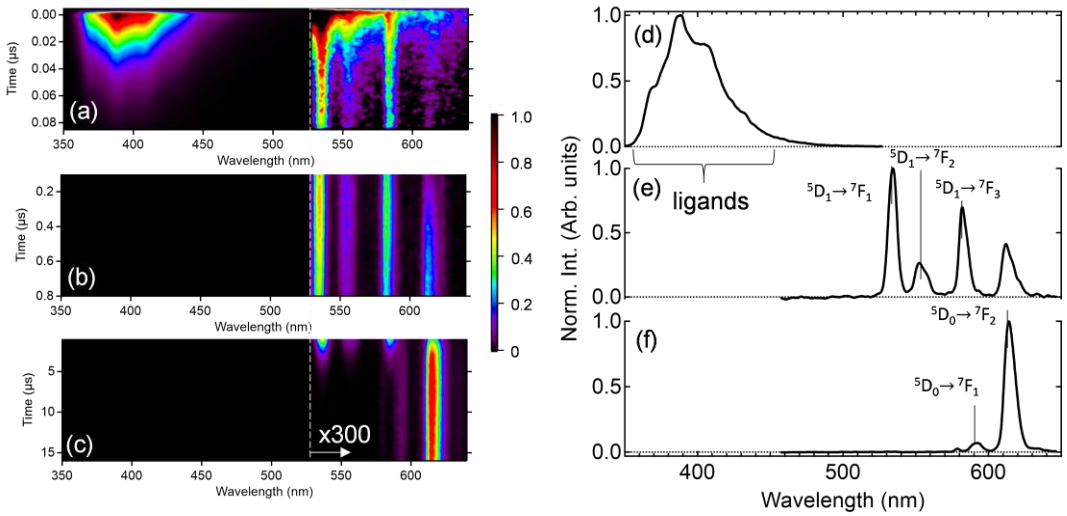

Figure 3-3 Pseudo-2D plot of spectral evolutions of the emission from an $Eu(hfa)_3(DPPTO)_2$/THF solution after optical excitation of triphenylene at 267 nm. (a) 0–0.08 μs, (b) 0.1–0.8 μs, and (c) 1–16 μs. The intensities above 530 nm are magnified by a factor of 300 for clarity. (d–f) Emission spectra at each delay time after optical excitation of triphenylene.

Eu(III) experienced an asymmetric field from the surrounding environment *(25, 26)*. The dominance of this band over the other emission bands implied the successful incorporation of an asymmetric field that made Eu(III) more emissive. Note that the emissions from $^5D_0$ were not significant at the beginning (<1 μs) but were dominant in the static emission spectrum *(7)* owing to its much longer lifetime than the other emissions from ligands or $^5D_1$. We succeeded in tracking the emission dynamics from the ligands to the lanthanide ion, by taking full advantage of the time- and spectrally-resolved emission measurements.

To investigate the dynamics of the energy transfer in $Eu(hfa)_3(DPPTO)_2$, we turned to the temporal change of the intensity of each emission (**Fig. 3-4**). The emission from the ligands at 490 nm decayed with two time constants of ~3 and ~20 ns (**Fig. 3-4a**), although the emission at 390 nm decayed with a single time constant of 20 ns (**Fig. 3-4d**). This implies that two different spectra with distinct lifetimes were overlapping in the region. In fact, the differential spectrum between the emission spectra in 0-2 and 50-80 ns showed a distinct spectral shape (**Fig. 3-4e**).

We also analyzed the emission using singular value decomposition (**Fig. 3-5a, b**) and global target analysis (**Fig. 3-5c-e**), confirming the existence of the distinct emission origin which has a shorter lifetime of ~3 ns and has a broader and redshifted spectrum (S_1') than the main component (S_1). The origin of the S_1' state is not necessarily clear at this point, but it could be another potential minimum in the singlet excited states or the excited states of the hfa ligands.

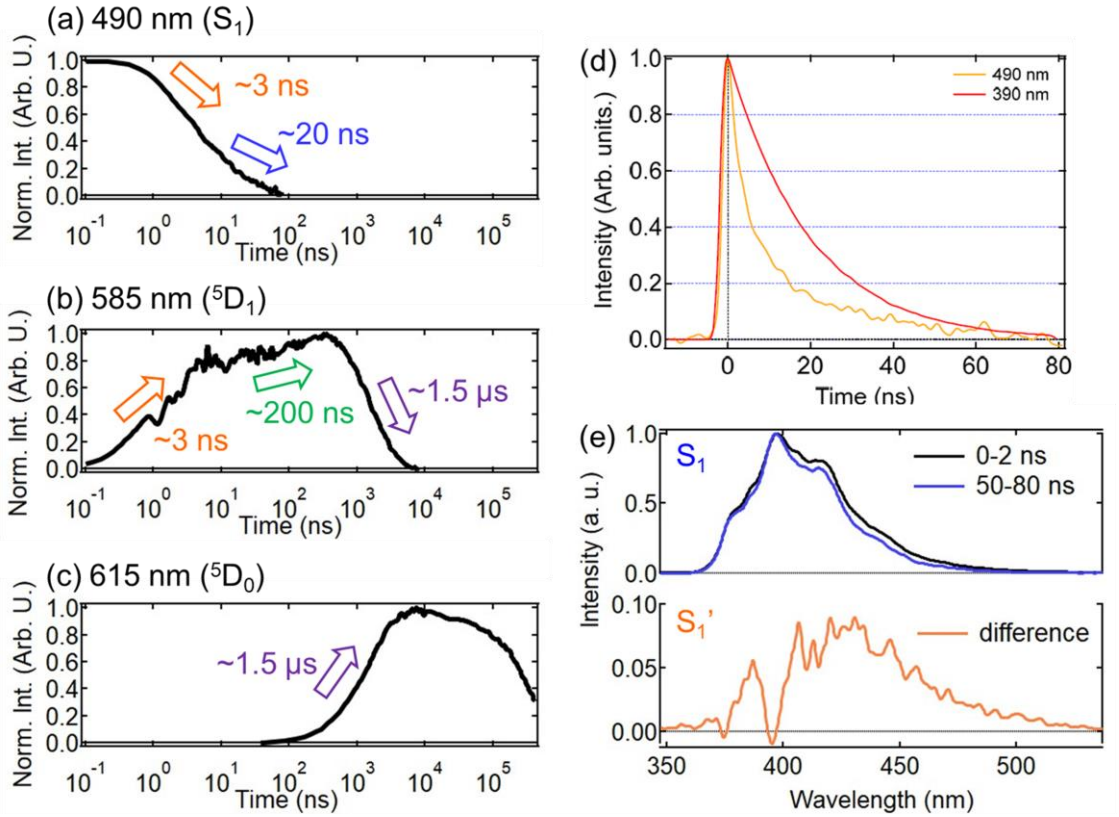

Figure 3-4 Temporal evolutions of the intensity of the emission from different origins. (a) The intensity of the emission at 490 nm which corresponds to fluorescence from ligands. (b) The intensity of the emission at 585 nm subtracted by the emission at 490 nm after normalization to extract the population kinetics of $^5D_1$. The increase of the emission clearly shows two time constants (3 and 200 ns). The time scale of the decay is 1.5 μs (c) The intensity of the emission at 615 nm, corresponding to the population kinetics of $^5D_0$, increases with a time constant of 1.5 μs. (d) The two time constants (3 and 20 ns) indicate two distinct emissions are overlapped (S_1 and S_1'). (e) Emission spectra in 0-2 and 50 - 80 ns. The differential spectrum corresponds to the emission from short lifetime component (S_1').

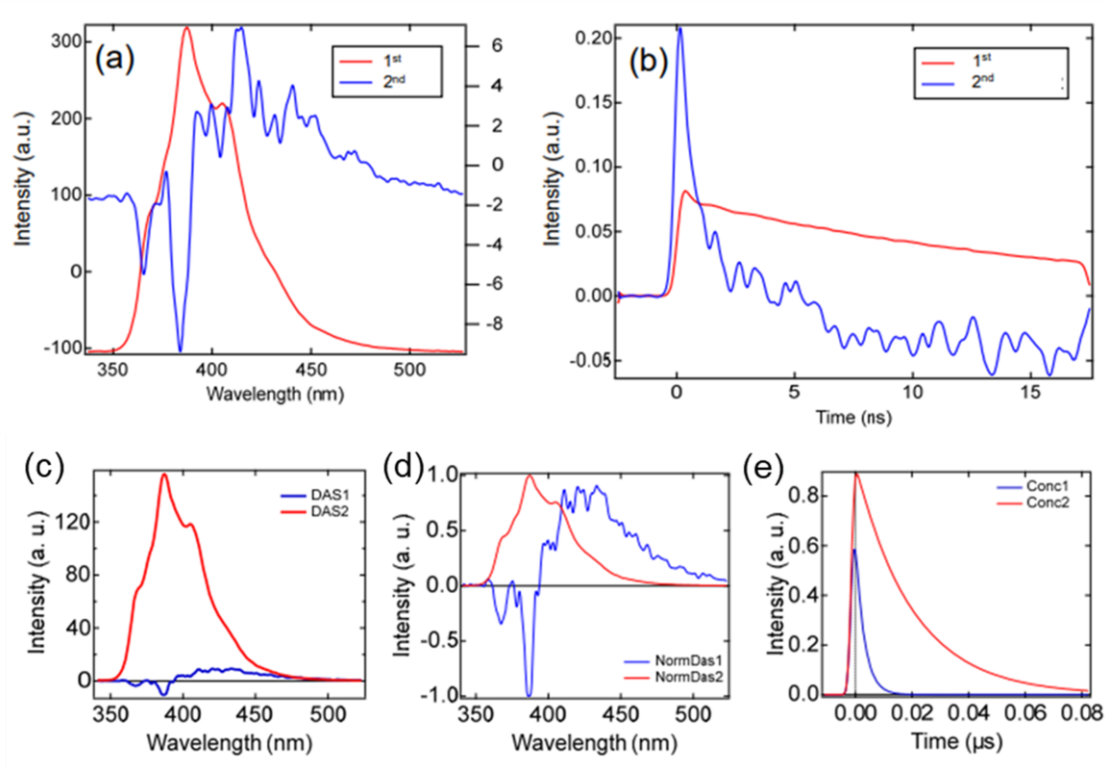

Figure 3-5 (a, b) The results of singular value decomposition analysis. Two major components are visualized. (a) Spectral components and (b) The temporal profiles of each component. The existence of broad and redshifted emission in short time scale (~3 ns) was indicated. (c-e) The results of global target analysis on the emission spectra from the ligands in <100 ns assuming two kinetic components. (c) Decay associated spectra, (d) normalized decay associated spectra, and (e) kinetic traces of the two components. The existence of broad and redshifted emission in short time scale (~3 ns) was further confirmed.

The dynamics of the emission assigned to the 4f-4f transition in the lanthanide ion is of great importance because it hints at the mechanisms of the ligand-to-metal energy transfer. The emission at 585 nm was mainly composed of the emission from $^5D_1$, which was a good indicator of the dynamics of the ligand-to-metal energy transfer. Because the emission at 585 nm contains the emission from S_1, we subtracted the temporal profile of the emission at 490 nm from that of 585 nm after normalization to discuss the population kinetics of $^5D_1$ independently. **Fig. 3-4b** shows the extracted kinetics of the $^5D_1$ state. The intensity increases with two distinct time constants of 3 and 200 ns, indicating the existence of two energy transfer pathways. Note that a significant amount of ultrafast energy transfer in 3 ns likely takes place from the S_1' state because the time constants coincide with each other. **Fig.3-4b** also shows the emission from $^5D_1$ decayed with a time constant of ~1.5 μs.

Concurrently, the intensity of the emission from the $^5D_0$ state increased with approximately the same time constant (**Fig. 3-4c**). This observation implied that (1) internal conversion from $^5D_1$ to $^5D_0$ occurs at ~1.5 μs and (2) the initial energy transfer from the ligands does not occur to $^5D_0$. Similar energy dynamics have also been reported for another trivalent europium complex previously *(22)*. Finally, the decay of the emission from $^5D_0$ was observed at ~700 μs, which was consistent with the previous reports and confirmed no degradation during the measurement.

3-3-3 Rate equation simulations using finite-difference time-domain methods (FDTD-RES).

The most intriguing dynamics are the mechanisms of the energy transfer from the ligands to the Eu(III). We analyzed the temporal change of the emission using a kinetic rate equation approach. We examined two distinct energy transfer models: the conventional energy transfer model, where the energy transfer to the central metal solely takes place from the T_1 state of the ligands (**Fig. 3-6a**), and the dual energy transfer model, where the energy transfer can take place from not only from T_1 but also from S_1' (**Fig. 3-6b**). We simulated the temporal population change based on kinetic rate equations analysis using the finite difference time domain method and compared the simulation to the observed population change to determine which model was consistent with the observation.

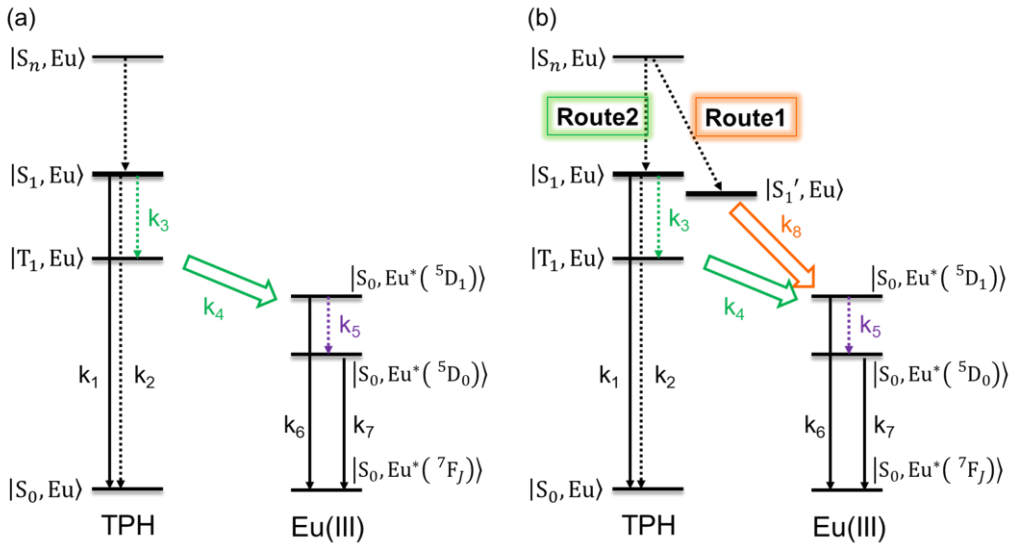

Figure 3-6 Jablonski diagrams of the two intramolecular energy transfer models examined by kinetic simulation. (a) Conventional Dexter energy transfer model where the energy transfer occurs via triplet excited states of the ligands. (b) The proposed dual energy transfer model where the energy transfers not only from the triplet excited state but also from another singlet excited state (S_1') of the ligands directly.

We constructed a set of kinetic equations from the models. For the Dexter energy transfer model, we obtain

$$\frac{\mathrm{d}}{\mathrm{d}t}D_{|\mathrm{S_1,Eu}\rangle}(t) = (k_1 + k_2 + k_3)D_{|\mathrm{S_1,Eu}\rangle}(t) \tag{3-1a}$$

$$\frac{\mathrm{d}}{\mathrm{d}t}D_{|\mathrm{T_1,Eu}\rangle}(t) = k_3 D_{|\mathrm{S_1,Eu}\rangle}(t) - k_4 D_{|\mathrm{T_1,Eu}\rangle}(t) \tag{3-1b}$$

$$\frac{\mathrm{d}}{\mathrm{d}t}D_{|\mathrm{S_0,Eu^*(\,^5D_1)}\rangle}(t) = k_4 D_{|\mathrm{T_1,Eu}\rangle}(t) - (k_5 + k_6)D_{|\mathrm{S_0,Eu^*(\,^5D_1)}\rangle}(t) \tag{3-1c}$$

$$\frac{\mathrm{d}}{\mathrm{d}t}D_{|\mathrm{S_0,Eu^*(\,^5D_0)}\rangle}(t) = k_5 D_{|\mathrm{S_0,Eu^*(^5D_1)>}}(t) - k_7 D_{|\mathrm{S_0,Eu^*(^5D_0)>}}(t), \tag{3-1d}$$

where $D_{|X\rangle}(t)$ is the population of a state *X* at *t*; k_i is the rate between corresponding transition *i* as described in the **Fig. 3-6**.

In order to analyze population kinetics using the above differential equations, we numerically simulated the temporal changes of the populations using finite-difference time-domain methods (FDTD). The equations 3-1a-d can be transformed to the finite difference representation as

$$D_{|\mathrm{S_1,Eu}\rangle}(t + \Delta t) = (k_1 + k_2 + k_3)D_{|\mathrm{S_1,Eu}\rangle}(t) \cdot \Delta t + D_{|\mathrm{S_1,Eu}\rangle}(t) \cdot \Delta t \tag{3-2a}$$

$$D_{|\mathrm{T_1,Eu}\rangle}(t + \Delta t) = \left\{k_3 D_{|\mathrm{S_1,Eu}\rangle}(t) - k_4 D_{|\mathrm{T_1,Eu}\rangle}(t)\right\} \cdot \Delta t + D_{|\mathrm{T_1,Eu}\rangle}(t) \cdot \Delta t \tag{3-2b}$$

$$\begin{aligned} D_{|\mathrm{S_0,Eu^*(\,^5D_1)}\rangle}(t) & \\ &= \left\{k_4 D_{|\mathrm{T_1,Eu}\rangle}(t) - (k_5 + k_6)D_{|\mathrm{S_0,Eu^*(\,^5D_1)}\rangle}(t)\right\} \cdot \Delta t \\ &+ D_{|\mathrm{S_0,Eu^*(\,^5D_1)}\rangle}(t) \cdot \Delta t \end{aligned} \tag{3-2c}$$

$$\begin{aligned} D_{|\mathrm{S_0,Eu^*(\,^5D_0)}\rangle}(t) & \\ &= \left\{k_5 D_{|\mathrm{S_0,Eu^*(^5D_1)>}}(t) - k_7 D_{|\mathrm{S_0,Eu^*(^5D_0)>}}(t)\right\} \cdot \Delta t \\ &+ D_{|\mathrm{S_0,Eu^*(\,^5D_0)}\rangle}(t) \cdot \Delta t \end{aligned} \tag{3-2d}$$

where Δt is the finite difference for time. The transformation allows us to simulate thorough temporal change of the populations under given set of kinetic parameters. We set $\Delta t = 0.1$ ns for the FDTD-RES, which is small enough to describe the population change we observed experimentally. We set $D_{|S_1,Eu\rangle}(t = 0) = 1$, and the populations of the other states at $t = 0$ as 0. We tried to achieve the best fitting between the kinetics simulation and the observed dynamics by tuning the rate constants.

First, we examined the conventional energy transfer model in which the energy transfer only through the T_1 state of the ligands (**Fig. 3-6a**). Because of the multiple and complex kinetics, we fitted the experimental data based on reasonable assumptions as follows. Judging from the dominant absorption coefficient of triphenylene moieties at 267 nm, we can safely assume that the initial excitation created the S_1 state in the ligands with almost unity. Because the excitation was localized to triphenylene moieties, we assumed the rates of the radiative decay (k_1), non-radiative decay (k_2), and intersystem crossing (k_3) were those obtained for triphenylene in a tetrahydrofuran (THF) solution *(25)*. Next, we tried to achieve the best fitting between the kinetics simulation and the observed dynamics by tuning the rest of the rate constants k_4–k_7 (**Fig. 3-7a-d, Table 3-1**), but ended up with the conclusion that the Dexter model cannot fully account for the experimental observation of the emission dynamics. In particular, there was a critical deviation in the fast generation of $^5D_1$ (**Fig. 3-7b**). The fundamental reason for this failure was because of the sequential population from S_1, to T_1, to $^5D_1$ (**Fig. 3-7e**), in which the delayed population of $^5D_1$ was unavoidable.

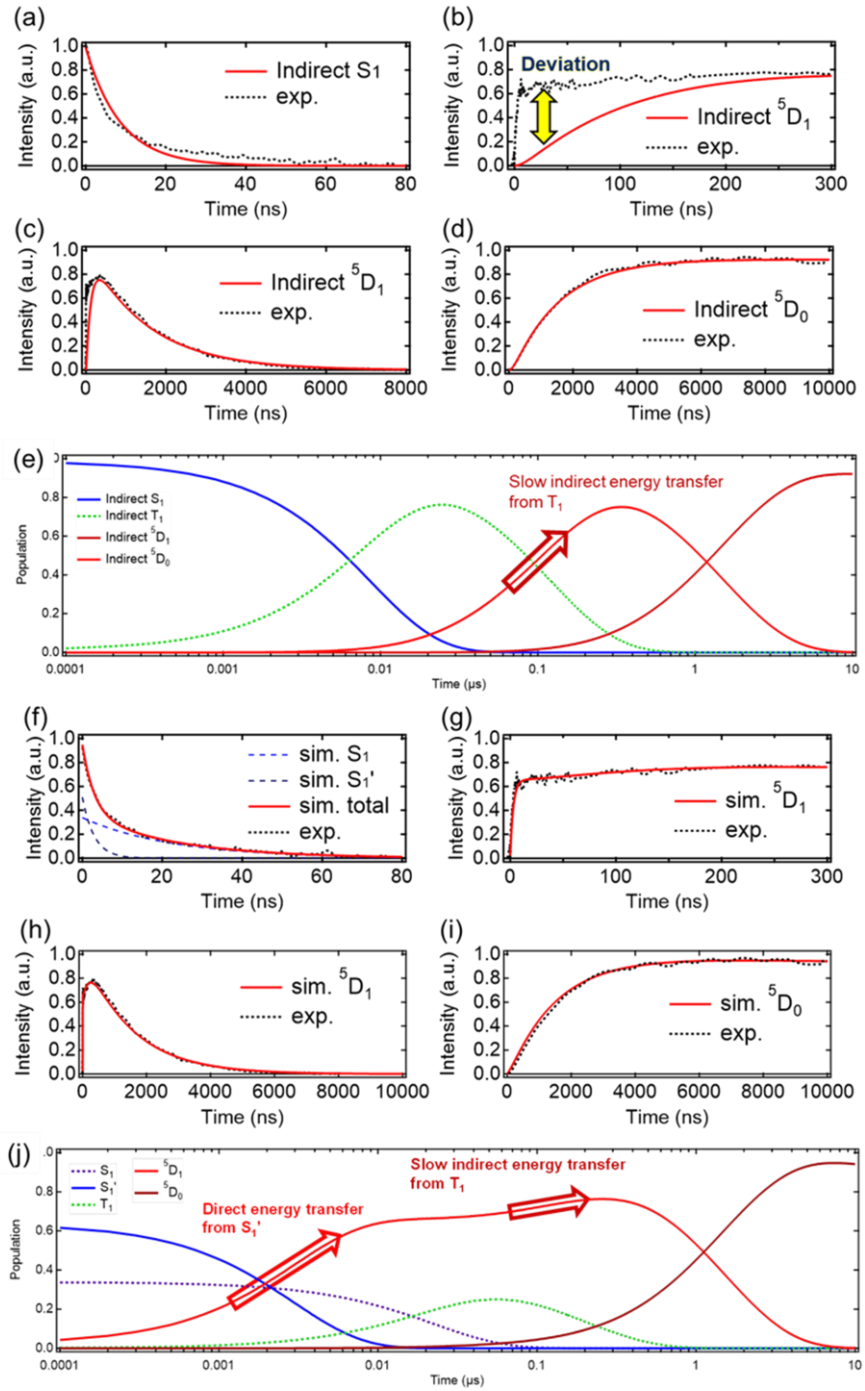

Figure 3-7 (a-e) Kinetic simulation of the conventional Dexter energy transfer model where the energy transfer occurs via triplet excited states of the ligands. (f-j) Proposed dual energy transfer model, where the energy transfers not only from the T_1 but also from the S_1 states of the ligands. (a-d, f-i) Comparison of experimental results and simulations regarding to the energy transfer from the ligands to the Eu(III). (e) Population dynamics from simulation. The slow energy transfer results in the failure of describing the quick generation of $^5D_1$. (f) Temporal changes of the excited states indicated from the kinetic simulation.

Table 3-1 The list of the rate constants employed in the fitting simulations.

Rate constants (μs^{-1})	k_1	k_2	k_3	k_4	k_5	k_6	k_7	k_8
Dexter ET model	7.4	0.0	106.7	8.3	0.66	1.4×10^{-3}	1.4×10^{-3}	
Dual ET model	3.3	0.0	46.7	5.0	0.7	1.4×10^{-3}	1.4×10^{-3}	333.0

The failure in the fitting of the fast population of $^5D_1$ using the conventional model motivated us to examine the model with an additional energy transfer pathway from the ligands: the dual energy transfer model from both S_1' and T_1 (**Fig. 3-6b**). Given the observation of the distinct singlet excited state, we can safely assume the existence of an additional energy level of S_1' and a rate constant (k_8) which represented rapid energy transfer from the S_1' to the $^5D_1$ state. By carefully fitting the experimental data with the rate constants, we were able to reproduce the experimental observation quantitatively (**Fig. 3-7f-i, Table 3-1**). The significant improvement resulted from the successful representation of the quicker population owing to energy transfer directly from the S_1' state (**Fig. 3-7j**). The branching ratio of the initial population between the S_1 and S_1' was estimated as S_1:S_1' = 42:58, based on the simulation and quantum efficiency of the complex. *(7)* From these comparisons, we concluded that the dual energy transfer from both the singlet and the triplet excited states took place in the phosphine oxide-bridged complex.

Even though the timescale of the energy transfer to Eu(III) was two-orders of magnitude slower than the recently reported time scale, *(21)* we emphasize that efficient energy transfer remained even with the stronger isolation owing to the phosphine-oxide. Because the T_1 of the ligands generally has a much longer lifetime, the isolation results in the benefit of the suppression of vibrational relaxation without losing the quantum yield

of sensitization.

The mechanisms of the energy transfer are of great importance and interest. Energy transfer from the S_1 state of ligands in Eu(III) complexes with β-diketone or tridentate ligands has been indicated in a previous report. *(22)* Our observation indicated that such fast energy transfer also occurs in a system that possesses weaker electronic coupling; in other words, that achieved with a phosphine oxide linker in between the ligands and the lanthanide ion. Although the intra-complex energy transfer tends to be assumed to occur through triplet excited states by Dexter energy transfer, a phosphine oxide linker acts as a spacer in between the chromophore that absorbs light, and the lanthanide ion. This separation results in a minimization of the overlap between molecular/atomic orbitals, which makes the short-range exchange process less effective and slow (~200 ns). Meanwhile, the strongest electric dipole allowed transition in the f-f transitions in Eu(III), $^7F_0$-$^5L_6$, is as high as the energy of the S_1 of the ligands, *(3)* which can serve as an energy acceptor state in the ligands-metal energy transfer via Förster-type mechanisms. Although quantitative analysis of the Förster energy transfer is not easy due to difficulties in predicting the oscillator strength and direction of the transition dipole moment of the acceptor transition ($^7F_0$-$^5L_6$), we anticipate that further controlled measurements on the Eu(III) complex derivatives with a different length between the antenna and the central metal or with different types of conjugation would uncover and manipulate the balance between two energy transfer pathways. In particular, the short-range Dexter energy transfer with electron exchange should be more sensitive to the length between the antenna and the central metal. We emphasize that such a coexistence of dual energy transfer with distinct time constants is unique and interesting from the viewpoint of physical chemistry. Such a unique situation might potentially be useful to

realize individual control of exciton flow of the singlet and triplet excited states, in complexes containing multiple central metals.

3-4 Conclusion

We observed the energy transfer dynamics in $Eu(hfa)_3(DPPTO)_2$ complexes after photoexcitation of the antenna moieties using TR-PL. We succeeded in unveiling the energy transfer dynamics from the ligands to the lanthanide ion. From a comparison of the emission dynamics of each excited state, we concluded that energy transfer takes place in less than a microsecond. Our in-depth analysis based on kinetic rate equations revealed that the energy transfer concurrently occurs from both the singlet and triplet excited states of the ligands to $^5D_1$ of the lanthanide ion with timescales of ~3 and ~200 nanoseconds, respectively, followed by much slower internal conversion at the central metal to finally populate $^5D_0$. While this kind of ligands-to-metal energy transfer in the trivalent lanthanide complexes is often assumed to take place through either the triplet or singlet excited state of ligands, we demonstrated that dual energy transfer takes place if Dexter and Förster energy transfers are balanced by a subtle change in the distance between the chromophore and Eu(III). The realization of dual energy transfer potentially opens a way for the drastic improvement of the efficiency of intramolecular energy transfer.

References

1. J. -C. G. Bünzli, On the design of highly luminescent lanthanide complexes. *Cood. Chem. Rev.* **293–294**, 19–47 (2015).
2. H. Xu, Q. Sun, Z. An, Y. Wei, X. Liu, Electroluminescence from Europium(III) Complexes. *Coord. Chem. Rev.* **293–294**, 228– 249 (2015).
3. K. Binnemans, Interpretation of Europium(III) Spectra. *Cood. Chem. Rev.* **295**, 1–45 (2015).
4. L. D. Carlos, R. A. S. Ferreira, V. De Zea Bermudez, S. J. L. Ribeiro, Lanthanide-Containing Light-Emitting Organic-Inorganic Hybrids: A Bet on the Future. *Adv. Mater.* **21**, 509– 534 (2009).
5. A. De Bettencourt-Dias, Lanthanide-Based Emitting Materials in Light-Emitting Diodes. *Dalt. Trans.* **22**, 2229– 2241 (2007).
6. Y. Kitagawa, R. Ohno, T. Nakanishi, K. Fushimi, Y. Hasegawa, Visible Luminescent Lanthanide Ions and a Large π-Conjugated Ligand System Shake Hands. *Phys. Chem. Chem. Phys.* **18**, 31012– 31016 (2016)
7. Y. Kitagawa, F. Suzue, T. Nakanishi, K. Fushimi, Y. Hasegawa, A Highly Luminescent Eu(III) Complex Based on an Electronically Isolated Aromatic Ring System with Ultralong Lifetime. *Dalt. Trans.* **47**, 7327– 7332 (2018).
8. K. Miyata, Y. Konno, T. Nakanishi, A. Kobayashi, M. Kato, K. Fushimi, Y. Hasegawa, Chameleon Luminophore for Sensing Temperatures: Control of Metal-to-Metal and Energy Back Transfer in Lanthanide Coordination Polymers. *Angew. Chem., Int. Ed.* **52**, 6413– 6416 (2013).
9. M. Hasegawa, A. Ishii, S. Kishi, Picosecond Time-Resolved Luminescence of Pr(III) Complexes: Intramolecular Excitation Energy Transfer from Ligand to Pr(III). *J. Photochem. Photobiol. A* **178**, 220– 224 (2006).
10. N. Filipescu, W. F. Sager, F. A. Serafin, Substituent Effects on Intramolecular Energy Transfer. II. Fluorescence Spectra of Europium and Terbium β-Diketone Chelates. *J. Phys. Chem.* **68**, 3324– 3346 (1964).
11. K. Miyata, T. Nakagawa, R. Kawakami, Y. Kita, K. Sugimoto, T. Nakashima, T. Harada, T. Kawai, Y. Hasegawa, Remarkable Luminescence Properties of Lanthanide Complexes with Asymmetric Dodecahedron Structures. *Chem. - Eur. J.* **17**, 521– 528 (2011).
12. Y. Hirai, T. Nakanishi, Y. Kitagawa, K. Fushimi, T. Seki, H. Ito, Y. Hasegawa, Luminescent Europium(III) Coordination Zippers Linked with Thiophene-Based Bridges. *Angew. Chem., Int. Ed.* **55**, 12059– 12062 (2016).

13. N. B. D. Lima, S. M. C. Gonçalves, S. A. Júnior, A. M. A. Simas, Comprehensive Strategy to Boost the Quantum Yield of Luminescence of Europium Complexes. *Sci. Rep.* **3**, 1– 8 (2013).
14. M. Congiu, M. Alamiry, O. Moudam, S. Ciorba, P. R. Richardson, L. Maron, A. C. Jones, B. S. Richards, N. Robertson, Preparation and Photophysical Studies of [Ln(Hfac)$_3$DPEPO], Ln = Eu, Tb, Yb, Nd, Gd; Interpretation of Total Photoluminescence Quantum Yields. *Dalt. Trans.* **42**, 13537– 13545 (2013).
15. E. E. S. Teotonio, G. M. Fett, H. F. Brito, W. M. Faustino, G. F. de Sá, M. C. F. C. Felinto, R. H. A. Santos, Evaluation of Intramolecular Energy Transfer Process in the Lanthanide(III) Bis- and Tris-(TTA) Complexes: Photoluminescent and Triboluminescent Behavior. *J. Lumin.* 128, 190– 198 (2008).
16. J. H. S. K. Monteiro, A. De Bettencourt-Dias, F. A. Sigoli, Estimating the Donor-Acceptor Distance to Tune the Emission Efficiency of Luminescent Lanthanide Compounds. *Inorg. Chem.* **56**, 709– 712 (2017).
17. M. Latva, H. Takalo, V-M. Mukkala, C. Matachescu, J. C. Rodriguez-Ubisd, J. Kankarea, Correlation between the Lowest Triplet State Energy Level of the Ligand and Lanthanide(III) Luminescence Quantum Yield. *J. Lumin.* **75**, 149– 169 (1997).
18. S. Sato, M. Wada, Relations between Intramolecular Energy Transfer Efficiencies and Triplet State Energies in Rare Earth β-Diketone Chelates. *Bull. Chem. Soc. Jpn.* 43, 1955– 1962 (1970).
19. N. M. Shavaleev, S. V. Eliseeva, R. Scopelliti, J. -C. G. Bünzli, Designing Simple Tridentate Ligands for Highly Luminescent Europium Complexes. *Chem. - Eur. J.* **15**, 10790– 10802 (2009).
20. N. M. Shavaleev, S. V. Eliseeva, R. Scopelliti, J. -C. G. Bünzli, Aryl Chromophore Ligands for Bright Europium Luminescence. *Inorg. Chem.* **49**, 3927– 3936 (2010).
21. M. W. Mara, D. S. Tatum, A. March, G. Doumy, E. G. Moore, K. N. Raymond, Energy Transfer from Antenna Ligand to Europium(III) Followed Using Ultrafast Optical and X-Ray Spectroscopy. *J. Am. Chem. Soc.* 141, 11071– 11081 (2019).
22. C. Yang, L. M. Fu, Y. Wang, J. P. Zhang, W. T. Wong, X. C. Ai, Y. F. Qiao, B. S. Zou, L. L. Gui, A Highly Luminescent Europium Complex Showing Visible-Light-Sensitized Red Emission: Direct Observation of the Singlet Pathway. *Angew. Chem., Int. Ed.* 43, 5010– 5013 (2004).
23. E. Kasprzycka, V. A. Trush, V. M. Amirkhanov, L. Jerzykiewicz, O. L. Malta, J. Legendziewicz, P. Gawryszewska, Contribution of Energy Transfer from the Singlet State to the Sensitization of Eu^{3+} and Tb^{3+} Luminescence by Sulfonylamidophosphates. *Chem. - Eur. J.* **23**, 1318– 1330 (2017).

24. R. D. Spencer, G. Weber, Influence of Brownian rotations and energy transfer upon the measurements of fluorescence lifetime. *J. Chem. Phys.* 52, 1654– 1663 (1970).
25. B. R. Judd, Optical Absorption Intensities of Rare-Earth Ions. *Phys. Rev.* **127**, 750–761 (1962).
26. G. S. Ofelt, Structure of the F6configuration with Application to Rare-Earth Ions. *J. Chem. Phys.* **38**, 2171– 2180 (1963).
27. J. W. Levell, A. Ruseckas, J. B. Henry, Y. Wang, A. D. Stretton, A. R. Mount, T. H. Galow, I. D. W. Samuel, Fluorescence Enhancement by Symmetry Breaking in a Twisted Triphenylene Derivative. *J. Phys. Chem. A* 114, 13291– 13295 (2010).

Chapter 4.

Novel Energy Transfer Pathway in Trivalent Europium Complexes with β-Diketonate Ligands

(*Manuscript in preparation*)

Abstract

Trivalent europium (Eu(III)) complexes exhibit sharp emission and long luminescence lifetimes, making them attractive for light-emitting applications. To achieve high emission efficiency, efficient intramolecular energy transfer from antenna ligands to Eu(III) ions is crucial. In this study, we investigated the energy transfer mechanism in $Eu(hfa)_3(TPPO)_2$ (hfa: hexafluoroacetylacetonate, TPPO: triphenylphosphine oxide) complex using time-resolved photoluminescence spectroscopy and femtosecond transient absorption spectroscopy. Our experimental results demonstrated a near unity efficiency of energy transfer from the T_1 state of β-diketonate ligands to the Eu(III) ions, unveiling a novel pathway to the $^5D_2$ state of the Eu(III) ion. This discovery holds important implications for the design strategies aiming to maximize the emission efficiency of Eu(III) complexes with β-diketonate ligands. These insights contribute to establishing efficient luminescent Eu(III) complexes and advancing the development of lanthanide-based light-emitting materials.

4-1 Introduction

Trivalent europium (Eu(III)) complexes have attracted attention as light-emitting materials such as displays and sensors because of their high color purity *(1-4)*. The emission of Eu(III) complex is almost the same as that of the central Eu(III) ion because the emission of Eu(III) ion is ascribed to 4f-4f transitions shielded by 5s and 5p orbitals and it is hardly affected by the ligands *(5,6)*. Nevertheless, the absorption coefficient of the Eu(III) ion is very low ($\varepsilon < 10\ M^{-1}\ cm^{-1}$); thus, the Eu(III) complexes utilize the energy transfer from antenna ligands to a metal center. The photoluminescence (PL) of Eu(III) complexes relies on photosensitization from antenna ligands. The overall PL quantum yield (ϕ_{tot}) of a Eu(III) complex is expressed as

$$\phi_{\mathrm{tot}} = \eta_{\mathrm{sens}} \times \phi_{\mathrm{Eu}} \tag{4-1}$$

where η_{sens} and ϕ_{Eu} represent the overall photosensitization efficiency and the quantum yield of Eu(III) luminescence, respectively. Because η_{sens} is governed by the energy transfer efficiency from ligands, it is necessary to improve the energy transfer efficiency for achieving high ϕ_{tot}.

Two significant energy transfer mechanisms are commonly considered: energy transfer from ligand singlet state or ligand triplet state. Both energy transfer mechanisms have been reported qualitatively. Many researchers have developed antenna ligands based on T_1 energy to improve energy transfer efficiency, which has been successful for several lanthanide complexes *(7–10)*. Contrary, the energy transfer pathway from the ligand S_1 state has been proposed in a few Eu(III) complexes *(11,12)*. However, the detailed mechanism and quantum yield of the energy transfer for the Eu(III) complex has not yet been demonstrated because of the difficulty of the direct observation.

Moreover, the energy-accepting states of the Eu(III) ion depend on the respective

energies of the sensitizer ligand. In the case of the Eu(III) complexes, the accepting state is $^5D_1$ or $^5D_0$ state of a Eu(III) ion. However, there is only a little evidence of the exact energy-accepting states. Yang *et al.* firstly reported energy transfer directly from the aniline ligands to the $^5D_1$ state *(13)*. We also reported the dual energy transfer after photoexcitation of triphenylene ligands to the $^5D_1$ state *(14)*. In order to optimize the energy transfer efficiency, it is crucial to understand the energy transfer mechanism in terms of not only the energy level of the ligand T_1 state but also the energy-accepting state of the Eu(III) ion.

The energy transfer mechanism is influenced by the energy levels of the ligands and the coordination geometry. Although theoretical studies have provided insight into the mechanisms of energy transfer (*15–20*), there are very few experimental demonstrations or quantitative evaluations of energy transfer. Mara *et al.* revealed that the importance of the quantum yields of the intersystem crossing (ISC) of the sensitizer ligands to suppress the energy loss in the sensitization process *(21)*. We demonstrated the enhancement of sensitization efficiency by improving the quantum yields of the ISC in the host-guest system *(22)*. Since these are the only observed examples of energy transfer and ligand design based on energy levels is common, no design strategies for Eu(III) complexes based on energy transfer mechanisms have been established.

In this study, we investigate the $Eu(hfa)_3(TPPO)_2$ (hfa: hexafluoroacetylacetonate, TPPO: triphenylphosphine oxide) complex (**Fig. 4-1**) containing a phosphine oxide linker and hfa ligands, which commonly used in Eu(III) complexes *(23–31)*. We employed time-resolved photoluminescence spectroscopy (TR-PL) and femtosecond transient absorption spectroscopy (fs-TAS) in a multiscale temporal range from sub-picoseconds to hundreds of microseconds to investigate ligand-to-metal

energy transfer mechanism of $Eu(hfa)_3(TPPO)_2$. The combination of TR-PL and fs-TAS enable us to elucidate the overall energy transfer dynamics and quantum yields, building upon our previous report *(22)*. Our observations revealed a near unity efficiency of intramolecular energy transfer from the T_1 state of the β-diketonate ligands (hfa) to the $^5D_2$ state of the Eu(III) ion. Additionally, we successfully unveiled the complete energy transfer pathway of $Eu(hfa)_3(DPPTO)_2$ we previously reported *(14)*. Importantly, this study presents the first experimental observation of energy transfer to the $^5D_2$ state of the Eu(III) ion. These findings have significant implications for the design strategies aimed at maximizing Eu(III) emission in Eu(III) complexes with β-diketonate ligands.

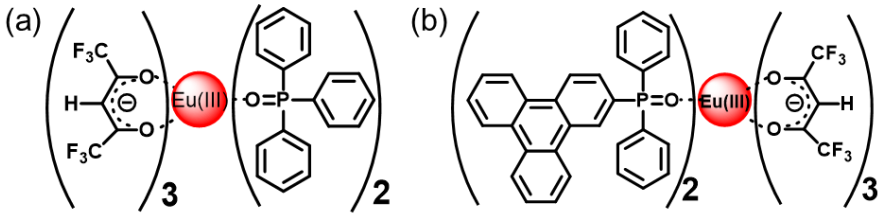

Figure 4-1 Molecular structure of (a) $Eu(hfa)_3(TPPO)_2$. (b) $Eu(hfa)_3(DPPTO)_2$.

4-2 Experimental section

4-2-1 Sample preparation

$Eu(hfa)_3(TPPO)_2$ was synthesized according to the reported procedure *(31)*. We prepared a solution of the complex in chloroform purchased from Kanto Kagaku, Tokyo, Japan. The all solution was Ar degassed.

4-2-2 Time-resolved photoluminescence (TR-PL) measurements

TR-PL measurements were performed using a streak camera system (Hamamatsu C4780, time resolution <30 ps) synchronized with a Ti:sapphire regenerative amplifier (Spectra-Physics, Spitfire Ace, pulse duration = 120 fs, repetition rate = 1 kHz, pulse energy = 4 mJ/pulse, central wavelength = 800 nm). Fourth harmonic generation of signal light from OPA seeded by the Ti:Sapphire femtosecond laser (315 nm). The polarization angles of the light for pumping/detection were set to the magic angle (54.7 deg) to avoid distortion of the temporal profiles from molecular orientation *(32)*. The excitation energy was kept to less than 0.8 mJ/cm^2. The concentration of the solutions was 1 mM.

4-2-3 Femtosecond transient absorption spectroscopy (fs-TAS)

Transient absorption (TA) measurements were conducted using the pump-probe method *(33)*. The light source was a Ti:sapphire regenerative amplifier system (Spectra-Physics, Spitfire Ace, pulse duration = 120 fs, repetition rate = 1 kHz, pulse energy = 4 mJ/pulse, central wavelength = 800 nm) seeded by a Ti:sapphire femtosecond mode-locked laser (Spectra-Physics, Tsunami). The output of the amplifier was divided into two pulses for the pump and probe. Fourth harmonic generation of signal light from OPA

seeded by the Ti:Sapphire femtosecond laser (315 nm). The broadband probe pulse (470–680 nm) was generated using a sapphire crystal of 1 mm thickness. The pump and probe pulse beam sizes at the sample position were <0.7 mmϕ and <0.5 mmϕ, respectively. A PC-controlled mechanical delay state was used to adjust the delay time between the pump and probe pulses. The probe pulse that passed through the sample films was dispersed by a polychromator (JASCO, CT-10, 300 grooves/500 nm), and the spectra were captured using a multichannel detection system with a CMOS sensor (UNISOKU, USP-PSMM-NP). The excitation energy was kept to less than 0.4 mJ/cm^2. The recorded data was analyzed using a Python-based homemade program.

4-2-4 Measurement of photoluminescence properties

The photoluminescence quantum yields were measured using a Hamamatsu Photonics Quantaurus-QY instrument equipped with an integrating sphere. A time-correlated single-photon counting lifetime spectroscopy system (HAMAMATSU Quantaurus-Tau C11367-21, C11567-02, and M12977-01) was used to PL measure lifetimes.

4-3 Results and discussion

4-3-1 Sensitization efficiency of $Eu(hfa)_3(TPPO)_2$

We investigated the sensitization ability of the antenna ligands by examining the luminescence properties of $Eu(hfa)_3(TPPO)_2$. The absorption spectra of the complex $Eu(hfa)_3(TPPO)_2$ and the ligand molecule TPPO are shown in **Fig. 4-2a**. The strong absorption band ranging from 280 to 340 nm was attributed to the S_0-S_n excitation of the hfa ligands, while the weak absorption observed at 250–270 nm mainly originated from TPPO. Upon photoexcitation of $Eu(hfa)_3(TPPO)_2$ with 315 nm light, Eu(III) emission bands were observed (**Fig. 4-2b**), corresponding to transitions from $^5D_0$ to $^7F_0$, $^7F_1$, $^7F_2$, $^7F_3$, and $^7F_4$ at wavelengths of 581, 594, 616, 654, and 701 nm, respectively. The most significant emission band at 615 nm was an electronic dipole allowed emission when Eu(III) experienced an asymmetric field from its surrounding environment *(34,35)*. The selective excitation of the hfa ligands at 315 nm confirmed the sensitization of the Eu(III) ion by these ligands in $Eu(hfa)_3(TPPO)_2$.

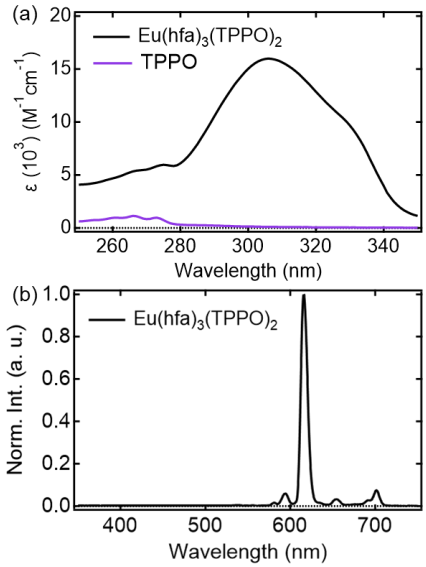

Figure 4-2 (a) Absorption spectra of the $Eu(hfa)_3(TPPO)_2$ (black line) and TPPO (purple line). (b) Emission spectra of the $Eu(hfa)_3(TPPO)_2$.

The sensitization efficiency of $Eu(hfa)_3(TPPO)_2$ was qualitatively discussed based on the luminescence spectra of Eu(III). The photophysical properties of $Eu(hfa)_3(TPPO)_2$ in $CHCl_3$ are summarized in **Table 4-1**. Firstly, we estimated the luminescence quantum yield of the Eu(III) ion (ϕ_{Eu}) in $Eu(hfa)_3(TPPO)_2$. The natural

radiative rate constant of the Eu(III) ion (k_r) was calculated from the ratio of the total Eu(III) ion transition to the magnetic dipole transition ($^5D_0 \rightarrow {}^7F_1$) in the observed emission spectrum *(36)*. The non-radiative rate constant (k_{nr}) was determined by the ratio of k_r to the observed decay rate constant of the $^5D_0$ state (τ_{obs}). The estimated ϕ_{Eu} value of 0.76 was attributed to a large radiative rate constant (960 s^{-1}) and a small non-radiative rate constant (310 s^{-1}), consistent with previous reports *(30)*. The overall PL quantum yield excited by the hfa ligands (ϕ_{tot}) and the sensitization efficiency (η_{sens}) of $Eu(hfa)_3(TPPO)_2$ were estimated to be 0.51 and 0.67, respectively.

Table 4-1 Optical properties of $Eu(hfa)_3(TPPO)_2$ in $CHCl_3$. The lifetime of the $^5D_0$ state (τ_{obs}) are determined by the lifetime at 615 nm (λ_{ex} = 315 nm). I_{tot}/I_{MD} is the ratio of the total area of the Eu(III) luminescence spectrum to the area of the $^5D_0 \rightarrow {}^7F_1$ transition band. Here, k_r, k_{nr}, ϕ_{Eu}, ϕ_{tot} and η_{sens} represent radiative rate constant of Eu(III) ions, non-radiative rate constant of Eu(III) ions, luminescence quantum yield of Eu(III) ions, total photoluminescence quantum yield, and overall photosensitization efficiency, respectively.

	I_{tot}/I_{MD}	τ_{obs}/ms	k_r/s^{-1}	k_{nr}/s^{-1}	ϕ_{Eu}	ϕ_{tot}	η_{sens}
$Eu(hfa)_3(TPPO)_2$	22	0.79	960	300	0.76	0.51	0.67

4-3-2 Initial process after photoexcitation of hfa ligands

To identify the factors contributing to the sensitization efficiency (η_{sens}), we investigated the efficiency of each energy transfer process. We performed fs-TAS on $Eu(hfa)_3(TPPO)_2$ to analyze the excited state dynamics of the hfa ligands following photoexcitation (**Fig. 4-3a-d**). The absorbance change (ΔAbs.) of the $Eu(hfa)_3(TPPO)_2$ solution exhibited an increase in the <550 nm range and a decrease in the >550 nm range. By conducting a global analysis of the fs-TAS spectra using a sequential model with two components *(37)*, we observed a conversion from the first component to the second component with a time constant of 3.8 ± 0.1 ps (**Fig. 4-3b**). The evolution associated spectra (EAS) and concentration kinetics of the two components are shown in **Fig. 4-3c, d**, respectively.

To assign the observed species, we also analyzed the fs-TAS of $Gd(hfa)_3(TPPO)_2$ in a similar way (**Fig. 4-3e-h**). The global analysis also resulted in similar EASs (**Fig. 4-3c, g**) with a time constant of 2.5 ± 0.01 ps (**Fig. 4-3f**). The two EAS components were reasonably assigned to the singlet excited state (S_1) and the lowest triplet excited state (T_1) of the hfa ligands in the case of $Gd(hfa)_3(TPPO)_2$, and the time constant represented the ISC rate. Therefore, the two components observed in the $Eu(hfa)_3(TPPO)_2$ solution were assigned to S_1 and T_1 of the hfa ligands. The rapid time constants observed can be attributed to the heavy metal effects of the lanthanide ion, which accelerate the ISC rate. Notably, the T_1 lifetime in $Eu(hfa)_3(TPPO)_2$, estimated from fs-TAS, was much shorter (68.5 ± 0.3 ps) compared to the T_1 lifetime in $Gd(hfa)_3(TPPO)_2$ estimated from TR-PL measurements (**Fig. 4-4**, 4.1 ± 0.01 μs). The short T_1 lifetime in the Eu(III) complex suggests rapid depopulation of the T_1 state via intramolecular energy transfer to the Eu(III) ion, which is absent in $Gd(hfa)_3(TPPO)_2$ (**Fig. 4-5**).

We concluded that the intramolecular energy transfer from the T_1 state of the hfa ligands to the Eu(III) ion occurs within approximately 69 ps. This time constant is extremely faster than that observed in $Eu(hfa)_3(DPPTO)_2$, which we previously reported (~200 ns) *(14)*. $Eu(hfa)_3(DPPTO)_2$ possesses a phosphine-oxide linker between the antenna chromophore DPPTO and the Eu(III) ion, whereas in $Eu(hfa)_3(TPPO)_2$, the antenna chromophore hfa is directly connected to the Eu(III) ion *(38)*. The shorter distance between the antenna chromophore and the Eu(III) ion in $Eu(hfa)_3(TPPO)_2$ is the reason for the observed fast energy transfer.

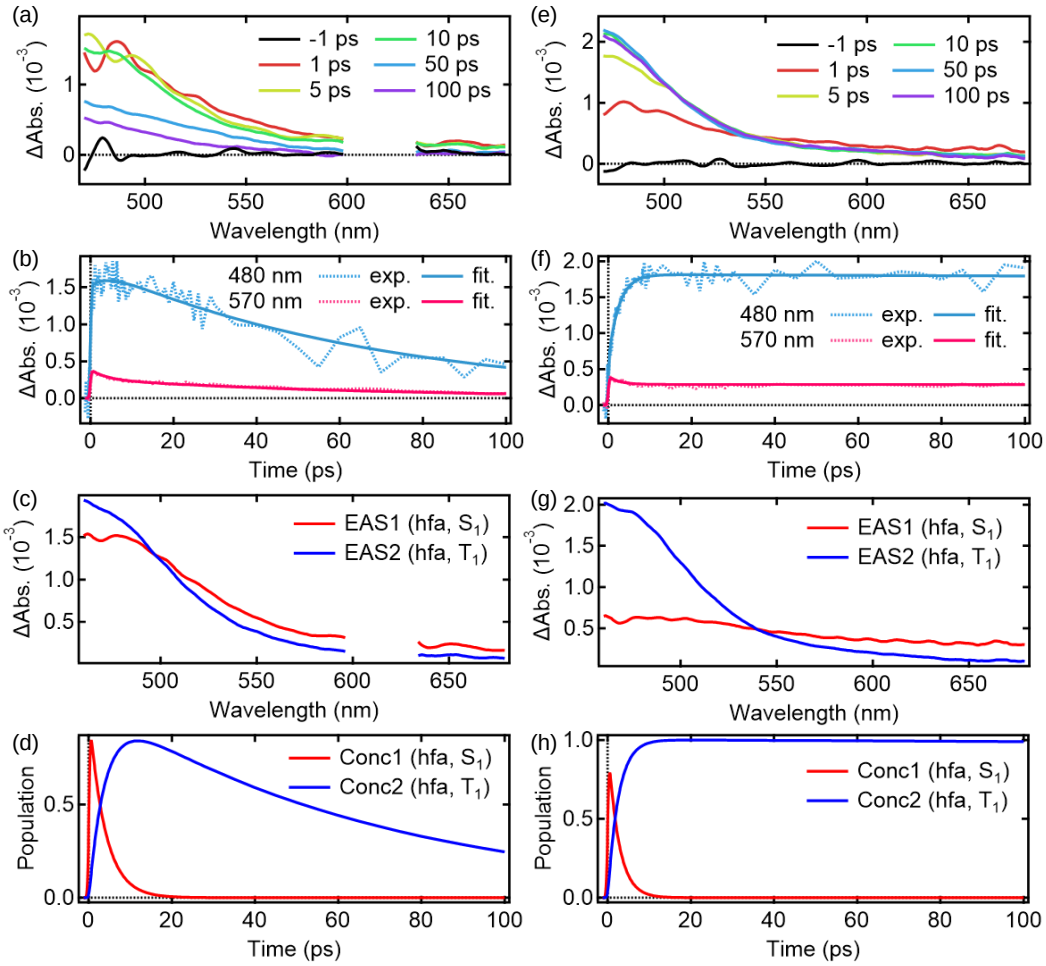

Figure 4-3 fs-TAS spectra and the results of their global analysis in $CHCl_3$ solution of (a–d) $Eu(hfa)_3(TPPO)_2$ and (e–h) $Gd(hfa)_3(TPPO)_2$. (a, e) Temporal evolutions of the fs-TAS spectra after photoexcitation at 315 nm. (b, f) Temporal profiles of the fs-TAS spectra at 480 nm (blue dotted line) and 570 nm (pink dotted line) and corresponding fitting curves resulted from the global analysis. (c, g) EAS. (d, h) Corresponding concentration kinetics were obtained from the global analysis. No TA data was available in the $Eu(hfa)_3(TPPO)_2$ solution due to the strong emission from Eu(III) ion in the region neighboring 615 nm.

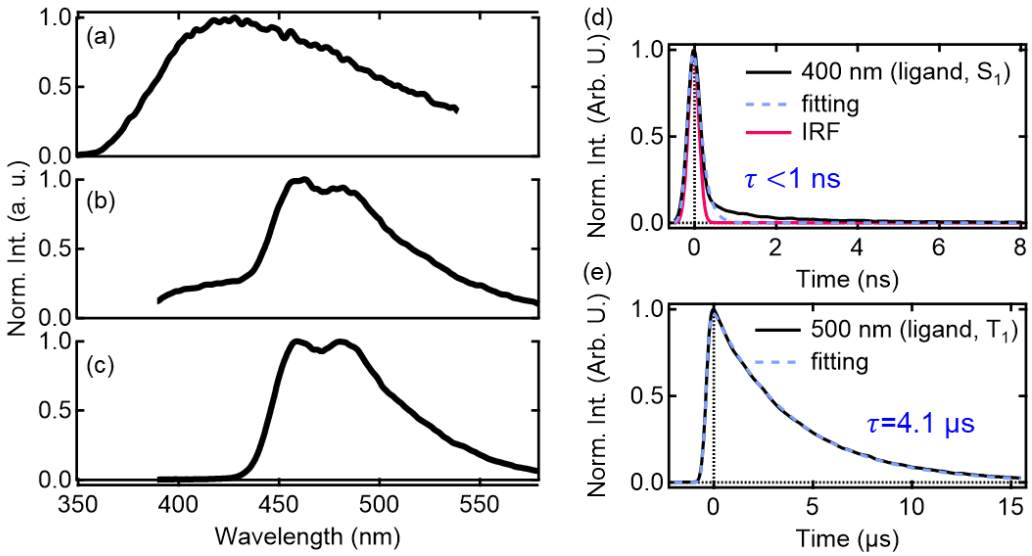

Figure 4-4 TR-PL spectra and their temporal profiles from the $Gd(hfa)_3(TPPO)_2$ solution. (a–c) Emission spectra at each delay time after optical excitation of hfa ligands at 315 nm by the time integration of (a) 0–1 ns, (b) 80–100 ns, and (c) 5–10 μs. (d) Temporal profile at 400 nm (black solid line), which is assigned to the fluorescence from the hfa ligands, and fitting curve assuming a single exponential decay (sky blue dashed line), and instrumental response function (IRF, pink solid line). (e) Temporal profile at 500 nm (black solid line), which is assigned to the phosphorescence from the hfa ligands, and a fitting curve assuming a single exponential decay (sky blue dashed line).

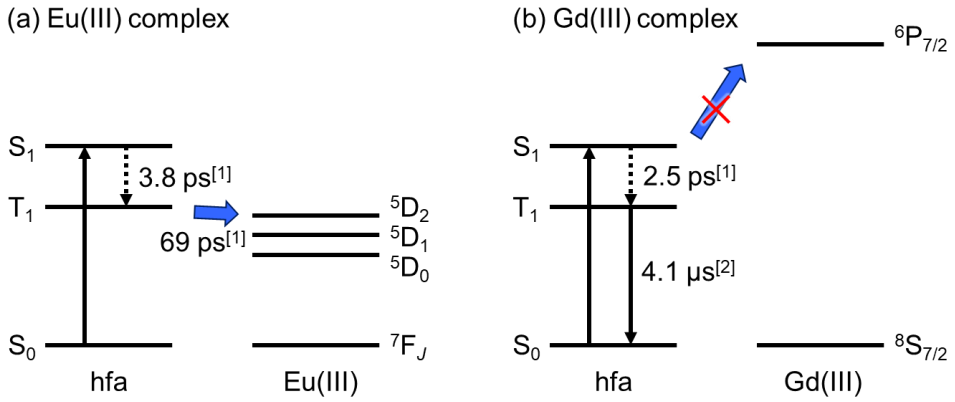

Figure 4-5 Schematic diagram of intra-molecular energy transfer in $CHCl_3$ solution of (a) $Eu(hfa)_3(TPPO)_2$ and (b) $Gd(hfa)_3(TPPO)_2$. The rate constants were determined by fs-TAS[1] (**Fig. 4-3**) and TR-PL[2] measurements (**Fig. 4-4**).

4-3-3 Time-domain view of the whole energy transfer process

Fig.4-6 shows the spectral evolution of the emission from $Eu(hfa)_3(TPPO)_2$. Immediately after the initial optical excitation of the hfa ligands at 315 nm, a broad emission in the range from 350 to 450 nm was observed (**Fig. 4-6a**). This emission is mainly originated from the fluorescence of the hfa ligands because it is broader and higher in energy compared to the emission from Eu(III). As the ligand emission decays, the sharp emission from Eu(III) becomes dominant. All the later observed bands are assigned to the 4f-4f transitions in Eu(III) according to the Dicke's diagram *(39)*.

The emission bands at 461, 473, 488, and 509 nm, occurring in the nanosecond time region (**Fig. 4-6b**), were assigned to the transitions of $^5D_2 \rightarrow {}^7F_0$, $^5D_2 \rightarrow {}^7F_1$, $^5D_2 \rightarrow {}^7F_2$, and $^5D_2 \rightarrow {}^7F_3$, respectively. The emission bands at 535, 556, and 583 nm, observed in the tens of nanoseconds time region (**Fig. 4-6c**), were assigned to the transitions of $^5D_1 \rightarrow {}^7F_1$, $^5D_1 \rightarrow {}^7F_2$, and $^5D_1 \rightarrow {}^7F_3$, respectively. The bands at 577, 592, and 614 exhibit the longest lifetime (**Fig. 4-6d**), and were assigned to $^5D_0 \rightarrow {}^7F_0$, $^5D_0 \rightarrow {}^7F_1$ and $^5D_0 \rightarrow {}^7F_2$, respectively. It should be noted that the emissions from $^5D_0$ were not significant at the beginning (<1 μs) but become dominant in the static emission spectrum, as its lifetime is much longer than the other emissions from ligands or $^5D_1$. By employing time- and spectrally-resolved emission measurements, the emission dynamics from the ligands to the lanthanide ion were tracked successfully.

To investigate the energy transfer dynamics in $Eu(hfa)_3(TPPO)_2$, the temporal change in the intensity of each emission was analyzed (**Fig. 4-6e-g**). The emission from the ligands at 400 nm decayed with time constants of <0.1 ns (**Fig. 4-6e**), indicating the occurrence of fast energy transfer in this region. Two possibilities are considered for the fast decay: (1) ISC, (2) nonradiative irradiation. However, based on the observation of

the ligand T_1 state in the fs-TAS measurement, this fast decay is attributed to the fast ISC process. This observation was further supported by the observation of the ligand T_1 state in the fs-TAS measurement.

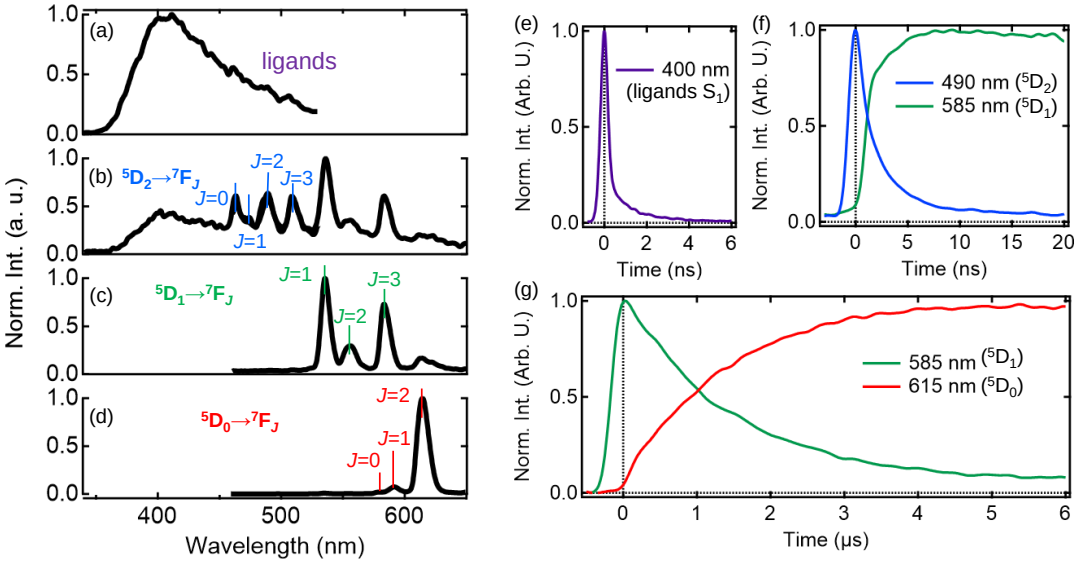

Figure 4-6 TR-PL spectra and their temporal profiles from the Eu(hfa)$_3$(TPPO)$_2$ solution. (a–d) Emission spectra at each delay time after optical excitation of hfa ligands at 315 nm. by the time integration of (a) -0.05–0.05 ns, (b) 0.95–1.05 ns, (c) 9.95–10.05 ns, and (d) 6.95–7.05 μs. (e–g) Temporal profiles of the emission at 400 nm (purple line), 490 nm (blue line), 585 nm (green line), and 615 nm (red line) in the different time region (a) -0.8–6 ns, (b) -3–20 ns, -0.5–6 μs.

The dynamics of the emission assigned to the 4f-4f transition in the lanthanide ion is of great importance because it hints at the mechanisms of the ligand-to-metal energy transfer. The emission at 490 nm was mainly composed of the emission from the $^5D_2$ state. The kinetics of the $^5D_2$ state (**Fig. 4-6f**) showed an increase in intensity with rapid time constants of less than 0.1 ns, indicating the presence of fast intramolecular energy transfer. To our best knowledge, this is the first observation of the energy transfer from the hfa ligand to the $^5D_2$ sate of the Eu(III) ion.

Furthermore, the emission from $^5D_2$ decayed with a time constant of approximately 2.0 ns (**Fig. 4-6e**). Associated with this decay, the intensity of the emission from the $^5D_1$ state increased with approximately the similar time constant (**Fig. 4-6f**). This result clearly indicates that the initial energy transfer from the ligands is not to $^5D_1$ but to $^5D_2$ and the time constant of internal conversion from $^5D_2$ to $^5D_1$ is ~2.0 ns. Furthermore, the emission from $^5D_1$ decays with a time constant of approximately 1.5 μs (**Fig. 4-6g**), and the intensity of the emission from the $^5D_0$ state increases with a similar time constant. This indicates that the time constant of internal conversion from $^5D_1$ to $^5D_0$ is ~1.5 μs. Finally, the decay of the emission from $^5D_0$ was approximately 790 μs, consistent with previous reports and confirming no degradation during the measurement.

4-3-4 Near unity intramolecular energy transfer from hfa ligands to Eu(III) ion

To estimate the intramolecular energy transfer efficiency (η_{ET}) from the ligand T_1 state to Eu(III) ion, we compared the T_1 lifetimes between Eu(III) and Gd(III) complex. The η_{ET} of the $Eu(hfa)_3(TPPO)_2$ was determined under the assumption that the radiative and non-radiative decay rates of the triplet state for the Gd(III) complexes reflect those of the Eu(III) complexes in the absence of energy transfer such that

$$\eta_{ET} = 1 - \frac{k_{Gd}^{T_1}}{k_{Eu}^{T_1}} \tag{4-2}$$

where k_{Gd}^{T1} and k_{Eu}^{T1} represent the rate constants of the T_1 states of the Gd (III) complex and the ligands in the Eu(III) complex ligands, respectively. By comparing the lifetimes of the ligand T_1 states between $Eu(hfa)_3(TPPO)_2$ and $Gd(hfa)_3(TPPO)_2$, the η_{ET} of $Eu(hfa)_3(TPPO)_2$ was determined to be greater than 0.99.

The high η_{ET} is presumably due to the direct bonding of the hfa chromophore to the Eu(III) ion, which minimizes the donor–acceptor distance. It is important to note that the Eu(III) complex exhibits a very high energy transfer efficiency (>0.99) despite the sensitization efficiency, η_{sens} being 0.67. The η_{sens} is determined by the quantum yield of the overall energy transfer process. In the case of $Eu(hfa)_3(TPPO)_2$, η_{sens} is expressed as

$$\eta_{sens} = \phi_{ISC} \times \eta_{ET} \tag{4-3}$$

where ϕ_{ISC} represents the yield of ISC of the ligands. Thus, we concluded that the ϕ_{ISC} is the dominant factor contributing to the low η_{sens}. This result indicates that once the ligand triplet state is generated, energy transfer occurs with near unity efficiency. Previous observations of near unity energy transfer in Eu(III) complexes with various antenna ligands, despite different η_{sens} values, support this conclusion *(21).*

The investigation of energy transfer dynamics in $Eu(hfa)_3(TPPO)_2$ has provided

valuable insights into the efficient transfer of energy from the ligands to the Eu(III) ion. However, despite the high energy transfer efficiency observed, there is still a significant loss of energy during the process. This rapid decay indicates that both radiative and, more likely, nonradiative relaxation pathways are efficiently competing with ISC, resulting in a small population of the ligand triplet state.

4-3-5 Comparison of energy transfer process with $Eu(hfa)_3(DPPTO)_2$

Fig. 4-7 shows the overview of the energy transfer dynamics in the $Eu(hfa)_3(TPPO)_2$ and $Eu(hfa)_3(DPPTO)_2$. From the TR-PL and fs-TAS measurements, we elucidated the energy transfer pathways and their time constants. Through a comprehensive investigation, we have successfully identified the previously ambiguous energy transfer process occurring within 3 ns in $Eu(hfa)_3(DPPTO)_2$. Our results reveal that this rapid energy transfer can be attributed to the ligand (hfa) $T_1 \rightarrow$ Eu(III) $^5D_2 \rightarrow$ Eu(III) $^5D_1$ state energy transfer pathway. The hfa T_1 state serves as an intermediate state, efficiently transferring energy to the $^5D_2$ state, which subsequently transfers energy to the $^5D_1$ state.

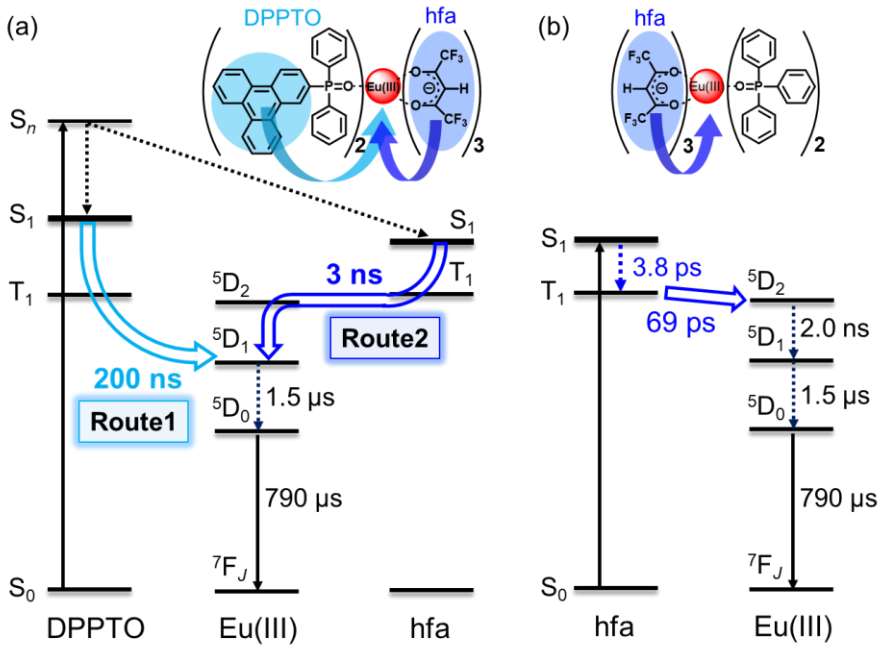

Fig. 4-7 Overview of the energy transfer dynamics in the (a) $Eu(hfa)_3(DPPTO)_2$ after photoexcitation of DPPTO ligands and (b) $Eu(hfa)_3(TPPO)_2$ after photoexcitation of hfa ligands.

The observation that both hfa and DPPTO, despite having the similar T_1 energy level, transfer energy to different excited states of the Eu(III) ion ($^5D_2$ and $^5D_1$, respectively) suggests that energy transfer in this system is not solely controlled by the energy levels. This finding highlights the influence of ligand coordination and the connectivity in determining the energy transfer pathways and their efficiencies. By modifying the ligand arrangement and coordination geometry, it may be possible to manipulate and optimize the energy transfer process in Eu(III) complexes.

Furthermore, our results emphasize the importance of considering not only the energy levels but also the ligand connectivity and arrangement when designing efficient energy transfer systems. The specific ligand arrangement can influence the pathways and efficiency of energy transfer, potentially offering opportunities for tailoring the energy transfer dynamics in Eu(III) complexes. Further investigations and theoretical studies are warranted to gain deeper insights into the interplay between ligand coordination, energy levels, and energy transfer dynamics, enabling the development of enhanced systems for various applications.

4-4 Conclusion

In conclusion, our investigation of the energy transfer mechanism in $Eu(hfa)_3(TPPO)_2$ complex has provided valuable insights into the efficient intramolecular energy transfer from the T_1 state of β-diketonate ligands to the Eu(III) ions. The observed near unity efficiency of energy transfer to the $^5D_2$ state of the Eu(III) ion highlights the potential of β-diketonate ligands as effective sensitizers for trivalent europium complexes. This discovery not only enhances our understanding of energy transfer processes in Eu(III) complexes, but also opens up new possibilities for the design and development of highly efficient luminescent materials. By optimizing the ligand structure and coordination environment, it may be possible to further manipulate energy transfer pathways and enhance the emission efficiency of Eu(III) complexes. These findings significantly contribute to the advancement of lanthanide-based light-emitting materials, offering promising prospects for their application in light-emitting devices and the development of more energy-efficient luminescent systems.

References

1. J. Kido, Y. Okamoto, Organo Lanthanide Metal Complexes for Electroluminescent Materials. *Chem. Rev.* **102**, 2357–2368 (2002).
2. L. Wang, Z. Zhao, C. Wei, H. Wei, Z. Liu, Z. Bian, C. Huang, Review on the Electroluminescence Study of Lanthanide Complexes. *Adv. Optical Mater.* **7**, 1801256 (2019).
3. S. V. Eliseeva, J.-C. G. Bünzli, Lanthanide luminescence for functional materials and bio-sciences. *Chem. Soc. Rev.* **39**, 189–227 (2010).
4. H. Xu, Q. Sun, Z. An, Y. Wei, X. Liu, Electroluminescence from Europium(III) Complexes. *Coord. Chem. Rev.* **293–294**, 228–249 (2015).
5. J. -C. G. Bünzli, On the design of highly luminescent lanthanide complexes. *Cood. Chem. Rev.* **293–294**, 19–47 (2015).
6. K. Binnemans, Interpretation of Europium(III) Spectra. *Cood. Chem. Rev.* **295**, 1–45 (2015).
7. S. Sato, M. Wada, Relations between Intramolecular Energy Transfer Efficiencies and Triplet State Energies in Rare Earth β-Diketone Chelates. *Bull. Chem. Soc. Jpn.* 43, 1955–1962 (1970).
8. M. Latva, H. Takalo, V-M. Mukkala, C. Matachescu, J. C. Rodriguez-Ubisd, J. Kankarea, Correlation between the Lowest Triplet State Energy Level of the Ligand and Lanthanide(III) Luminescence Quantum Yield. *J. Lumin.* **75**, 149–169 (1997).
9. N. M. Shavaleev, S. V. Eliseeva, R. Scopelliti, J. -C. G. Bünzli, Designing Simple Tridentate Ligands for Highly Luminescent Europium Complexes. *Chem. - Eur. J.* **15**, 10790–10802 (2009).
10. N. M. Shavaleev, S. V. Eliseeva, R. Scopelliti, J. -C. G. Bünzli, Aryl Chromophore Ligands for Bright Europium Luminescence. *Inorg. Chem.* **49**, 3927–3936 (2010).
11. M. Kleinerman, Energy Migration in Lanthanide Chelates. *J. Chem. Phys.* **51**, 2370–2381 (1969).
12. E. Kasprzycka, V. A. Trush, V. M. Amirkhanov, L. Jerzykiewicz, O. L. Malta, J. Legendziewicz, P. Gawryszewska, Contribution of Energy Transfer from the Singlet State to the Sensitization of Eu^{3+} and Tb^{3+} Luminescence by Sulfonylamidophosphates. *Chem. - Eur. J.* **23**, 1318–1330 (2017).
13. C. Yang, L. M. Fu, Y. Wang, J. P. Zhang, W. T. Wong, X. C. Ai, Y. F. Qiao, B. S. Zou, L. L. Gui, A Highly Luminescent Europium Complex Showing Visible-Light-Sensitized Red Emission: Direct Observation of the Singlet Pathway. *Angew. Chem., Int. Ed.* 43, 5010–5013 (2004).

14. S. Miyazaki, K. Miyata, H. Sakamoto, F. Suzue, Y. Kitagawa, Y. Hasegawa, K. Onda, Dual Energy Transfer Pathways from an Antenna Ligand to Lanthanide Ion in Trivalent Europium Complexes with Phosphine-Oxide Bridges. *J. Phys. Chem. A* **124**, 6601–6606 (2020).
15. R. A. Sá Ferreira, L. D. Carlos, R. R. Gonçalves, S. J. L. Ribeiro, V. de Zea Bermudez, Energy-Transfer Mechanisms and Emission Quantum Yields In Eu^{3+}-Based Siloxane-Poly(oxyethylene) Nanohybrids. *Chem. Mater.* **13**, *9*, 2991–2998 (2001).
16. N. B. D. Lima, J. D. L. Dutra, S. M. C. Gonçalves, R. O. Freire, A. M. Simas, Chemical Partition of the Radiative Decay Rate of Luminescence of Europium Complexes. *Sci. Rep.* **6**, 21204 (2016).
17. M. Hatanaka, Y. Hirai, Y. Kitagawa, T. Nakanishi, Y. Hasegawa, K. Morokuma, Organic linkers control the thermosensitivity of the emission intensities from Tb(III) and Eu(III) in a chameleon polymer. *Chem. Sci.* **8**, 423–429 (2017).
18. L. Wu, Y. Fang, W. Zuo, J. Wang, J. Wang, S. Wang, Z. Cui, W. Fang, H.-L. Sun, Y. Li, X. Chen, Excited-State Dynamics of Crossing-Controlled Energy Transfer in Europium Complexes. *JACS Au* **2**, *4*, 853–864 (2022).
19. M. J. Beltrán-Leiva, P. C.-López, C. Zúñiga, A. Bulhões-Figueira, D. Páez-Hernández, R. Arratia-Pérez, Theoretical Method for an Accurate Elucidation of Energy Transfer Pathways in Europium(III) Complexes with Dipyridophenazine (dppz) Ligand: One More Step in the Study of the Molecular Antenna Effect. *Inorg. Chem.* **56**, *15*, 9200–9208 (2017).
20. José Diogo L. Dutra, Ricardo O. Freire, Theoretical tools for the calculation of the photoluminescent properties of europium systems – A case study. *J. Photochem. Photobiol. A* **256**, 29–35 (2013).
21. M. W. Mara, D. S. Tatum, A. March, G. Doumy, E. G. Moore, K. N. Raymond, Energy Transfer from Antenna Ligand to Europium(III) Followed Using Ultrafast Optical and X-Ray Spectroscopy. *J. Am. Chem. Soc.* 141, 11071–11081 (2019).
22. S. Miyazaki, K. Goushi, Y. Kitagawa, Y. Hasegawa, C. Adachi, K. Miyata, K. Onda, Highly efficient light harvesting of a Eu(iii) complex in a host–guest film by triplet sensitization. *Chem. Sci.* **14**, 6867–6875 (2023).
23. N. Filipescu, W. F. Sager, F. A. Serafin, Substituent Effects on Intramolecular Energy Transfer. II. Fluorescence Spectra of Europium and Terbium β-Diketone Chelates. *J. Phys. Chem.* **68**, 3324–3346 (1964).
24. H. Kataoka, T. Kitano, T. Takizawa, Y. Hirai, T. Nakanishi, Y. Hasegawa, Photo- and thermo-stable luminescent beads composed of Eu(III) complexes and PMMA

for enhancement of silicon solar cell efficiency. *J. Alloys Compd.* **601**, 293–297 (2014).

25. D. B. A. Raj, B. Francis, M. L. P. Reddy, R. R. Butorac, V. M. Lynch, A. H. Cowley, Highly Luminescent Poly(Methyl Methacrylate)-Incorporated Europium Complex Supported by a Carbazole-Based Fluorinated β-Diketonate Ligand and a 4,5-Bis(diphenylphosphino)-9,9-dimethylxanthene Oxide Co-Ligand. *Inorg. Chem.* **49**, *19*, 9055–9063 (2010).
26. K. Miyata, T. Nakagawa, R. Kawakami, Y. Kita, K. Sugimoto, T. Nakashima, T. Harada, T. Kawai, Y. Hasegawa, Remarkable Luminescence Properties of Lanthanide Complexes with Asymmetric Dodecahedron Structures. *Chem. - Eur. J.* **17**, 521–528 (2011).
27. N. B. D. Lima, S. M. C. Gonçalves, S. A. Júnior, A. M. A. Simas, Comprehensive Strategy to Boost the Quantum Yield of Luminescence of Europium Complexes. *Sci. Rep.* **3**, 1–8 (2013).
28. Y. Kitagawa, R. Ohno, T. Nakanishi, K. Fushimi, Y. Hasegawa, Visible Luminescent Lanthanide Ions and a Large π-Conjugated Ligand System Shake Hands. *Phys. Chem. Chem. Phys.* **18**, 31012–31016 (2016)
29. K. Nakamura, Y. Hasegawa, H. Kawai, N. Yasuda, N. Kanehisa, Y. Kai, T. Nakamura, S. Yanagida, Y. Wada, Enhanced Lasing Properties of Dissymmetric Eu(III) Complex with Bidentate Phosphine Ligands. *J. Phys. Chem. A* **111**, 3029–3037 (2007).
30. Y. Kitagawa, F. Suzue, T. Nakanishi, K. Fushimi, Y. Hasegawa, A Highly Luminescent Eu(III) Complex Based on an Electronically Isolated Aromatic Ring System with Ultralong Lifetime. *Dalt. Trans.* **47**, 7327–7332 (2018).
31. Y. Hasegawa, M. Yamamuro, Y. Wada, N. Kanehisa, Y. Kai, A. Yanagida, Luminescent Polymer Containing the Eu(III) Complex Having Fast Radiation Rate and High Emission Quantum Efficiency. *J. Phys. Chem. A* **107**, 1697–1702 (2003).
32. R. D. Spencer, G. Weber, Influence of Brownian rotations and energy transfer upon the measurements of fluorescence lifetime. *J. Chem. Phys.* 52, 1654– 1663 (1970).
33. M. Saigo, Y. Shimoda, T. Ehara, T. Ryu, K. Miyata, K. Onda, Characterization of Excited States in a Multiple-Resonance-Type Thermally Activated Delayed Fluorescence Molecule Using Time-Resolved Infrared Spectroscopy. *Bull. Chem. Soc. Jpn.* **95**, 381–388 (2022).
34. B. R. Judd, Optical Absorption Intensities of Rare-Earth Ions. *Phys. Rev.* **127**, 750–761 (1962).

35. G. S. Ofelt, Structure of the F6configuration with Application to Rare-Earth Ions. *J. Chem. Phys.* **38**, 2171–2180 (1963).
36. M. H. V. Werts, R. T. F. Jukes, J. W. Verhoeven, The emission spectrum and the radiative lifetime of Eu^{3+} in luminescent lanthanide complexes. *Phys. Chem. Chem. Phys.* **4**, 1542–1548 (2002).
37. J. J. Snellenburg, S. P. Laptenok, R. Seger, K. M. Mullen, I. H. M. van Stokkum, Glotaran: A Java-Based Graphical User Interface for the R Package TIMP. *J. Stat. Softw.* **49**, *3*, 1–22 (2012).
38. J. H. S. K. Monteiro, A. De Bettencourt-Dias, F. A. Sigoli, Estimating the Donor-Acceptor Distance to Tune the Emission Efficiency of Luminescent Lanthanide Compounds. *Inorg. Chem.* **56**, 709–712 (2017).
39. C. -G. Ma, M. G. Brik, D.-X. Liu, B. Feng, Y. Tian, A. Suchocki, Energy level schemes of f^N electronic configurations for the di-, tri-, and tetravalent lanthanides and actinides in a free state. *J. Lumin.* **170**, 369–374 (2016).

Chapter 5.

Highly Efficient Light Harvesting of a Eu(III) Complex in a Host–guest Film by Triplet Sensitization

Shiori Miyazaki, Kenichi Goushi, Yuichi Kitagawa, Yasuchika Hasegawa, Chihaya Adachi, Kiyoshi Miyata and Ken Onda

Chemical Science **2023**, *14*, 6867–6875.

Abstract

Trivalent lanthanide complexes are attractive light emitters owing to their ideal high color purity. Sensitization using ligands with high absorption efficiency is a powerful approach to enhancing photoluminescence intensity. However, the development of antenna ligands that can be used for sensitization is limited due to difficulties in controlling the coordination structures of lanthanides. When compared to conventional luminescent Eu(III) complexes, a system composed of triazine-based host molecules and $Eu(hfa)_3(TPPO)_2$ (hfa: hexafluoroacetylacetonato, TPPO: triphenylphosphine oxide) significantly increased total photoluminescence intensity. Energy transfer from host molecules to Eu(III) ion occurs via triplet states over several molecules, according to time-resolved spectroscopic studies, with nearly 100% efficiency. Our discovery paves the way for efficient light harvesting of Eu(III) complexes with simple fabrication using a solution process.

5-1 Introduction

Molecule-based light-emission technologies have been intensively developed over the last few decades owing to their various applications, such as display panels, bioimaging sensors, optical telecommunications, and laser diodes *(1–3)*. Light-emitting materials must emit narrow-band light to achieve high color purity in their applications. However, general organic molecular emitters exhibit broadband emissions with a full width at a half-maximum (FWHM) of 70–100 nm. Trivalent lanthanide (Ln(III)) complexes exhibit narrow-band emissions with FWHMs of 10–20 nm caused by transitions between f-orbitals in Ln(III) that are shielded by electrons in the occupied 5s, 5p orbitals *(4)*; however, direct photoexcitation of the Laporte-forbidden f–f transition in Ln(III) with a small absorption coefficient ($\varepsilon < 10\ M^{-1}\ cm^{-1}$) is difficult *(5)*. Many efforts have been made to overcome this difficulty by synthesizing organic ligands with large absorption coefficients and appropriate energy levels, which play an important role in efficient photosensitizers and intra-molecular ligand-to-Ln(III) energy transfer in complexes *(6–8)*.

The overall photoluminescence (PL) intensity (I_{PL}) *(9,10)* of an Ln(III) complex in a dilute solution or thin film is expressed as

$$I_{PL} = \varepsilon_{ligands} \times \phi_{tot} \tag{5-1}$$

where $\varepsilon_{ligands}$ and ϕ_{tot} represent the sum of all ligand absorption coefficients and the overall luminescence quantum yield of Ln(III) from ligand photoexcitation via intra-molecular energy transfer, respectively. This equation indicates that high PL intensity requires high light-absorption ability and luminescence quantum yield. Eu(III)$(hfa)_3(DPPTO)_2$ (hfa: hexafluoroacetylacetonato, DPPTO: 2-ddiphenyl

phosphoryl triphenylene **Fig. 5-1**) is one of the Ln(III) complexes with the highest luminescence intensity in solution, I_{PL} = 90,000 M^{-1} cm^{-1}. The following three factors contribute to this high I_{PL}: (i) high $\varepsilon_{\mathrm{ligands}}$ = 170,000 M^{-1} cm^{-1} of the two DPPTO ligands owing to their triphenylene chromophores *(11)*, (ii) high ϕ_{tot} = 0.53 owing to suppression of nonradiative decay due to low vibrational frequencies of the phosphine-oxide linker in the DPPTO ligand and CF bonds in the hfa ligand *(12–16)*, and (iii) enhancement of transition intensities in Eu(III) due to the asymmetric structure *(17–21)* formed by the hfa and DPPTO ligands. However, further improvement of luminescence intensity by designing new ligands is limited due to the difficulty in synthesizing ligands that simultaneously contain multiple chromophores with a large absorption coefficient and stable coordination to Ln(III) compared to general transition metal ions.

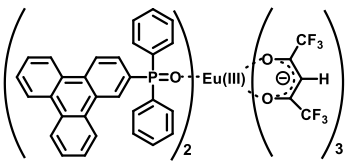

Figure 5-1 Chemical structure of $Eu(hfa)_3(DPPTO)_2$.

We propose that a host-guest system, composed of π-conjugated molecules and Ln(III) complex emitters, are an ideal system for drastically increasing the PL intensity of Ln(III) complexes while requiring minimal fabrication. Multiple π-conjugated molecules with high absorption coefficients serve as antennae for photosensitizing Ln(III) complexes in this system; therefore, a much higher absorption coefficient, denoted by $\varepsilon_{\mathrm{hosts}}$ in this case, is expected in Eq. (5-1) when compared to the molecular Ln(III) complex. Moreover, no linkers were required to coordinate Ln(III). However, to achieve high ϕ_{tot}, such a host-guest system must overcome additional challenges; not only intra-molecular energy transfer but also inter-molecular energy transfer processes from host molecules to the Ln(III) complex are involved, and each process must be highly efficient. To achieve a very high I_{PL} for the host-gust system, it is essential to understand the

mechanisms of the entire energy transfer process and design lossless energy transfer processes. To address these concerns, we chose a simple Eu(III) complex, Eu(III)$(hfa)_3(TPPO)_2$ (TPPO: triphenylphosphine oxide) *(22,23)*, in which intra-molecular energy transfer occurs from the hfa ligands. We discovered that a host-guest system composed of a 2,4,6-tris(biphenyl-3-yl)-1,3,5-triazine (mT2T) host and the Eu(III) complex achieves an I_{PL} three orders of magnitude greater than the I_{PL} of the Eu(III) complex itself and that ~40 host molecules work for light harvesting of one Eu(III) complex via lossless triplet–triplet inter-molecular energy transfer.

In general, host-guest systems of Ln(III) complexes have been fabricated as emitting layers in organic light-emitting diodes (OLEDs) *(24–26)*. Host molecules are known to affect the emission properties of Ln(III) complexes. Pietraszkiewicz *et al.* fabricated a 5 wt% Eu(nta)3SFXPO-complex-doped host-guest film (nta:1-(2-naphthoyl)-3,3,3-trifluoroacetonate, SFXPO: spiro-fluorene-xanthene diphosphine oxide) with a higher PL quantum yield (PLQY) of 0.86 than 0.64 in a neat film *(27)*. This shows that host-guest systems may improve the efficiency of energy transfer processes when compared to molecular Ln(III) complexes. Buczko *et al.* fabricated a film of 0.17 wt% $(N(C_2H_5)_4)[Eu(hfa)_4]$-complex in $(N(C_2H_5)_4)[Ln(hfa)_4]$-complex, Ln = Gd(III) or Lu(III), and found 347 times larger emission intensity compared to the neat film due to inter-molecular energy transfer from ligands of $(N(C_2H_5)_4)[Ln(hfa)_4]$ and diminishment of concentration quenching *(28)*. Nonetheless, there are no design strategies apart from matching the energy of their lowest excited states *(29–33)*, and there are few direct observations of inter- and intra-molecular energy transfer processes in host and guest systems *(34–38)*.

We fabricated 10 wt% $Eu(hfa)_3(TPPO)_2$-doped films with the five host molecules demonstrated below, and a polymethyl methacrylate (PMMA) polymer with no photosensitization ability. We measured their I_{PL} and discovered that the mT2T host molecule exhibited the highest I_{PL} = 3,600,000 M^{-1} cm^{-1}, which was approximately five hundred times greater than the PMMA host (**Fig. 5-2**). To investigate the source of the relatively high I_{PL}, we used time-resolved PL spectroscopy (TR-PL) and femtosecond transient absorption spectroscopy (fs-TAS) in a multiscale temporal range from sub-picoseconds to hundreds of microseconds to investigate the emission mechanisms of the host-guest film. Beginning with the initial excitation of the host molecules and ending with the emission of the Eu(III) complex, we elucidated the mechanisms of all processes in the film: (1) the intersystem crossing (ISC) in the host molecule, (2) the inter-molecular energy transfer process from the host molecules to the ligands of the guest Eu(III) complex, (3) the intra-molecular energy transfer process from the ligands to Eu(III) ion, and (4) the emission processes of f–f transitions in Eu(III) ion. Furthermore, we discovered that the yields of all energy transfer processes, (1)–(3), were nearly unity and that the yield of the Eu(III) ion emission process (4) determined the overall quantum yield

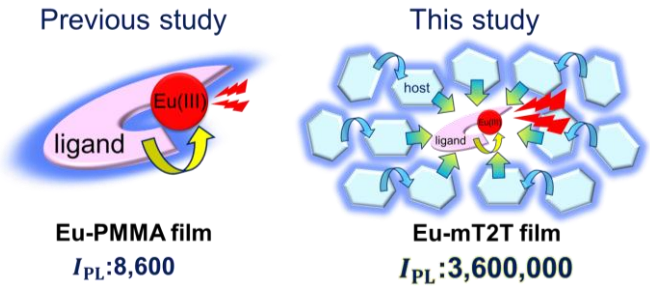

Figure 5-2 Drastic improvement of the overall photoluminescence intensity (I_{PL}) by efficient photosensitization from many host molecules. Schematic view of photo-sensitization by intra-molecular energy transfer from the ligands to Eu(III) ion in the $Eu(hfa)_3(TPPO)_2$-doped PMMA film (Eu-PMMA film, left) and light harvesting by inter-molecular energy transfer from many hosts to Eu(III) complex in the $Eu(hfa)_3(TPPO)_2$-doped mT2T film (Eu-mT2T film, right).

of the film. This highly efficient PL is attributed to the ideal triplet sensitization processes: rapid and efficient ISC in mT2T results in efficient triplet–triplet inter-molecular energy transfers with no losses.

5-2 Experimental section

5-2-1 Materials

A previously reported procedure was used to synthesize $Eu(hfa)_3(TPPO)_2$ *(22)*. mT2T, SF3TRZ, and mCBP were purchased from the NARD Institute Ltd. (Hyogo, Japan). CBP was purchased from Angene International Ltd. (Nanjing, China). T2T was purchased from Tokyo Chemical Industry Co., Ltd. (Tokyo, Japan). mT2T, SF3TRZ, mCBP, and CBP were purified via sublimation. Chloroform, dichloromethane, and methanol were purchased from Kanto Kagaku Co., Ltd. (Tokyo, Japan). Without further purification, all solvents were used as received.

5-2-2 Fabrication of thin films

Thin films for optical measurements were fabricated by spin-coating on quartz substrates. The quartz substrates were washed by ultrasonic cleaning with acetone and isopropanol. For the preparation of neat films, the emitter compounds were dissolved in chloroform (10 wt%). To prepare the host-guest films, a weight ratio of 1:9 of the guest molecule and the host molecule was dissolved in chloroform to obtain an overall concentration of 10 wt%. Before use, the solution was filtered through a 0.2 μm filter, and the quartz substrates were heated to 80 °C. The solution was spin-coated onto quartz substrates for 60 s at 1000 rpm and then annealed at 70 °C for 10 min. **Table 5-1** shows the thicknesses of the films.

Thin films for refractive index measurements were fabricated on silicon substrates using vacuum vapor deposition at a pressure of less than 10^{-3} Pa. We used a fixed deposition rate of 0.5 nm/s and a thickness of 100 nm.

Table 5-1 Film thicknesses of the host-guest films. The concentration of $Eu(hfa)_3(TPPO)_2$ in the host-guest films is 10 wt%.

guest	host	Thickness (nm)
$Eu(hfa)_3(TPPO)_2$	-	83.0
	PMMA	166
	mT2T	118
	SF3TRZ	117
	mCBP	123
	pCBP	124
	pT2T	97.5

5-2-3 Measurement of photoluminescence properties

UV-vis absorption spectra were measured using a PerkinElmer LAMDA950 spectrophotometer. Excitation and PL spectra of the $Eu(hfa)_3(TPPO)_2$-doped PMMA film (excitation wavelength for PL spectra: λ_{ex} = 315 nm and probe wavelength for excitation spectra: λ_{em} = 615 nm), $Eu(hfa)_3(TPPO)_2$-doped mT2T film (λ_{ex} = 267 nm, λ_{em} = 615 nm), $Eu(hfa)_3(TPPO)_2$-doped T2T film (λ_{ex} = 260 nm, λ_{em} = 615 nm), $Eu(hfa)_3(TPPO)_2$-doped SF3TRZ film (λ_{ex} = 267 nm, λ_{em} = 615 nm), $Eu(hfa)_3(TPPO)_2$-doped mCBP film (λ_{ex} = 267 nm, λ_{em} = 615 nm), and $Eu(hfa)_3(TPPO)_2$-doped CBP film (λ_{ex} = 260 nm, λ_{em} = 615 nm) were measured using spectrofluorometers (FP-8600, JASCO; PMA-12, Hamamatsu Photonics). The phosphorescence spectra of the neat films of $Gd(hfa)_3(TPPO)_2$, TPPO (λ_{ex} = 335 nm), $Gd(hfa)_3(TPPO)_2$-doped mT2T (λ_{ex} = 267 nm), mT2T (λ_{ex} = 267 nm), T2T (λ_{ex} = 315 nm), SF3TRZ (λ_{ex} = 267 nm), mCBP (λ_{ex} = 267 nm), and T2T (λ_{ex} = 267 nm) at 77 K were measured using a spectrofluorometer (FP-8600, JASCO; PMA-12, Hamamatsu Photonics).

The photoluminescence quantum yields were measured using a Hamamatsu Photonics Quantaurus-QY instrument equipped with an integrating sphere. A time-correlated single-photon counting lifetime spectroscopy system (HAMAMATSU Quantaurus-Tau C11367-21, C11567-02, and M12977-01) was used to PL measure lifetimes.

The refractive indexes and thicknesses of the films were measured using variable-angle spectroscopic ellipsometry (M-2000U, J. A. Woollam Co., Inc., United States).

5-2-4 Time-resolved photoluminescence (TR-PL)

TR-PL measurements were performed using a streak camera system (Hamamatsu C4780, time resolution <30 ps) synchronized with a Ti:sapphire regenerative amplifier (Spectra-Physics, Spitfire Ace, pulse duration = 120 fs, repetition rate = 1 kHz, pulse energy = 4 mJ/pulse, central wavelength = 800 nm). The samples were excited by the third harmonic of the fundamental pulse from an amplifier (267 nm). Before measuring, all films were encapsulated. The excitation energy was kept to less than 0.8 mJ/cm^2.

5-2-5 Femtosecond transient absorption spectroscopy (fs-TAS)

Transient absorption (TA) measurements were conducted using the pump-probe method *(39)*. The light source was a Ti:sapphire regenerative amplifier system (Spectra-Physics, Spitfire Ace, pulse duration = 120 fs, repetition rate = 1 kHz, pulse energy = 4 mJ/pulse, central wavelength = 800 nm) seeded by a Ti:sapphire femtosecond mode-locked laser (Spectra-Physics, Tsunami). The output of the amplifier was divided into two pulses for the pump and probe. The samples were pumped by the third harmonic of the fundamental pulse from an amplifier (267 nm). The broadband probe pulse (450–750 nm) was generated using a sapphire crystal of 1 mm thickness. The pump and probe pulse beam sizes at the sample position were <0.7 mmϕ and <0.5 mmϕ, respectively. A PC-controlled mechanical delay state was used to adjust the delay time between the pump and probe pulses. The probe pulse that passed through the sample films was dispersed by a polychromator (JASCO, CT-10, 300 grooves/500 nm), and the spectra were captured using a multichannel detection system with a CMOS sensor (UNISOKU, USP-PSMM-NP). To avoid damage, all the films were encapsulated before being measured and were

mechanically moved continuously. The excitation energy was kept to less than 0.4 mJ/cm^2. The recorded data was analyzed using a Python-based homemade program. In this study, the Eu(III) ion emission in the Eu-mT2T film is too strong to avoid its scattered emission. Therefore, the TA spectra around 615 nm was unavailable.

5-3 Results and Discussion

5-3-1 Contribution of host molecules to I_{PL}

Five different host molecules were used to fabricate $Eu(hfa)_3(TPPO)_2$-doped films: mT2T, 2-(9,9'-spirobi[fluoren]-3-yl)-4,6-diphenyl-1,3,5-triazine (SF3TRZ), 3,3′-di(9H-carbazol-9-yl)biphenyl (mCBP), 4,4′-N,N′-dicarbazole-biphenyl (CBP), and 2,4,6-tris(1,1′-biphenyl-4-yl)-[1,3,5]triazine (T2T) (**Fig. 5-3**). These host molecules have been used in conventional OLED applications. To evaluate the intrinsic optical properties of isolated $Eu(hfa)_3(TPPO)_2$, we also fabricated an $Eu(hfa)_3(TPPO)_2$-doped PMMA (Eu-PMMA) film. Because PMMA is transparent in the >250 nm range *(40)*, the absorption spectrum of the Eu-PMMA film in the >250 nm range is identical to that of $Eu(hfa)_3(TPPO)_2$. The absorption range of 250–350 nm for isolated $Eu(hfa)_3(TPPO)_2$ is primarily assigned to the S_0–S_n transition of the hfa ligands *(41)*, and the absorption of TPPO in this range is much weaker (**Fig. 5-4a**). The host-guest systems significantly enhanced their overall absorption coefficients because all of the host molecules have higher absorption coefficients in the range of 250–280 nm than the hfa ligands (**Table 5-2**, **Fig. 5-4b**).

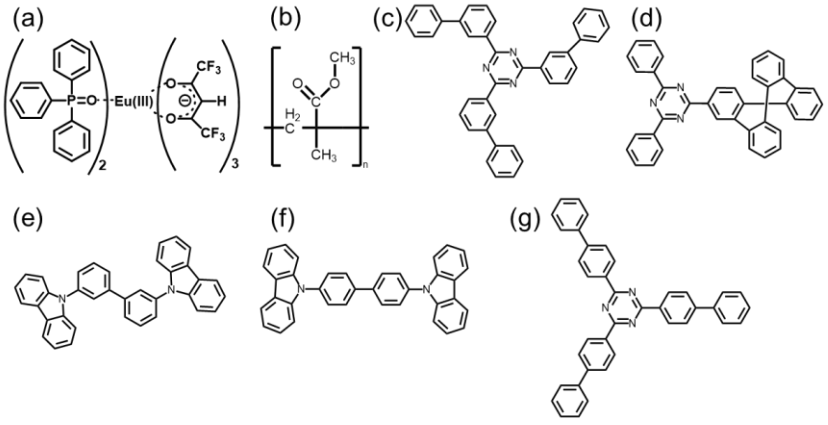

Figure 5-3 Chemical structures. (a) Eu(hfa)3(TPPO)2, (b) PMMA, (c) mT2T, (d) SF3TRZ, (e) mCBP, (f) CBP, and (g) T2T.

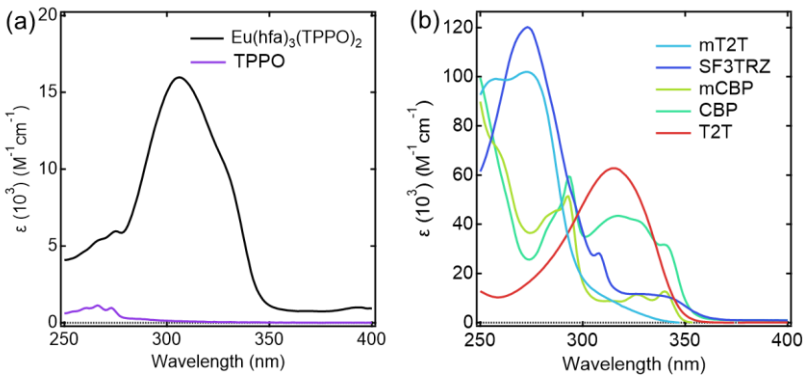

Figure 5-4 Absorption spectra. (a) Absorption spectra of $Eu(hfa)_3(TPPO)_2$ (black line) and TPPO (purple line). (b) Absorption spectra of mT2T (sky blue line), SF3TRZ (blue line), mCBP (yellow green line), CBP (green line), and T2T (red line). The spectrum of $Eu(hfa)_3(TPPO)_2$ was measured in $CHCl_3$. The spectra of TPPO and all host molecules were measured in CH_2Cl_2.

Table 5-2 Absorption and emission properties of the $Eu(hfa)_3(DPPTO)_2$ and $Eu(hfa)_3(TPPO)_2$-doped films. The values of $\varepsilon_{\text{host}}^{\text{mol}}$ and $\varepsilon_{\text{ligands}}$ of $Eu(hfa)_3(DPPTO)_2$-PMMA film were evaluated at 267 nm. The values of $\varepsilon_{ligands}$ of $Eu(hfa)_3(TPPO)_2$-PMMA film was evaluated at 315 nm. I_{PL} was calculated using eq. (1) and eq. (2). The PLQYs (ϕ_{tot}) were measured each photoexcitation wavelength (λ_{ex}) ($\varepsilon_{\text{ligands}}$, $\varepsilon_{\text{host}}^{\text{mol}}$, n_{host}, I_{PL}; see text for details).

guest	host	Eu conc. /wt%	$\varepsilon_{\text{ligands}}$ /$M^{-1}cm^{-1}$	$\varepsilon_{\text{host}}^{\text{mol}}$ /$M^{-1}cm^{-1}$	n_{host}	ϕ_{tot}	λ_{ex} /nm	I_{PL} /$M^{-1}cm^{-1}$
$Eu(hfa)_3(DPPTO)_2$	PMMA	10	1.7×10^5	-	-	0.52	267	8.8×10^4
$Eu(hfa)_3(TPPO)_2$	PMMA	10	1.4×10^4	-	-	0.60	315	8.6×10^3
	mT2T	5	-	1.0×10^5	47	0.76	267	3.6×10^6
		10			22	0.84		1.9×10^6
		30			5.8	0.83		4.8×10^5
		50			2.5	0.78		1.9×10^5
	SF3TRZ	10	-	1.1×10^5	22	0.52	267	1.3×10^6
	mCBP	10	-	4.6×10^4	25	0.30	267	3.4×10^5
	CBP	10	-	4.0×10^4	25	0.24	267	2.1×10^5
	T2T	10	-	1.2×10^4	22	0.22	267	6.1×10^4

To investigate the sensitization ability of the host molecules, we compared the PL properties of the host-guest films to those of the Eu-PMMA film (**Fig. 5-5a**). After photoexciting the Eu-PMMA film with 315 nm light, emission bands from Eu(III) ion were observed at 581, 594, 615, 654, and 701 nm (**Fig. 5-5b**) and are assigned to the transitions $^5D_0 \rightarrow {}^7F_J$ and $J = 0$, 1, 2, 3, and 4, respectively *(4)*. The Eu(III) ion sensitization by the hfa ligands in the Eu-PMMA film was confirmed because excitation at 315 nm selectively excites the hfa ligands (**Fig. 5-4a**). Also, after photoexcitation with 260–267 nm light, the same emission bands in Eu(III) ion were observed in all of the host-guest films (**Fig. 5-5c, 5-6**). Given that the absorption coefficients of the host molecules in this wavelength range are much larger than those of the guest complex (**Fig. 5-4**), this

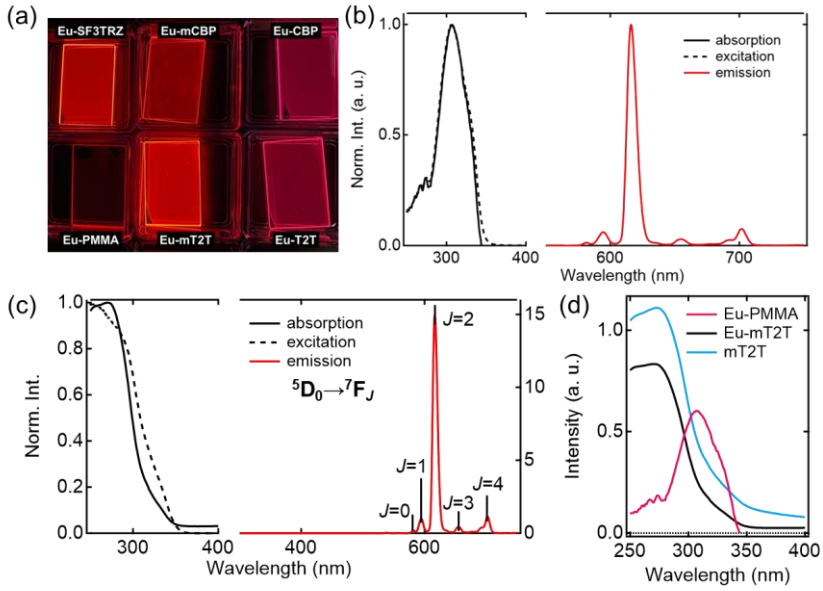

Figure 5-5 Optical properties of $Eu(hfa)_3(TPPO)_2$-doped films. (a) Photos of emission from the fabricated films upon photoexcitation with 254 nm. (b) Absorption (solid line), excitation (broken line, probed at 615 nm), and emission (red line, λ_{ex} = 315 nm) spectra of the Eu-PMMA film. (c) Absorption (solid line), excitation probed at 615 nm (broken line), and emission (red line) spectra of the Eu-mT2T film. (d) Absorption spectra of the Eu-PMMA film (pink line), Eu-mT2T film (black line), and mT2T neat film (sky blue line).

indicates that inter-molecular energy transfer from the host molecules to Eu(III) complex occurs in all host-guest films.

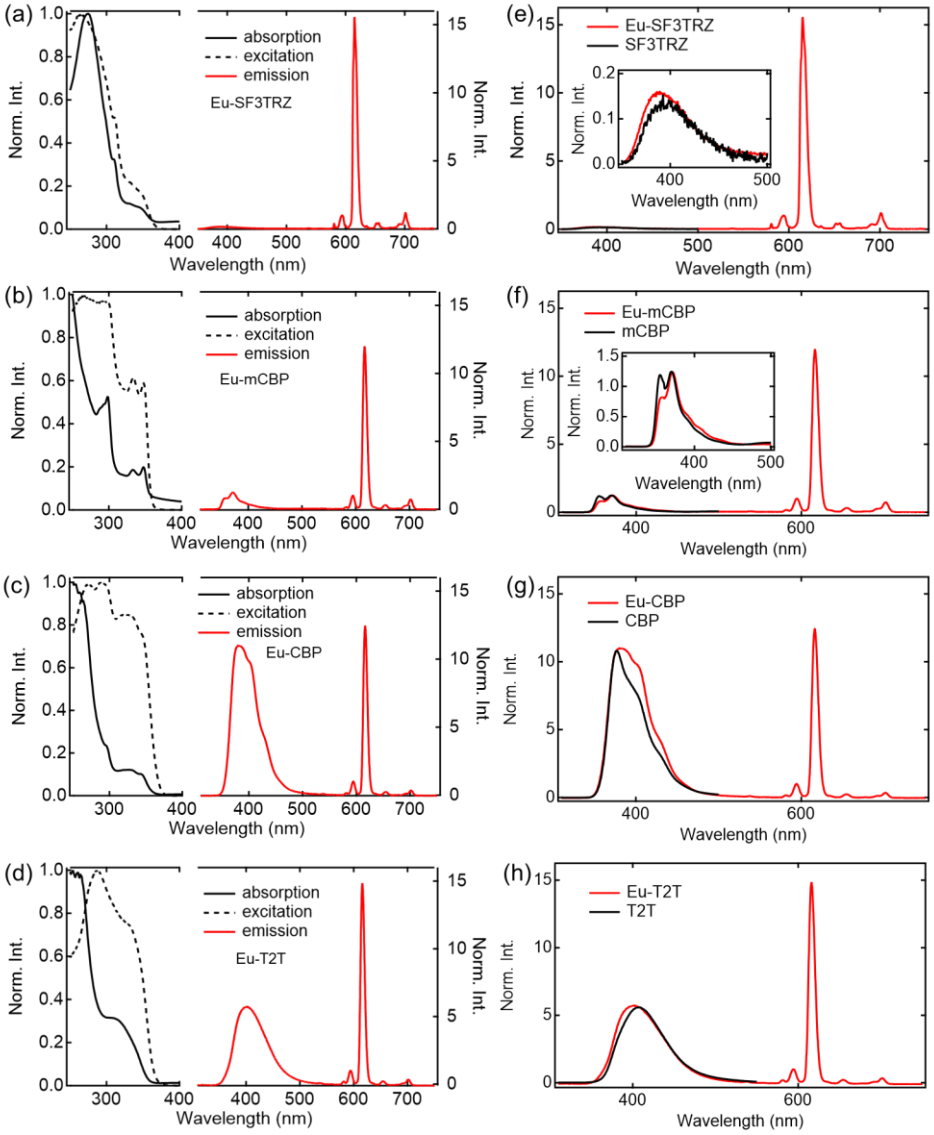

Figure 5-6 Optical spectra of the host-guest films. (a-d) Absorption (black line), excitation (broken line, probed at 615 nm), and emission spectra (red line) of the (a) Eu-SF3TRZ film (λ_{ex} = 267 nm), (b) Eu-mCBP film (λ_{ex} = 267 nm), (c) Eu-CBP film (λ_{ex} = 260 nm), and (d) Eu-T2T film (λ_{ex} = 260 nm). (e-h) Comparison of emission spectra between host-guest and host-molecule neat films. (e) Eu-SF3TRZ film (red line, λ_{ex} = 267 nm) and SF3TRZ neat film (black line, λ_{ex} = 275 nm). (f) Eu-mCBP film (red line, λ_{ex} = 267 nm) and mCBP neat film (black line, λ_{ex} = 297 nm). (g) Eu-CBP film (red line, λ_{ex} = 260 nm) and CBP neat film (black line, λ_{ex} = 267 nm). (h) Eu-T2T film (red line, λ_{ex} = 260 nm) and T2T neat film (black line, λ_{ex} = 267 nm).

The sensitization efficiencies of the host-guest films are discussed qualitatively based on their emission spectra. A broad emission band located at around 400 nm was observed for $Eu(hfa)_3(TPPO)_2$-doped SF3TRZ (Eu-SF3TRZ), mCBP (Eu-mCBP), CBP (Eu-CBP), and T2T (Eu-T2T) films, in addition to the emission from Eu(III) ion (**Fig.5-6a-d**). These bands were assigned to the fluorescence from the lowest singlet excited state (S_1) of each host molecule (**Fig. 5-6e-h**), indicating imperfect energy transfer to the Eu(III) complex. In contrast, no-host molecule emission band was observed in the $Eu(hfa)_3(TPPO)_2$-doped mT2T (Eu-mT2T) film (**Fig. 5-5c**). This finding suggests that inter-molecular energy transfer from the host mT2T molecules to the Eu(III) complex occurs extremely efficiently in the film. In fact, ϕ_{tot} of Eu-mT2T (ϕ_{tot} = 0.84) was significantly higher than Eu-PMMA (ϕ_{tot} = 0.60) (**Table 5-2**). The excitation spectra probed at the Eu(III) ion emission, which coincided with the absorption spectra of these films, further supported efficient sensitization (**Fig. 5-5c, d**).

We measured the photophysical properties of Eu-mT2T films with different doping ratios of Eu(III) complex to mT2T to estimate the number of host molecules that contributed to one Eu(III) ion emission (**Table 5-2**). Considering this result, I_{PL} of host-guest films can be expressed as

$$I_{\mathrm{PL}} = \varepsilon_{\mathrm{hosts}} \times \phi_{\mathrm{tot}} = \varepsilon_{\mathrm{host}}^{\mathrm{mol}} \times n_{\mathrm{host}} \times \phi_{\mathrm{tot}} \qquad (5\text{-}2)$$

where $\varepsilon_{\mathrm{host}}^{\mathrm{mol}}$ and n_{host} represent the molar absorption coefficient of the host molecule and the number of host molecules contributed to one Eu(III) ion emission which is calculated from the doped molar ratio between the host molecule and the Eu(III) complex, respectively. The ϕ_{tot} was highest when the mixing ratio was 10%, implying that ~22 host molecules contributed to the emission of one Eu(III) complex via energy transfer between the host and guest molecules. The I_{PL} is plotted as a function of n_{host}

in **Fig. 5-7**. The I_{PL} for the Eu(hfa)$_3$(TPPO)$_2$-doped films increases monotonically even when n_{host} = 47, indicating that more than 47 host molecules work as photosensitizers for one Eu(III) complex. Note that the maximum I_{PL} is more than two order of magnitude greater than that of the conventional highly luminescent complex Eu(hfa)$_3$(DPPTO)$_2$ *(11)*.

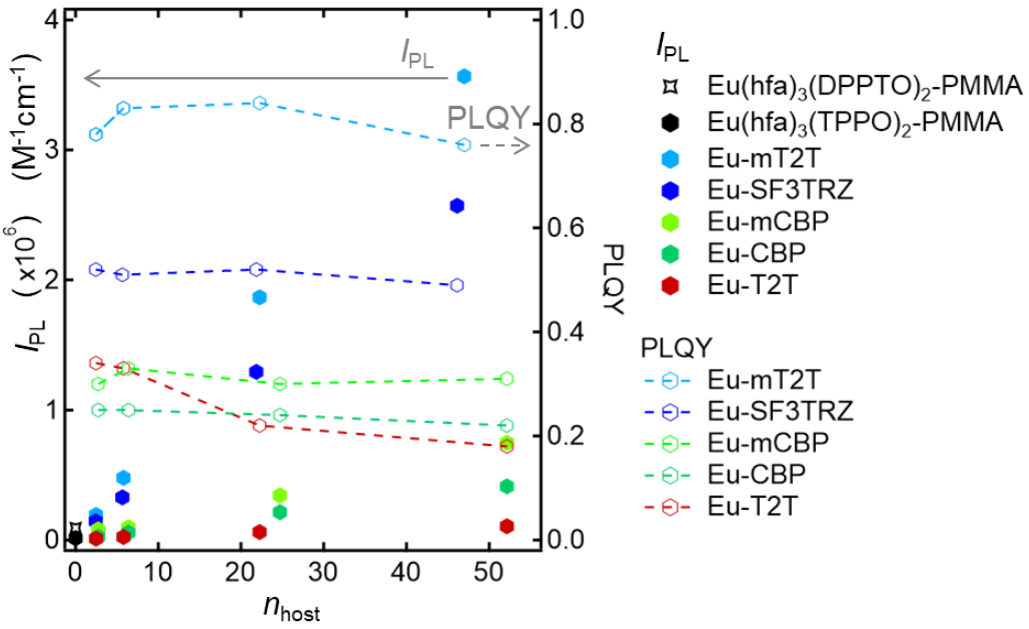

Figure 5-7 Host and its ratio dependence of overall luminescence intensities (I_{PL}) and PLQY. I_{PL} of Eu(hfa)$_3$(DPPTO)$_2$-doped PMMA film (black star marker), Eu(hfa)$_3$(TPPO)$_2$-doped PMMA film (black hexagon marker), Eu-mT2T film (sky blue hexagon markers), Eu-SF3TRZ film (blue hexagon marker), Eu-mCBP film (yellow green hexagon marker), and Eu-T2T film (red hexagon marker), calculated using Eq. (1) and Eq. (2). PLQY of Eu-mT2T film (sky blue line), Eu-SF3TRZ film (blue line), Eu-mCBP film (yellow green line), and Eu-T2T film (red line). n_{host} is the number of host molecules contributed to one Eu(III) ion emission.

5-3-2 Initial process after photoexcitation: rapid and efficient ISC in mT2T

Understanding the mechanisms of intra- and inter-molecular energy transfer processes requires understanding the photophysical processes occurring in host molecules. To investigate the processes in the time domain, we measured and compared the fs-TAS spectra of the Eu-mT2T film (**Fig. 5-8a**) and the mT2T neat film (**Fig. 5-8e**). The absorbance change (ΔAbs.) of the Eu-mT2T film increased in the <600 nm range, whereas it decreased in the >600 nm range, with an isosbestic point at 600 nm. We note that the isosbestic point does not appear as an intersection at one point due to slight spectral shift over time. This is presumably due to dynamical effect uniquely seen in a solid state, for example, dielectric relaxation. We performed a global analysis of the fs-TAS spectra, assuming a sequential model with two components because the isosbestic point indicates an exclusive transition between two states *(42)*. With a time constant of 71.2 ± 0.6 ps, the first component was converted to the second component (**Fig. 5-8b**). The evolution associated spectra (EAS) and concentration kinetics of the two components are shown in **Fig. 5-8c** and **5-8d**, respectively. We analyzed the fs-TAS of the mT2T neat film in the same way to assign the observed species. The global analysis also resulted in similar EASs (**Fig. 5-8g**), with a time constant of 44.9 ± 0.4 ps (**Fig. 5-8h**). The two EAS components were reasonably assigned to S_1 and the lowest triplet excited state (T_1) in the case of the neat film, and the time constant represented the ISC rate. Therefore, the two components observed in the Eu-mT2T film were assigned to S_1 and T_1 of the host mT2T molecule. These time constants are much faster than those of the ISC process for aromatic organic molecules in general, which can be explained by the presence of lone pairs in the triazine moieties in mT2T accelerating the ISC rate *(43, 44)*. We conclude that mT2T undergoes a rapid and nearly unity ISC before exciton diffusion and energy transfer in the

host-guest film.

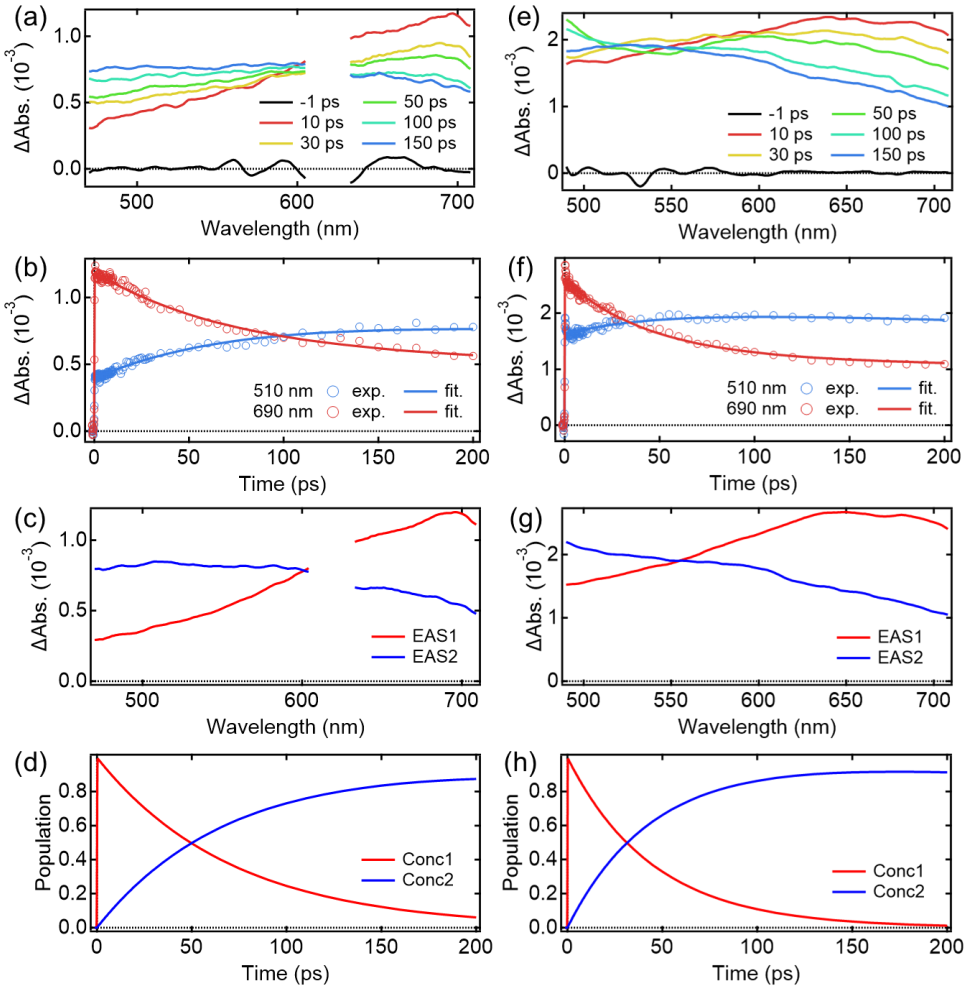

Figure 5-8 fs-TAS spectra and the results of their global analysis. (a-d) Eu-mT2T film. (e-h) mT2T neat film. (a, e) Temporal evolutions of the fs-TAS spectra after photoexcitation at 267 nm. (b, f) Temporal profiles of the fs-TAS spectra at 510 nm (blue circles) and 690 nm (red circles) and corresponding fitting curves resulted from the global analysis. (c, g) EAS. (d, h) Corresponding concentration kinetics were obtained from the global analysis. No TA data was available due to the strong emission from Eu(III) ion in the region neighboring 615 nm.

5-3-3 Quantum yields of each energy transfer process

Given that rapid ISC occurs first in the host film, **Fig. 5-9** shows the predicted energy transfer processes in the Eu-mT2T film after photoexcitation. We first estimated the luminescence quantum yield of Eu(III) ion (ϕ_{Eu}) in the host-guest films to estimate the quantum yield of each process. The natural radiative rate constant of Eu(III) ion ($k_{\mathrm{r}}^{\mathrm{Eu}}$) can be calculated from the ratio of the total Eu(III) ion transition to the magnetic dipole transition ($^5D_0 \rightarrow {}^7F_1$) in the observed emission spectrum of Eu(III) ion (**Fig. 5-5c**, Eq. (5-3)) *(45)*. The transitions $^5D_0 \rightarrow {}^7F_{0,\,2,\,3,\,4}$ are electric dipole transitions whose intensities are increased by reducing the coordination symmetry of the Eu(III) complex. The $^5D_0 \rightarrow {}^7F_1$ transition, in contrast, is a magnetic dipole transition that is independent of the coordination structure. We can assume that the energy of the $^5D_0 \rightarrow {}^7F_1$ transition and the dipole strength are constant.

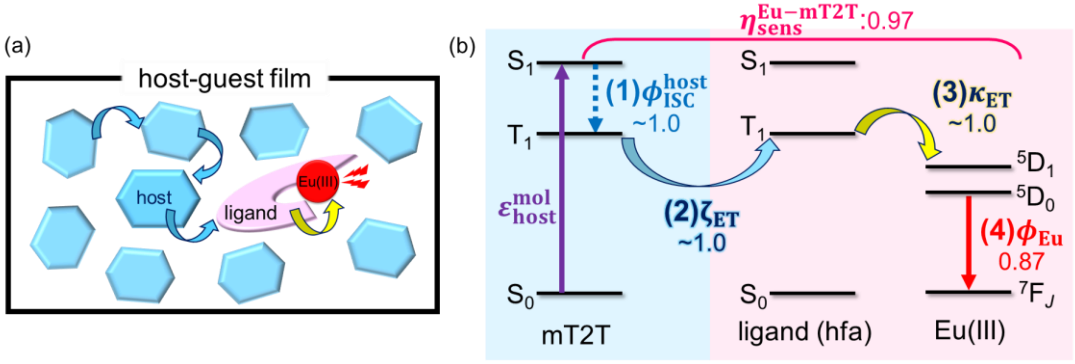

Figure 5-9 Overview of inter- and intra-molecular energy transfer processes in the Eu-mT2T film. (a) Schematic in real space. (b) Schematic in energy levels. $\phi_{\mathrm{ISC}}^{\mathrm{host}}$, ζ_{ET}, κ_{ET}, ϕ_{Eu} represent the quantum yields of (1) ISC in mT2T, (2) inter-molecular energy transfer from mT2T to the hfa ligands, (3) intra-molecular energy transfer from the hfa ligands to Eu(III) ion, and (4) the emission in Eu(III) ion, respectively. $\eta_{\mathrm{sens}}^{\mathrm{Eu-mT2T}}$ is the overall photosensitization efficiency in the Eu-mT2T film (Eq. (5-8)).

The relationship between the shape of the emission spectrum of Eu(III) ion and its k_r^{Eu} is expressed as

$$k_r^{Eu} = A_{MD,0} n^3 \left(\frac{I_{tot}}{I_{MD}}\right) \quad (5\text{-}3)$$

Here, $A_{MD,0}$, n, and (I_{tot}/I_{MD}) represent the spontaneous luminescence rate of the $^5D_0 \rightarrow {}^7F_1$ transition *in vacuo* (14.65 s^{-1}), refractive index of the medium, and ratio of the total area of the Eu(III) luminescence spectrum to the area of the $^5D_0 \rightarrow {}^7F_1$ transition band, respectively.

ϕ_{Eu} is also determined by the ratio of k_r^{Eu} to the observed decay rate constant of the $^5D_0$ state (k_{obs}^{Eu}) (Eq. (5-4) and (5-5)). The k_{obs}^{Eu} of the $^5D_0$ state is expressed as

$$k_{obs}^{Eu} = \frac{1}{\tau_{obs}^{Eu}} = k_r^{Eu} + k_{nr}^{Eu} \quad (5\text{-}4)$$

Here, τ_{obs}^{Eu}, k_r^{Eu}, and k_{nr}^{Eu} represent the observed lifetimes of the $^5D_0$ state, the radiative rate constant of Eu(III) ion, and the non-radiative rate constant of Eu(III) ion, respectively. The quantum yield of Eu(III) luminescence (ϕ_{Eu}) and overall photosensitization efficiency (η_{sens}) were determined as follows:

$$\phi_{Eu} = \frac{k_r^{Eu}}{k_r^{Eu} + k_{nr}^{Eu}} = \frac{k_r^{Eu}}{k_{obs}^{Eu}} \quad (5\text{-}5)$$

$$\phi_{tot} = \eta_{sens} \times \phi_{Eu} \quad (5\text{-}6)$$

The estimated ϕ_{Eu}, rate constants, and parameters are summarized in **Table 5-3**. We calculated η_{sens} because ϕ_{tot} represents the product of ϕ_{Eu} and overall photosensitization efficiency (η_{sens}; Eq. (5-6); **Table 5-3**). It is worth noting that η_{sens} in the 10 wt% Eu-mT2T film is nearly unity, with $\eta_{sens}^{Eu-mT2T}$ = 0.97. This indicates approximately perfect sensitization of photoexcited mT2T to Eu(III) complex in the Eu-mT2T film, which is more efficient than sensitization of hfa ligands in the Eu-PMMA film, $\eta_{sens}^{Eu-PMMA}$ = 0.71.

Table 5-3 Optical properties of $Eu(hfa)_3(TPPO)_2$-doped films. The decay rate constants of the $^5D_0$ state (k_{obs}^{Eu}) are determined by the lifetime at 615 nm (λ_{ex} = 320 nm). I_{tot}/I_{MD} is the ratio of the total area of the Eu(III) luminescence spectrum to the area of the $^5D_0 \rightarrow {}^7F_1$ transition band. Here, n, k_r^{Eu}, k_{nr}^{Eu}, ϕ_{Eu}, and η_{sens} represent a refractive index of a medium, radiative rate constant of Eu(III) ions, non-radiative rate constant of Eu(III) ions, luminescence quantum yield of Eu(III) ions, and overall photosensitization efficiency, respectively.

host	k_{obs}^{Eu}/s^{-1}	I_{tot}/I_{MD}	n	k_r^{Eu}/s^{-1}	k_{nr}^{Eu}/s^{-1}	ϕ_{Eu}	η_{sens}
PMMA	1.2×10^3	21	1.5	1.0×10^3	1.8×10^2	0.85	0.71
mT2T	1.4×10^3	18	1.7	1.2×10^3	1.9×10^2	0.87	0.97
SF3TRZ	1.4×10^3	17	1.7	1.2×10^3	1.9×10^2	0.86	0.88
mCBP	1.4×10^3	15	1.7	1.1×10^3	2.9×10^2	0.79	0.42
CBP	1.4×10^3	15	1.7	1.1×10^3	3.4×10^2	0.76	0.38
T2T	1.4×10^3	17	1.8	1.3×10^3	1.1×10^2	0.92	0.17

To identify the factor that improves energy transfer efficiency in the Eu-mT2T film, we compared the sensitization efficiencies of intra-molecular energy transfer in the Eu-PMMA film ($\eta_{sens}^{Eu-PMMA}$) and the inter- and intra-molecular energy transfer in the Eu-mT2T film ($\eta_{sens}^{Eu-mT2T}$). $\eta_{sens}^{Eu-PMMA}$ is expressed as follows:

$$\eta_{sens}^{Eu-PMMA} = \phi_{ISC}^{ligand} \times \kappa_{ET} \quad (5\text{-}7)$$

where ϕ_{ISC}^{ligand} and κ_{ET} represent the ISC yield of the ligand and the efficiency of intra-molecular energy transfer, respectively. In contrast, $\eta_{sens}^{Eu-mT2T}$ is expressed as

$$\eta_{sens}^{Eu-mT2T} = \phi_{ISC}^{host} \times \zeta_{ET} \times \kappa_{ET} \quad (5\text{-}8)$$

where ϕ_{ISC}^{host} and ζ_{ET} represent the yield of ISC of the host and the efficiency of inter-molecular energy transfer, respectively. **Fig. 5-9b** shows the symbols for the Eu-mT2T film. We conducted time-resolved measurements in $Eu(hfa)_3(TPPO)_2$-doped neat (Eu-neat) and $Gd(hfa)_3(TPPO)_2$-doped neat (Gd-neat) films to estimate the κ_{ET} of the Eu(III) complex **(Fig. 5-10, 5-11**). We can observe intrinsic emission from the hfa ligands in the Gd-neat film because there is no intra-molecular energy transfer to Gd(III) due to

the energy level mismatch. We compared the time constants of the fs-TAS and TR-PL measurements to analyze each time constant in the energy transfer process (**Fig. 5-12**). The κ_{ET} of the Eu(III) complex was >0.99 when the lifetimes of the T_1 ligands between in the Eu-neat film and the Gd-neat film were compared (**Table 5-4**, Eq. (5-9)). The κ_{ET} was determined under the assumption that the radiative and non-radiative decay rates of the triplet state for the Gd(III) complexes reflect those of the Eu(III) complexes in the absence of energy transfer such that

$$\kappa_{\mathrm{ET}} = 1 - \frac{k_{\mathrm{Gd}}^{\mathrm{T_1}}}{k_{\mathrm{Eu}}^{\mathrm{T_1}}} \tag{5-9}$$

where $k_{\mathrm{Gd}}^{\mathrm{T1}}$ and $k_{\mathrm{Eu}}^{\mathrm{T1}}$ represent the rate constants of the T_1 states of the Gd (III) complex and the ligands in the Eu(III) complex ligands, respectively.

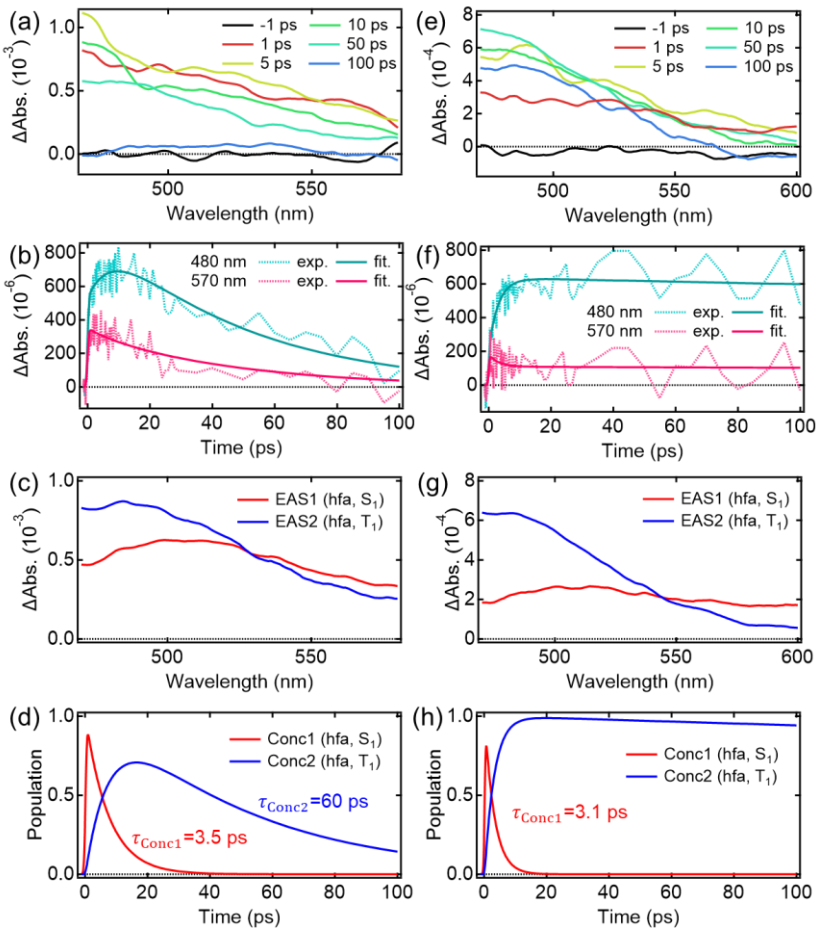

Figure 5-10 fs-TAS and their global analysis of neat films. (a-d) $Eu(hfa)_3(TPPO)_2$ neat films (e-h) $Gd(hfa)_3(TPPO)_2$ neat film. (a, e) Temporal evolutions of the fs-TAS spectra after photoexcitation at 315 nm. (b, f) Temporal profiles of the fs-TAS spectra at 480 nm (green dotted line) and at 580 nm (pink dotted line), and the corresponding fitting curves resulted from the global analysis. (c, g) EAS and (d, h). Corresponding concentration kinetics were obtained from the global analysis based on sequential models *(42)*.

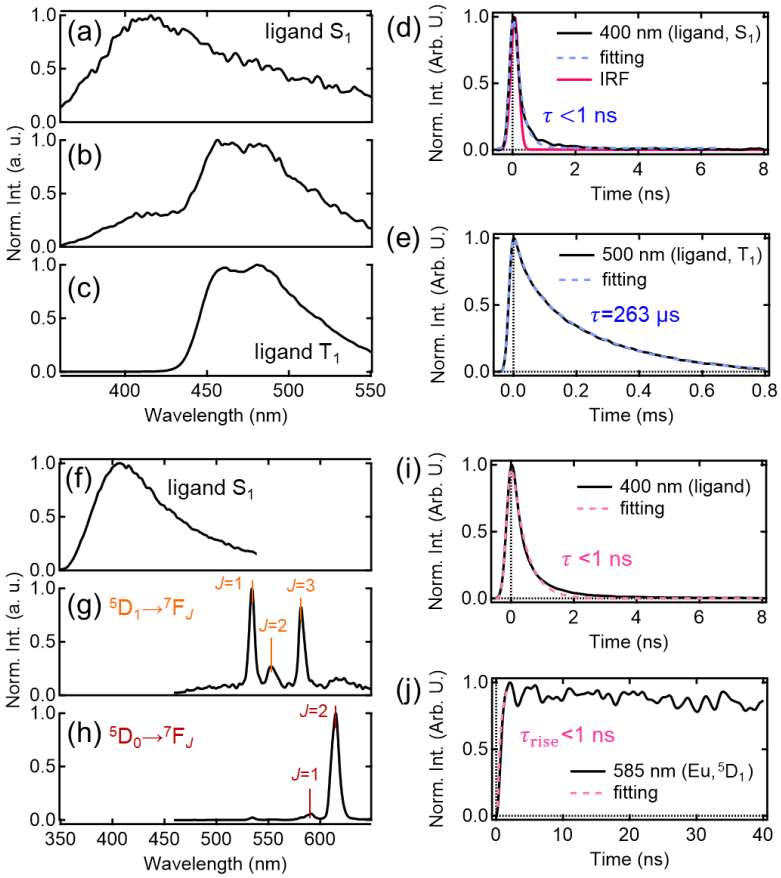

Figure 5-11 TR-PL and their analysis of neat films. (a-e) TR-PL data of $Gd(hfa)_3(TPPO)_2$ neat film. Integrated spectra at (a) 0–1 ns, (b) 80–100 ns, and (c) 10–30 μs. (d) Temporal profile at 400 nm (black solid line), which is assigned to the fluorescence from the hfa ligands, and fitting curve assuming a single exponential decay (sky blue dashed line), and instrumental response function (IRF). (e) Temporal profile at 500 nm (black solid line), which is assigned to the phosphorescence from the hfa ligands, and a fitting curve assuming a single exponential decay (sky blue dashed line). (f-j) TR-PL data of the $Eu(hfa)_3(TPPO)_2$ neat film. Integrated spectra at (f) 0–1 ns, (g) 10–20 ns, and (h) 6–8 μs. (i) Temporal profile at 400 nm, which is assigned to the fluorescence from hfa ligands, and a fitting curve assuming a double exponential decay (pink dashed line). (j) Temporal profile at 585 nm (black solid line), which is assigned to the emission from $^5D_1$ of Eu(III) ions, and fitting curve assuming a single exponential rise (pink dashed line).

We conclude that the quantum yield of the ISC at the ligands, $\phi_{\mathrm{ISC}}^{\mathrm{ligand}}$, in the Eu-PMMA film is the dominant factor in the relatively low $\eta_{\mathrm{sens}}^{\mathrm{Eu-PMMA}}$. Sensitization processes in the case of the Eu-mT2T film, in contrast, occur via inter-molecular energy transfer via T_1 states between the mT2T and hfa ligands. Because the quantum yield of ISC in mT2T is nearly unity, the Eu-T2T film achieves more efficient sensitization.

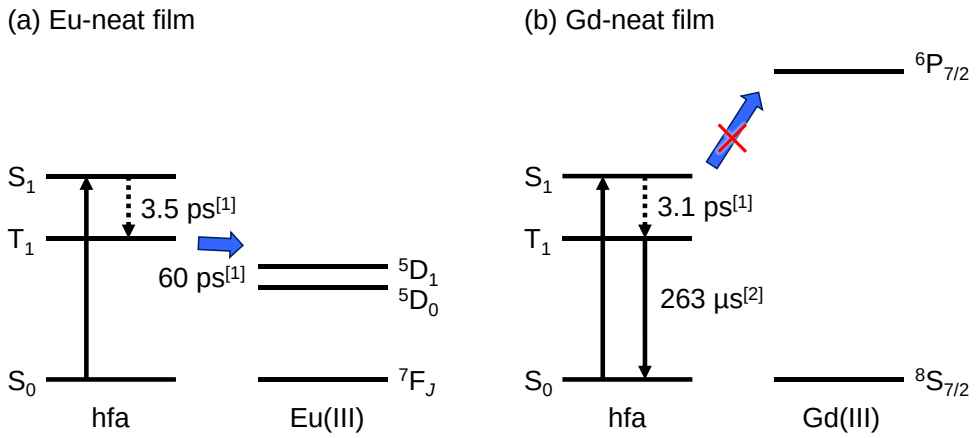

Figure 5-12 Schematic diagram of intra-molecular energy transfer in neat films. (a) $Eu(hfa)_3(TPPO)_2$-doped film. (b) $Gd(hfa)_3(TPPO)_2$-doped neat film. The rate constants were determined by fs-TAS[1] (**Fig. 5-10**) and TR-PL[2] measurements (**Fig. 5-11**)

Table 5-4 Lifetimes of the T_1 state of the ligands and intra-molecular energy transfer efficiency. The rate constants ($\boldsymbol{k_{\mathrm{L}}^{\mathrm{T_1}}}$) were determined by the lifetimes of the T_1 of the hfa ligands in the $Eu(hfa)_3(TPPO)_2$ and $Gd(hfa)_3(TPPO)_2$ neat films (**Fig. 5-12**) after photoexcitation of hfa (excitation wavelength: $\lambda_{ex} = 315$ nm). The efficiencies of the intra-molecular energy transfer ($\boldsymbol{\kappa_{\mathrm{ET}}}$) were calculated by Eq. (5-9).

guest	$\boldsymbol{k_{\mathrm{L}}^{\mathrm{T_1}}}$/s^{-1}	$\boldsymbol{\kappa_{\mathrm{ET}}}$
$Eu(hfa)_3(TPPO)_2$	1.7×10^{10}	>0.99
$Gd(hfa)_3(TPPO)_2$	3.8×10^{3}	-

5-3-4 Time-domain view of the whole sensitization processes

Multiscale TR-PL measurements were performed to quantify energy transfer processes in the time domain. The pseudo-2D color plot of the TR-PL of the Eu-mT2T film after photoexcitation at 267 nm is shown in **Fig. 5-13a-c**. Following photoexcitation, a broad emission band in the 350–500 nm range was observed (**Fig. 5-13a, d**). This band shape is approximately identical to the fluorescence observed in the mT2T neat film (**Fig. 5-14**); this emission is attributed to the S_1 emission in the mT2T. Note that no emission from mT2T was observed in the steady-state emission spectrum (**Fig. 5-5c**) because its time-integrated intensity was much smaller than that of Eu(III) ion. The decay time constant of mT2T emission was estimated to be <100 ps (**Fig. 5-13g**), which agrees with the time constant of ISC in mT2T (~70 ps) estimated from fs-TAS spectra.

Following the rapid decay of the fluorescence from mT2T, narrow-band emissions in the nanosecond to microsecond time range were observed (**Fig. 5-13b, c, e, f**). According to Dicke's diagram, all of these emission bands were assigned to the f–f transitions in Eu(III) ion *(46)*. The 535, 555, and 585 nm bands in the nanosecond region (**Fig. 5-13a, e**) were assigned to the transitions $^5D_1 \rightarrow {}^7F_1$, $^5D_1 \rightarrow {}^7F_2$, and $^5D_1 \rightarrow {}^7F_3$, respectively. The bands at 590 and 615 nm in the microsecond region (**Fig. 5-13b, f**) were assigned to $^5D_0 \rightarrow {}^7F_1$ and $^5D_0 \rightarrow {}^7F_2$, respectively. The rise time constant of the $^5D_1$ state was estimated to be 41.0 ± 0.8 ns (**Fig. 5-13h**), which is much longer than the time constant of the ISC in mT2T (<100 ps). The direct energy transfer from the T_1 state in mT2T to the excited states in Eu(III) ion is ruled out because this energy transfer occurs by the Dexter mechanism with electron exchange and the distance between mT2T and Eu(III) ion in the film is too long for such energy transfer to occur.

Therefore, this result indicates that the energy transfer to Eu(III) complex is ~40

ns and is mediated via the T_1 states. The rise time is determined by multiple processes: (1) the ISC of mT2T (<100 ps), (2) the triplet exciton diffusion in the host matrix, (3) the triplet-triplet energy transfer between mT2T and hfa ligand, and (4) the intramolecular energy transfer from hfa ligand to Eu(III) ion.

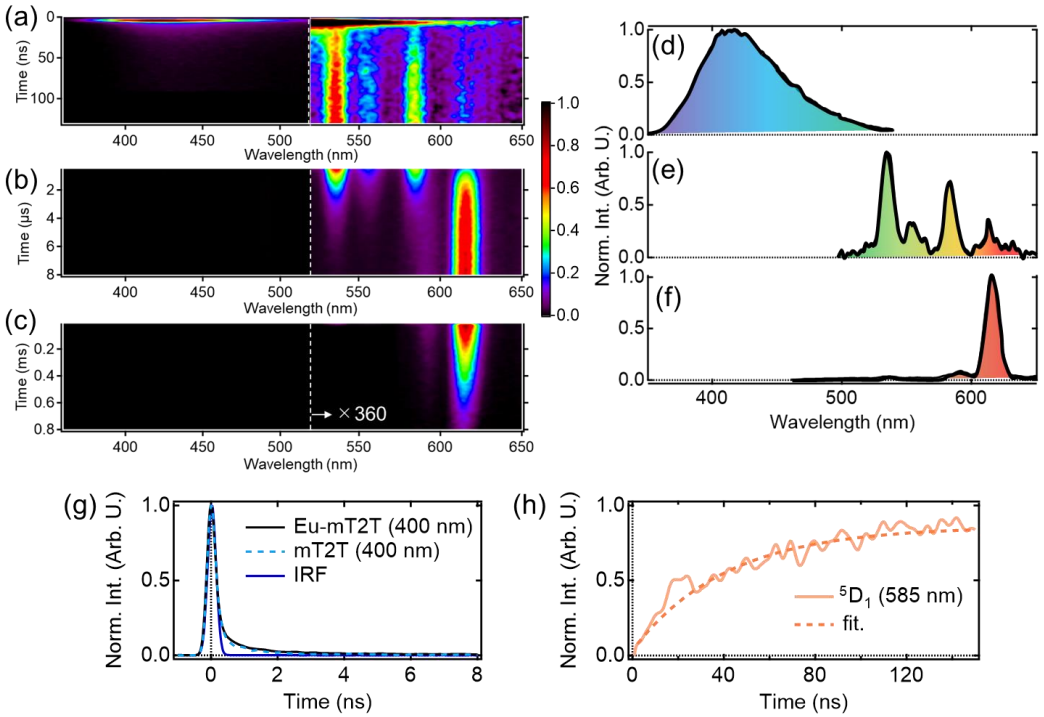

Figure 5-13 TR-PL spectra and their temporal profiles. (a–c) Pseudo-2D plot of the emission from the Eu-mT2T film after photoexcitation at 267 nm in the time range of (a) 0–130 ns, (b) 0.5–8 μs, and (c) 0.01–0.8 ms. For clarity, the intensities above 520 nm are magnified by a factor of 360. (d–f) Normalized emission intensity spectra were obtained from the streak images by the time integration of (d) 0.05–0.15 ns, (e) 145–155 ns, and (f) 6.5–7.5 μs. (g) Temporal profiles of the emission at 400 nm after photoexcitation of the Eu-mT2T film (solid black line) and the mT2T neat film (broken sky blue line) together with the instrumental response function (IRF, solid blue line). (h) Temporal profiles of the emission at 585 nm subtracted the overlapped fluorescence of the host molecules after photoexcitation of the Eu-mT2T film (orange line) and fitting curve (broken orange line).

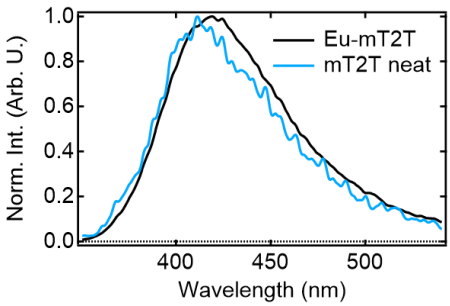

Figure 5-14 Comparison of TR-PL spectra between the doped and neat films. Integrated TR-PL spectra of the Eu-mT2T film at 0–10 ns (black line) and the mT2T neat film at 0–10 ns (sky blue line). The excitation wavelength was 267 nm. The spectrum of the Eu-mT2T film is assigned to the fluorescence from mT2T.

5-3-5 Mechanisms of efficient triplet-state mediated energy transfer and sensitization

Here, we discuss the origins of efficient inter-molecular energy transfer in the Eu-mT2T film in terms of T_1 energy matching. We compared the T_1 energies of the mT2T molecule to those of the hfa ligands of the Eu(III) complex. The T_1 energies for mT2T and hfa were estimated from the phosphorescence spectra (**Fig. 5-15**) to be 2.66 and 2.70 eV, respectively. Due to the close proximity of the energies, an efficient energy transfer from mT2T to the Eu(III) complex is anticipated. We also compared the T_1 energies of the other host molecules to those of hfa, confirming that energetically resonant conditions in the T_1 energies of the host and hfa are important for the higher PLQYs in the host-guest films **(Fig. 5-15g**). This indicates that inter-molecular energy transfer from host molecules to Eu(III) ion occurs via the T_1 of hfa. Furthermore, the phosphorescence of hfa ligands was observed following energy transfer from T_1 in mT2T (**Fig. 5-15a, 5-16**) in the $Gd(hfa)_3(TPPO)_2$-doped mT2T (Gd-mT2T) film, consistent with efficient host-to-hfa energy transfer based on triplet-triplet energy transfer. We concluded that the energy resonance in T_1 between mT2T and hfa causes highly efficient inter-molecular energy transfer sensitization (ζ_{ET}~1.0).

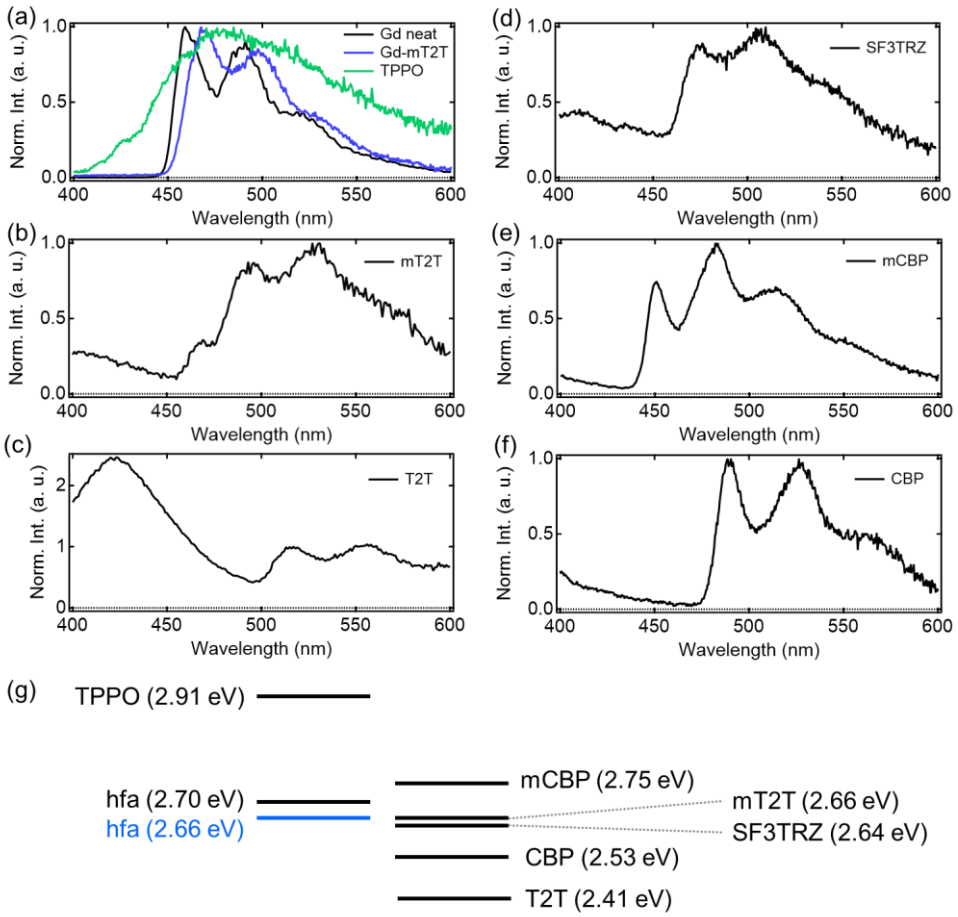

Figure 5-15 Phosphorescence spectra of host molecules and ligands measured at 77 K. (a) $Gd(hfa)_3(TPPO)_2$ neat film (black line), $Gd(hfa)_3(TPPO)_2$-doped mT2T film (blue line), and TPPO neat film (green line). (b) mT2T, (c) pT2T, (d) SF3TRZ, (e) mCBP, and (f) pCBP neat films. (g) Schematic energy diagram of the T_1 excited states estimated from the phosphorescence spectra. Note that the energy level of hfa ligands in the $Gd(hfa)_3(TPPO)_2$ neat film (black line) differs from that in the $Gd(hfa)_3(TPPO)_2$-doped mT2T film (blue line).

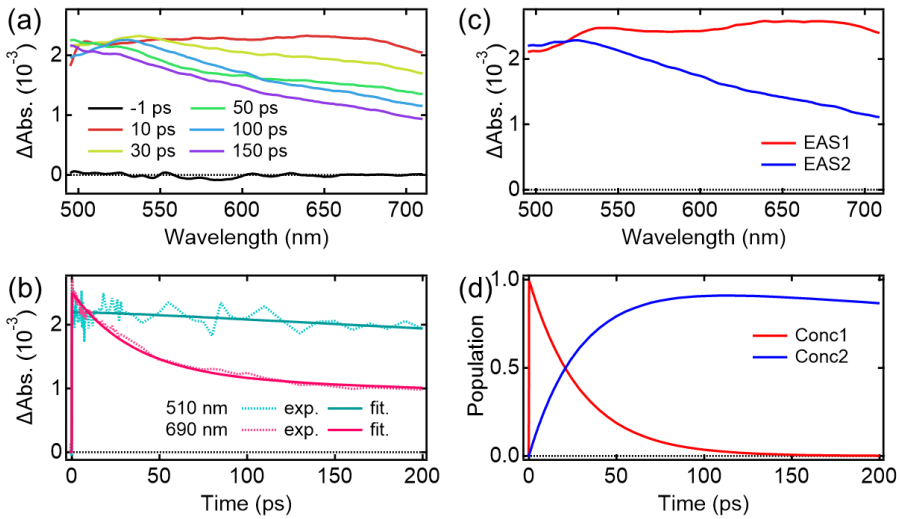

Figure 5-16 fs-TAS and their global analysis of the $Gd(hfa)_3(TPPO)_2$-doped mT2T film. (a) Temporal evolution of the fs-TAS spectra after photoexcitation at 267 nm. (b) Temporal profiles at 510 nm (green dotted line) and at 690 nm (pink dotted line). The corresponding fitting curves resulted from the global analysis. (c) EAS and (d) corresponding concentration kinetics were obtained from the global analysis based on sequential models *(42)*. The transition timescale from EAS1 to EAS2 was 36.3 ± 0.3 ps.

It is worth mentioning that our triplet-based emission enhancement strategy offers several advantages over the co-fluorescence effect, in which Gd or Lu complex works as a sensitizer, described in ref. 28. Firstly, we achieved a significantly greater enhancement in emission compared to the previous work. Secondly, we utilize organic compounds as host molecules, resulting in a substantial improvement in absorption ability. Thirdly, the host-guest films are fabricated through a simple solution process.

There are two possible assignments to the slow rise time. One is the energy transfer from the T_1 of the mT2T to the T_1 of the ligand and the other is the triplet exciton diffusion in the host matrix. Finally, we discuss triplet exciton diffusion in the host matrix by comparing energy transfer to Eu(III) complex and PLQYs in Eu-mT2T films with different mT2T and Eu(III) complex ratios (**Fig. 5-17, Table 5-5**). As the concentration

of the Eu(III) complex increased, the rise time constant of $^5D_1$ got shorter. The rise time constant of the low ratio of the mT2T (Eu(III) complex concentration of 50 wt%) film exhibits the fastest rise time constant (~29 ns). Because the lifetime of T_1 in mT2T is likely to be much longer than the diffusion time scale, sensitization processes mediated by triplet–triplet energy transfer are effective in realizing ideal sensitization for Eu(III) ion emission (**Fig. 5-18**).

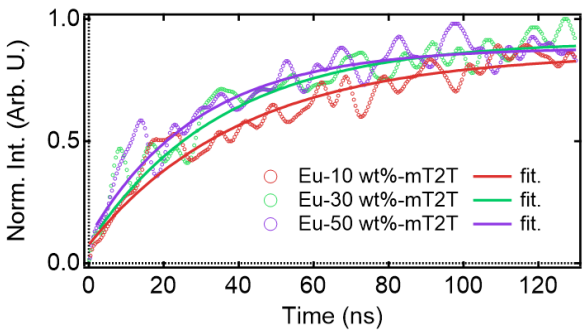

Figure 5-17 Comparison of temporal profiles of emission from Eu(III) in a doped film with different doping ratios. Temporal profiles of the TR-PL spectra at 585 nm, which is assigned to the emission of $^5D_1$ of Eu(III) in $Eu(hfa)_3(TPPO)_2$ 10 wt%-doped Eu-mT2T (Eu-10 wt%-mT2T, red circle) film, 30 wt%-doped Eu-mT2T (Eu-30 wt%-mT2T, green circle) film, and 50 wt%-doped Eu-mT2T (Eu-50 wt%-mT2T, purple circle) film. The corresponding solid curves are fitting curves assuming a single exponential rise. The obtained rise time constant of the Eu-10 wt%-mT2T film is 41.0 ± 0.8 ns, the rise time constant of the Eu-30 wt%-mT2T film is 35.5 ± 1.2 ns, and the rise time constant of the Eu-50 wt%-mT2T film is 29.1 ± 1.0 ns.

Table 5-5 Environmental dependency of PLQY of Eu(III)-complex-doped films. PLQYs were measured under ambient atmosphere or under the argon (Ar) atmosphere.

guest	host	Eu conc. /wt%	environment	ϕ_{tot}	λ_{ex} /nm
$Eu(hfa)_3(TPPO)_2$	PMMA	10	ambient	0.60	315
			Ar	0.61	
	mT2T	10	ambient	0.79	267
			Ar	0.84	
		30	ambient	0.78	267
			Ar	0.83	
		50	ambient	0.77	267
			Ar	0.78	

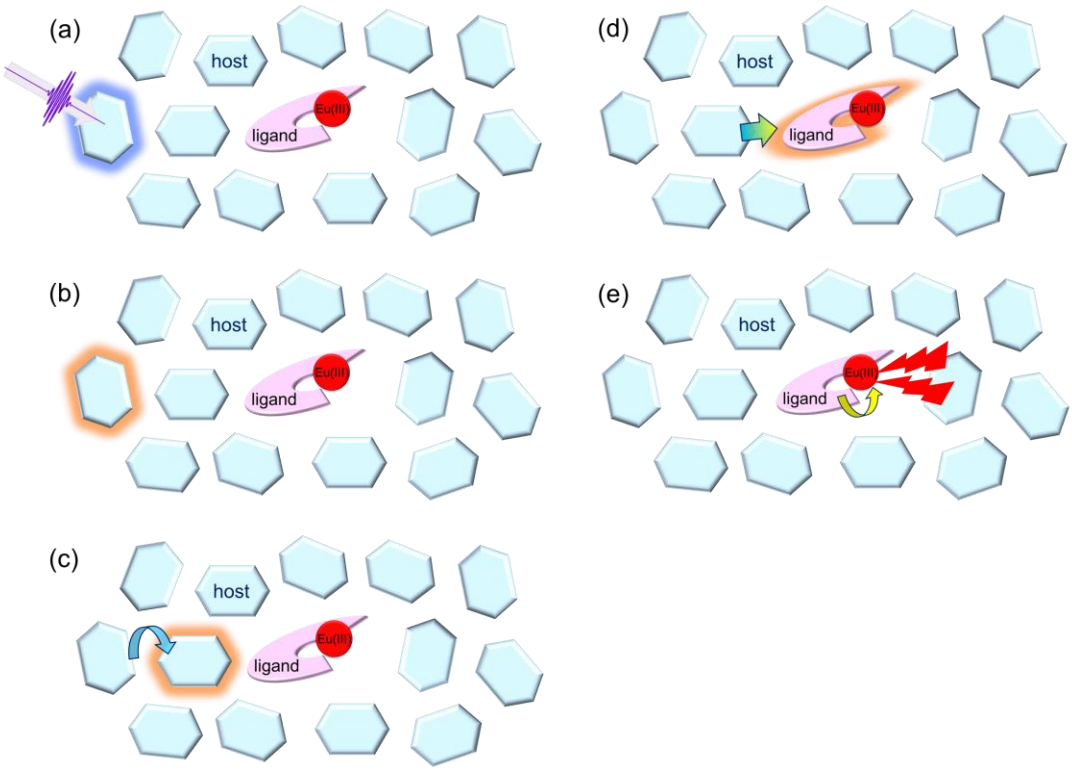

Figure 5-18 Overview of energy transfer processes in the Eu-mT2T film. (a) Photoexcitation of a mT2T host molecule. (b) ISC occurs in the mT2T host molecule. (c) Excitation diffusion between mT2T occurs in ~40 ns. (d) Intermolecular energy transfer occurs from the nearest mT2T generated from the excitation diffusion to a hfa ligand of a Eu(III) complex. (e) Intramolecular energy transfer occurs from the ligand to the Eu(III) ion.

5-4 Conclusion

We demonstrated highly efficient light harvesting of Eu(III) ion in complex-doped host-guest films with $Eu(hfa)_3(TPPO)_2$. When we used mT2T, a triazine derivative thet works well as an energy-harvesting antenna, we observe a significant increase in the luminescence intensity of Eu(III) ion. After photoexcitation of host molecules to Eu(III) ion emission, we estimated the quantum yields of all energy transfer processes and discovered that all energy transfer processes occur with nearly unity quantum yield. We conclude from the TR-PL and fs-TAS measurements that efficient energy transfer occurs via resonant energy transfer from T_1 of mT2T to T_1 of hfa following rapid and highly efficient ISC in mT2T. This mechanism can avoid energy loss in the ISC process in the hfa ligands of an Eu(III) complex and overcome the intrinsic limitations of conventional direct sensitization by the ligands. Based on these results, we propose a novel light harvesting method for Ln(III) with simple fabrication: a host-guest film composed of host molecules with efficient ISC, which works as an efficient photosensitizer, and a guest Ln(III) complex with ligands having a T_1 state whose energy matches that of T_1 in the host, which works as an efficient energy accepter and emitter.

References

1. M. A. Baldo, O. F. O'Brien, Y. You, A. Shoustikov, S. Sibley, M. E. Thompson, S. R. Forrest, Highly efficient phosphorescent emission from organic electroluminescent devices. *Nature* **395**, 151–154 (1998).
2. H. Uoyama, K. Goushi, K. Shizu, H. Nomura, C. Adachi, Highly efficient organic light-emitting diodes from delayed fluorescence. *Nature* **492**, 234–238 (2012).
3. A. S. D. Sandanayaka, T. Matsushima, F. Bencheikh, S. Terakawa, W. J. Potscavage Jr., C. Qin, T. Fujihara, K. Goushi, J.-C. Ribierre, C. Adachi, Indication of current-injection lasing from an organic semiconductor. *Appl. Phys. Express* **12**, 061010 (2019).
4. K. Binnemans, Interpretation of Europium(III) Spectra. *Cood. Chem. Rev.* **295**, 1–45 (2015).
5. B. R. Judd, Optical Absorption Intensities of Rare-Earth Ions. *Phys. Rev.* **127**, 750 (1962).
6. L. R. Melby, N. J. Rose, E. Abramson, J. C. Caris, Synthesis and Fluorescence of Some Trivalent Lanthanide Complexes. *J. Am. Chem. Soc.* **86** (23), 5117–5125 (1964).
7. Y. Hasegawa, Y. Wada, S. Yanagida, Strategies for the design of luminescent lanthanide(III) complexes and their photonic applications. *J. Photochem. Photobiol. C Rev.* **5**, 183–202 (2004).
8. J. -C. G. Bünzli, On the design of highly luminescent lanthanide complexes. *Cood. Chem. Rev.* **293–294**, 19–47 (2015).
9. J. Yuan, K. Matsumoto, Fluorescence Enhancement by Electron-Withdrawing Groups on -Diketones in Eu(III)-diketonato-topo Ternary Complexes. *Analytical Sciences* **12**, 31–36, (1996).
10. K.-L. Wong, J.-C. G. Bünzli, P. A. Tanner, Quantum yield and brightness. *J. Lumin.* **224**, 117256 (2020).
11. Y. Kitagawa, F. Suzue, T. Nakanishi, K. Fushimi, Y. Hasegawa, A highly luminescent Eu(III) complex based on an electronically isolated aromatic ring system with ultralong lifetime. *Dalton Trans.* **47**, 7327–7332 (2018).
12. N. Filipescu, W. F. Sager, and F. A. Serafin, Substituent effects on intramolecular energy transfer. II. Fluorescence spectra of europium and terbium β-diketone chelates. *J. Phys. Chem.* **68**, 3324–3346 (1964).
13. S. Sato, M. Wada, Relations between Intramolecular Energy Transfer Efficiencies and Triplet State Energies in Rare Earth β-diketone Chelates. *Bull. Chem. Soc. Jpn.* **43**, 1955–1962 (1970).

14. D. B. A. Raj, B. Francis, M. L. P. Reddy, R. R. Butorac, V. M. Lynch, A. H. Cowley, Highly Luminescent Poly(Methyl Methacrylate)-Incorporated Europium Complex Supported by a Carbazole-Based Fluorinated β-Diketonate Ligand and a 4,5-Bis(diphenylphosphino)-9,9-dimethylxanthene Oxide Co-Ligand. *Inorg. Chem.* **49**, *19*, 9055–9063 (2010).
15. N. B. D. Lima, S. M. C. Gonçalves, S. A. Júnior, A. M. A. Simas, A Comprehensive Strategy to Boost the Quantum Yield of Luminescence of Europium Complexes. *Sci. Rep.* **3**, 1–8 (2013).
16. Y. Hasegawa, K. Murakoshi, Y. Wada, S. Yanagida, J. Kim, N. Nakashima, T. Yamanaka, Enhancement of luminescence of Nd^{3+} complexes with deuterated hexafluoroacetylacetonato ligands in organic solvent. *Chem. Phys. Lett.*, **248**, 8–12 (1996).
17. K. Miyata, T. Nakagawa, R. Kawakami, Y. Kita, K. Sugimoto, T. Nakashima, T. Harada, T. Kawai, Y. Hasegawa, Remarkable Luminescence Properties of Lanthanide Complexes with Asymmetric Dodecahedron Structures. *Chem. Eur. J.* **17**, 521–528 (2011).
18. K. Nakamura, Y. Hasegawa, H. Kawai, N. Yasuda, N. Kanehisa, Y. Kai, T. Nagamura, S. Yanagida, Y. Wada, Enhanced Lasing Properties of Dissymmetric Eu(III) Complex with Bidentate Phosphine Ligands. *J. Phys. Chem. A* **111**, 3029–3037 (2007).
19. P. A. Tanner, Some misconceptions concerning the electronic spectra of tri-positive europium and cerium. *Chem. Soc. Rev.* **42**, 5090–5101 (2013).
20. B. G. Vats, S. Kannan, M. Kumar, M. G. B. Drew, Ligand-Field Asymmetry-Controlled Luminescent Europium (III) and Samarium(III) Tris(β-diketonate) Complexes of Diphenyl-(2- pyridyl-N-oxide)- Phosphine Oxide. *ChemistrySelect* **2,** *13*, 3683–3689 (2017).
21. A. F. Kirby, D. Foster, F. S.Richardson, Comparison of $^7F_J \leftarrow {}^5D_0$ emission spectra for Eu(III) in crystalline environments of octahedral, near-octahedral, and trigonal symmetry. *Chem. Phys. Lett.* **95**, 507–512 (1983).
22. Y. Hasegawa, M. Yamamuro, Y. Wada, N. Kanehisa, Y. Kai, A. Yanagida, Luminescent Polymer Containing the Eu(III) Complex Having Fast Radiation Rate and High Emission Quantum Efficiency. *J. Phys. Chem. A* **107**, 1697–1702 (2003).
23. A. Nakajima, T. Nakanishi, Y. Kitagawa, T. Seki, H. Ito, K. Fushimi, Y. Hasegawa, Hyper-stable organo-Eu^{III} luminophore under high temperature for photo-industrial application. *Sci Rep.* **6**, 24458 (2016).

24. H. Xu, Q. Sun, Z. An, Y. Wei, X. Liu, Electroluminescence from Europium(III) Complexes. *Cood. Chem. Rev.* **293-294**, 228–249 (2015).
25. L. Wang, Z. Zhao, C. Wei, H. Wei, Z Liu, Z. Bian, C. Huang, Review on the Electroluminescence Study of Lanthanide Complexes. *Adv. Opt. Mater.* **7**, 1801256 (2019).
26. J. Kido, Y. Okamoto, Organo Lanthanide Metal Complexes for Electroluminescent Materials. *Chem. Rev.* **102**, 2357 (2002).
27. M. Pietraszkiewicz, M. Maciejczyk, I. D. W. Samuel, S. Zhang, Highly photo- and electroluminescent 1,3-diketonate Eu(III) complexes with spiro-fluorene-xantphos dioxide ligands: synthesis and properties. *J. Mater. Chem. C* **1**,8028–8032 (2013).
28. K. Buczko, M. Karbowiak, Co-fluorescence enhanced tuneable emission of lanthanide β-diketonate complexes in solid thin films. *J. Lumin.* **136**, 130–140 (2013).
29. H. Xu, K. Yin, W. Huang, Comparison of the Electrochemical and Luminescence Properties of Two Carbazole-Based Phosphine Oxide Eu^{III} Complexes: Effect of Different Bipolar Ligand Structures. *ChemPhysChem.* **9**, 1752 (2008).
30. J. Wang, C. Han, G. Xie, Y. Wei, Q. Xue, P. Yan, H. Xu. Solution-Processible Brilliantly Luminescent Eu^{III} Complexes with Host-Featured Phosphine Oxide Ligands for Monochromic Red-Light-Emitting Diodes. *Chem.-Eur. J.* **20**, 11137–11148 (2014).
31. D. B. A. Raj, S. Bijua, M. L. P. Reddy, 4,4,5,5,5-Pentafluoro-1-(9H-fluoren-2-yl)-1,3-pentanedione complex of Eu^{3+} with 4,5-bis(diphenylphosphino)-9,9-dimethylxanthene oxide as a promising light-conversion molecular device. *Dalton Trans.* 7519–7528 (2009).
32. H. Xu, L.-H. Wang, X.-H. Zhu, K. Yin, G.-Y. Zhong, X.-Y. Hou, and W. Huang, Application of Chelate Phosphine Oxide Ligand in Eu^{III} Complex with Mezzo Triplet Energy Level, Highly Efficient Photoluminescent, and Electroluminescent Performances. *J. Phys. Chem.* **110**, 3023–3029 (2006).
33. H. Xu, K. Yin, W. Huang, Novel Light-Emitting Ternary Eu^{3+} Complexes Based on Multifunctional Bidentate Aryl Phosphine Oxide Derivatives: Tuning Photophysical and Electrochemical Properties toward Bright Electroluminescence. *J. Phys. Chem. C* **114**, 1674–1683 (2010).
34. M. Latva, H. Takalo, V.-M. Mukkala, C. Matachescu, J. C. Rodriguez-Ubisd, J. Kankarea, Correlation between the Lowest Triplet State Energy Level of the Ligand and Lanthanide(III) Luminescence Quantum Yield. *J. Lumin.* **75**, 149–169 (1997).

35. S. Miyazaki, K. Miyata, H. Sakamoto, F. Suzue, Y. Kitagawa, Y. Hasegawa, K. Onda, Dual Energy Transfer Pathways from an Antenna Ligand to Lanthanide Ion in Trivalent Europium Complexes with Phosphine-Oxide Bridges. *J. Phys. Chem. A* **124**, 6601–6606 (2020).
36. M. W. Mara, D. S. Tatum, A. March, G. Doumy, E. G. Moore, K. N. Raymond, Energy Transfer from Antenna Ligand to Europium(III) Followed Using Ultrafast Optical and X-Ray Spectroscopy. *J. Am. Chem. Soc.* **141**, 11071–11081 (2019).
37. C. Yang, L.-M. Fu, Y. Wang, J.-P. Zhang, W.-T. Wong, X-C. Ai, Y.-F. Qiao, B. S. Zou, L.-L. Gui, A Highly Luminescent Europium Complex Showing Visible-Light-Sensitized Red Emission: Direct Observation of the Singlet Pathway. *Angew. Chem., Int. Ed.* **43**, 5010–5013 (2004).
38. E. Kasprzycka, V. A. Trush, V. M. Amirkhanov, L. Jerzykiewicz, O. L. Malta, J. Legendziewicz, P. Gawryszewska, Contribution of Energy Transfer from the Singlet State to the Sensitization of Eu^{3+} and Tb^{3+} Luminescence. *Chem.-Eur. J.* **23**, 1318–1330 (2017).
39. M. Saigo, Y. Shimoda, T. Ehara, T. Ryu, K. Miyata, K. Onda, Characterization of Excited States in a Multiple-Resonance-Type Thermally Activated Delayed Fluorescence Molecule Using Time-Resolved Infrared Spectroscopy. *Bull. Chem. Soc. Jpn.* **95**, 381–388 (2022).
40. A. Skumanich, M. Jurich, J. D. Swalen, Absorption and scattering in nonlinear optical polymeric systems. *Appl. Phys. Lett.* **62**, 446 (1993).
41. H. Kataoka, T. Kitano, T. Takizawa, Y. Hirai, T. Nakanishi, Y. Hasegawa, Photo- and thermo-stable luminescent beads composed of Eu(III) complexes and PMMA for enhancement of silicon solar cell efficiency. *J. Alloys Compd.* **601**, 293–297 (2014).
42. J. J. Snellenburg, S. P. Laptenok, R. Seger, K. M. Mullen, I. H. M. van Stokkum, Glotaran: A Java-Based Graphical User Interface for the R Package TIMP. *J. Stat. Softw.* **49**, *3*, 1–22 (2012).
43. J. Zhao, W. Wu, J. Sun, S. Guo, Triplet photosensitizers: from molecular design to applications. *Chem. Soc. Rev.* **42**, 5323–5351 (2013).
44. Z. An, C. Zheng, Y. Tao, R. Chen, H. Shi, T. Chen, Z. Wang, H. Li, R. Deng, X. Liu, W. Huang, Stabilizing triplet excited states for ultralong organic phosphorescence. *Nat. Mater.* **14**, 685–690 (2015).
45. M. H. V. Werts, R. T. F. Jukes, J. W. Verhoeven, The emission spectrum and the radiative lifetime of Eu^{3+} in luminescent lanthanide complexes. *Phys. Chem. Chem. Phys.* **4**, 1542–1548 (2002).

46. C. -G. Ma, M. G. Brik, D.-X. Liu, B. Feng, Y. Tian, A. Suchocki, Energy level schemes of f^N electronic configurations for the di-, tri-, and tetravalent lanthanides and actinides in a free state. *J. Lumin.* **170**, 369–374 (2016).

Chapter 6. Summary and perspective

6-1 Summary

The author employed TR-PL and TAS to investigate the energy transfer mechanisms in Eu(III) complexes. The goal was to gain a better understanding of the emission mechanism and facilitate materials development.

In **Chapter 1 and 2**, the author explained the background and experimental methods in this thesis, respectively.

In **Chapter 3**, the author conducted an investigation into the energy transfer processes in the $Eu(hfa)_3(DPPTO)_2$ complex using TR-PL. In addition to the conventional energy transfer pathway through the T_1 state of the ligands, a fast energy transfer pathway from the singlet excited states of the ligands to the $^5D_1$ state of Eu(III) was discovered. This dual energy transfer mechanism contributes to the high photoluminescence quantum yield observed in the complex, offering important insights for the design strategies of luminescent complexes.

In **Chapter 4**, the author explores the energy transfer mechanism in the $Eu(hfa)_3(TPPO)_2$ complex, utilizing TR-PL and fs-TAS. The experimental results demonstrate nearly unity efficiency of energy transfer from the T_1 state of β-diketonate ligands to the Eu(III) ions, unveiling a novel pathway to the $^5D_2$ state of the Eu(III) ion. These findings have important implications for designing efficient luminescent Eu(III) complexes and advancing the development of lanthanide-based light-emitting materials.

In **Chapter 5**, the author investigates the enhancement of photoluminescence intensity through sensitization using a host-guest system. Specifically, they explore a system composed of triazine-based host molecules and $Eu(hfa)_3(TPPO)_2$. By conducting TR-PL and fs-TAS measurements, the author reveals an energy transfer mechanism from the host molecules to the Eu(III) ions, occurring via triplet states over several molecules

with an impressive efficiency of nearly 100%. This discovery enables efficient light harvesting in Eu(III) complexes and provides a simple solution-based fabrication process, promising advancements in light-emitting applications.

In these studies, TR-PL and fs-TAS were employed to investigate the energy transfer mechanisms in Eu(III) complexes. This research not only enhanced our understanding of the emission mechanism but also played a crucial role in advancing materials development in this field.

6-2 Future perspective

Based on the findings of this research, there are several potential directions for future work in the field of Eu(III) complexes and their energy transfer mechanisms. One promising avenue is the application of these complexes in organic light-emitting diodes (OLEDs). By utilizing the knowledge gained about the energy transfer pathways and efficiency, it becomes possible to design and optimize Eu(III)-based OLEDs with enhanced performance and efficiency. This could lead to the development of more efficient and vibrant displays, lighting, and other optoelectronic devices.

Additionally, further investigations can be conducted to explore the potential of other antenna ligands and coordination structures for Eu(III) complexes. By studying different ligand systems and their energy transfer mechanisms, it is possible to discover novel pathways and improve the overall efficiency of energy transfer in these complexes. This would open up new possibilities for the design and synthesis of luminescent Eu(III) complexes with tailored properties for various applications.

Moreover, the study of host-guest systems, as demonstrated in Chapter 5, holds promise for enhancing the photoluminescence intensity in Eu(III) complexes. Future

research can focus on developing new host molecules and optimizing their interaction with Eu(III) ions to achieve even higher energy transfer efficiencies. This could lead to the creation of highly efficient light-harvesting systems that can be utilized in a wide range of applications.

Overall, the investigations presented in this thesis provide a solid foundation for future research in the field of Eu(III) complexes. By further exploring their energy transfer mechanisms and applying the gained knowledge to practical applications such as OLEDs, significant advancements can be made in the development of luminescent materials and optoelectronic devices.

Publication lists

Original papers

1. "Dual Energy Transfer Pathways from an Antenna Ligand to Lanthanide Ion in Trivalent Europium Complexes with Phosphine-Oxide Bridges"
   Shiori Miyazaki, Kiyoshi Miyata, Haruna Sakamoto, Fumiya Suzue, Yuichi Kitagawa, Yasuchika Hasegawa, and Ken Onda
   The Journal of Physical Chemistry A **2020**, *124*, 33, 6601–6606.

2. "Novel Energy Transfer Pathway in Trivalent Europium Complexes with β-Diketonate Ligands"
   Shiori Miyazaki, Kiyoshi Miyata, Yuichi Kitagawa, Yasuchika Hasegawa and Ken Onda
   (*Manuscript in preparation*)

3. "Highly Efficient Light Harvesting of a Eu(III) Complex in a Host–guest Film by Triplet Sensitization"
   Shiori Miyazaki, Kenichi Goushi, Yuichi Kitagawa, Yasuchika Hasegawa, Chihaya Adachi, Kiyoshi Miyata and Ken Onda
   Chemical Science **2023**, *14*, 6867–6875.

Joint papers

1. "Coordination Geometrical Effect on Ligand-to-Metal Charge Transfer-Dependent Energy Transfer Processes of Luminescent Eu(III) Complexes"
   Pedro Paulo Ferreira da Rosa, **Shiori Miyazaki**, Haruna Sakamoto, Yuichi Kitagawa, Kiyoshi Miyata, Tomoko Akama, Masato Kobayashi, Koji Fushimi, Ken Onda, Tetsuya Taketsugu, and Yasuchika Hasegawa
   The Journal of Physical Chemistry A **2021**, *125*, 1, 209–217.

Acknowledgments

This doctoral thesis is the summary of the author's studies conducted under the supervision of Professor Ken Onda at the Department of Chemistry, Graduated School of Science, Kyushu University, from April 2018 to August 2023.

The author would like to express my deepest gratitude to Professor Ken Onda for supervising this thesis, providing an excellent research environment, helpful discussion, and supporting all my works. The author would also like to express my deep appreciation to Associate Professor Kiyoshi Miyata for his insightful comments and guidance for my work and life.

The author would like to appreciate Professor Yasuchika Hasegawa and Associate Professor Yuichi Kitagawa at Hokkaido University for providing the samples and valuable discussions.

The author would like to appreciate Professor Chihaya Adachi and Assistant Professor Kenichi Goushi at Center for Organic Photonics and Electronics Research (OPERA), Kyushu University, for valuable discussions.

The author would like to thank all the members of Onda laboratory for their kind support not only for my work but also for his daily life. The author also would like to thank all the collaborators.

The author also thanks Japan Society for the Promotion of Science for the financial support of the Research Fellowship for Young Scientists.

Finally, the author would like to express his gratitude to his family for always supporting her during her long student life.

Shiori Miyazaki

August 2023